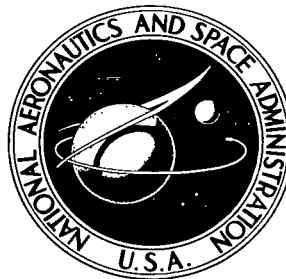


NASA TECHNICAL NOTE



NASA TN D-7976 *cl*

NASA TN D-7976



LOAN COPY: RETURN TO
AFWL TECHNICAL LIBRARY
KIRTLAND AFB, N. M.

EXPERIMENTAL AND NUMERICAL INVESTIGATION
OF BOUNDARY-LAYER DEVELOPMENT AND TRANSITION
ON THE WALLS OF A MACH 5 NOZZLE

*William D. Harvey, Aubrey M. Cary, Jr.,
and Julius E. Harris*

*Langley Research Center
Hampton, Va. 23665*



NATIONAL AERONAUTICS AND SPACE ADMINISTRATION • WASHINGTON, D. C. • DECEMBER 1975



0133535

1. Report No. NASA TN D-7976		2. Government Accession No.		3. Recipient's Catalog No.	
4. Title and Subtitle EXPERIMENTAL AND NUMERICAL INVESTIGATION OF BOUNDARY-LAYER DEVELOPMENT AND TRANSITION ON THE WALLS OF A MACH 5 NOZZLE				5. Report Date December 1975	
7. Author(s) William D. Harvey, Aubrey M. Cary, Jr., and Julius E. Harris				6. Performing Organization Code	
9. Performing Organization Name and Address NASA Langley Research Center Hampton, Va. 23665				8. Performing Organization Report No. L-10119	
12. Sponsoring Agency Name and Address National Aeronautics and Space Administration Washington, D.C. 20546				10. Work Unit No. 505-06-41-01	
15. Supplementary Notes Appendix by William D. Harvey and Aubrey M. Cary, Jr.				11. Contract or Grant No.	
16. Abstract Measurements of mean pitot pressure have been made across the wall boundary layer at several axial stations in a Mach 5, axisymmetric, contoured nozzle in air. Total temperature measurements near the nozzle exit were also made. The exit Reynolds number was varied from 0.41×10^5 to 0.68×10^6 per centimeter (1.04×10^5 to 1.73×10^6 per in.). The free-stream total temperature varied from approximately 319 K (575° R) to 378 K (680° R) for a corresponding wall-to-total temperature ratio of 0.8 to 1.3. When the wall-to-total temperature ratio was varied from about 0.8 to 0.9, the nozzle-wall boundary layer was laminar downstream of the throat for about 80 percent of the nozzle length at the lowest exit test Reynolds number of 10.10×10^4 per centimeter (2.56×10^5 per in.) and completely turbulent for the exit test Reynolds number of 1.145×10^5 per centimeter (2.91×10^5 per in.). In general, the implicit finite-difference theoretical method gave acceptable predictions of the experimental boundary-layer profile shapes and thickness for both laminar and turbulent flow. When the nozzle wall was heated to a wall-to-total temperature ratio of approximately 1.4, the boundary layer over most of the nozzle was laminar for a high exit Reynolds number of about 12.3×10^4 per centimeter (3.1×10^5 per in.) compared to 1.01×10^5 per centimeter (2.56×10^5 per in.) at the lower wall temperature. Disturbance effects from settling-chamber screen configurations, upstream two-dimensional steps, and upstream piping and valves had no effect on transition but did influence the boundary-layer thickness. Roughness located in the nozzle subsonic approach section promoted boundary-layer transition on the nozzle wall at a Reynolds number of about 7.0×10^4 per centimeter (1.8×10^5 per in.).				13. Type of Report and Period Covered Technical Note	
17. Key Words (Suggested by Author(s)) Boundary-layer stability and transition Nozzle and channel flow Supersonic and hypersonic flow				14. Sponsoring Agency Code	
18. Distribution Statement Unclassified - Unlimited				Subject Category 34	
19. Security Classif. (of this report) Unclassified		20. Security Classif. (of this page) Unclassified		21. No. of Pages 86	
				22. Price* \$4.75	

EXPERIMENTAL AND NUMERICAL INVESTIGATION
OF BOUNDARY-LAYER DEVELOPMENT AND TRANSITION
ON THE WALLS OF A MACH 5 NOZZLE

William D. Harvey, Aubrey M. Cary, Jr., and Julius E. Harris
Langley Research Center

SUMMARY

Measurements of mean pitot pressure were made across the boundary layer at various longitudinal stations in an axisymmetric contoured nozzle. The Mach number at the nozzle exit was approximately 5 and the exit diameter was 10.67 centimeters (4.2 in.). Total temperature was measured across the boundary layer at a single station near the nozzle exit. The test gas was air and the Reynolds number at the nozzle exit varied from 0.41×10^5 to 0.68×10^6 per centimeter (1.04×10^5 to 1.73×10^6 per in.). The free-stream total temperature varied from about 319 K (575° R) to 378 K (680° R).

During the first set of tests, the wall-to-total temperature ratio was varied from about 0.8 to 0.9. For these tests, the nozzle-wall boundary layer was laminar downstream of the throat for about 80 percent of the nozzle length for the exit test Reynolds number of 10.10×10^4 per centimeter (2.56×10^5 per in.). The boundary layer was completely turbulent at the exit test Reynolds number of 1.145×10^5 per centimeter (2.91×10^5 per in.). The presence of laminar, transitional, or turbulent flow on the nozzle wall was ascertained primarily on the basis of comparisons between measured and theoretical profile shapes and boundary-layer thicknesses. In general, the implicit finite-difference theoretical method gave acceptable predictions of the experimental pitot pressure, Mach number, and velocity profiles for both laminar and turbulent flow. The disagreement between the measured and theoretical profiles near the exit may be attributed to free-stream disturbances or the presence of Taylor-Görtler vortices that develop in the concave region of the nozzle.

The relation between the normalized total temperature and velocity parameters at the exit was nearly quadratic at the lowest Reynolds number and for wall-to-total temperature ratios less than about 0.85. For higher Reynolds numbers and for wall-to-total temperature ratios greater than about 0.85, however, there was significant deviation from the quadratic relation towards a linear variation with temperature overshoot near the boundary-layer edge. Tests were made with and without settling-chamber screens. The settling-chamber screens did not affect the temperature profiles. Pitot profile shapes along the nozzle were affected by the screens; however, boundary-layer thicknesses were only slightly affected.

When the nozzle wall was heated to a wall-to-total temperature ratio of approximately 1.4, the boundary layer over most of the nozzle length was laminar for a high exit Reynolds number of 12.3×10^4 per centimeter (3.1×10^5 per in.) where transitional flow was observed previously at a lower Reynolds number of 10.10×10^4 per centimeter (2.56×10^5 per in.) at a lower wall temperature. The increased transition Reynolds number for the hot wall tests is believed to be a result of reduced roughness effects by increased boundary-layer thickness. Effects of two-dimensional-type steps in the nozzle settling chamber, disturbances from various changes in screen configurations, and disturbances from inlet air-supply piping and control valves over a range of Reynolds numbers had no effect on transition but only on boundary-layer thickness. Three-dimensional-type roughness generated in the nozzle subsonic approach section by producing random cross hatchings in a powder deposit of alumina oxide caused transition to occur at a lower exit Reynolds number of about 7.0×10^4 per centimeter (1.8×10^5 per in.). Polishing the nozzle wall has been found to delay transition significantly ($R_\infty \approx 1.312 \times 10^5$ per cm or 3.33 per in.) compared to that for the unpolished wall ($R_\infty = 10.10 \times 10^4$ per cm or 2.56×10^5 per in.). Recommendations for the development of a laminar-flow nozzle with high Reynolds numbers are given, based on the present results.

INTRODUCTION

Investigations of boundary-layer flow along nozzle walls are useful in order to define nozzle flow characteristics and for basic studies of high Reynolds number turbulent boundary layers. The boundary layer along the walls of most large supersonic nozzles is turbulent and thicker than the boundary layer on a model in the nozzle flow; consequently, the former can be probed more accurately than the model boundary layer. Thus, well-documented nozzle-wall boundary layers provide useful test data for comparison with turbulent-boundary-layer prediction methods.

Recent results show that aerodynamic noise radiated from the turbulent boundary layer along a rigid nozzle wall profoundly affects boundary-layer transition on a model (refs. 1 to 8). The noise levels in the free stream with laminar flow along the walls are reduced by at least an order of magnitude (see ref. 3 and fig. 22 of ref. 4). Hence, it can be expected that a laminar-flow nozzle with sufficiently high Reynolds numbers would provide a test environment that more closely simulates flight conditions where disturbance levels are presumably small (ref. 9). Concepts are currently being considered and developed to specify design criteria of a supersonic-hypersonic quiet tunnel at the Langley Research Center as reported by Beckwith (ref. 9). A quiet tunnel would be essential for transition-related studies and for the study of turbulent boundary layer and shear-layer development in the absence of noise radiation from the turbulent nozzle-wall boundary layer.

Unfortunately, the nozzle-wall boundary layers were turbulent for all boundary-layer transition investigations in supersonic wind tunnels now available. Only a few investigations have ever reported the existence of laminar flow on wind-tunnel side walls (downstream of the throat region) in high-speed flow (see, for example, refs. 10 and 11).

In the present investigation, boundary-layer profiles were measured along the walls of a Mach 5 nozzle for a wide range of Reynolds numbers and wall temperature in order to determine whether a laminar boundary layer on the side walls could be maintained for high Reynolds numbers. These profiles are compared with finite-difference calculations for laminar, transitional, and turbulent flow by the method of reference 12 to evaluate the state of the boundary layer. Factors affecting transition of the nozzle-wall boundary layer such as settling-chamber screens, wall temperature, and wall roughness are evaluated.

SYMBOLS

Measurements and calculations were made in the U.S. Customary Units. They are presented herein in the International System of Units (SI) with the equivalent values given parenthetically in the U.S. Customary Units.

D	nozzle-exit internal diameter
h	step height
L	model length (test rhombus, fig. 18)
M	Mach number
p	pressure
R	local Reynolds number per unit length, $\frac{\rho \mu}{u}$
R_{∞}	free-stream Reynolds number per unit length at nozzle exit
r	nozzle radius
T	temperature
u	velocity in streamwise direction

x	axial distance along nozzle
y	coordinate normal to center line of nozzle
γ	ratio of specific heats
δ	boundary-layer thickness based on pitot pressure
δ^*	displacement thickness
θ	momentum thickness
μ	viscosity
ρ	mean density
ϕ	Mach angle

Subscripts:

D	nozzle-exit diameter
e	boundary-layer edge value
L	length
p	total-temperature probe
t	total conditions
w	wall conditions
x	axial distance
∞	free stream
1	settling chamber
2	pitot pressure

APPARATUS AND TESTS

Facility

A schematic sketch of the Mach 5 facility, survey probes, and strut support is shown in figure 1(a). Figure 1(b) shows detailed sketches of the nozzle, settling chamber (with screens), and survey probes. Nozzle coordinates are given in table I. Tests were made with and without screens in the settling chamber. The settling-chamber parts are given in table II and the screen configurations tested in table III. Configuration 1 (table III) was used in all tests unless otherwise noted. The entire screen configuration was removed for tests without screens.

The maximum air-supply pressure and temperature to the nozzle test chamber is 3.45 MPa (500 psi) and 534 K (960° R), respectively. The contoured nozzle was designed for an exit Mach number of 5 and a stagnation pressure of 3.45 MPa (500 psi). Flow through the nozzle exhausts into a diffuser and vacuum system (18.29-m diameter; 60-ft diameter vacuum sphere). The nozzle is 50 centimeters (19.7 in.) in length from the throat (Radius = 1.008 cm or 0.397 in.) to the exit (Radius = 5.283 cm or 2.08 in.) and has wall static-pressure ports located at 1.27 centimeters (0.50 in.) and 2.54 centimeters (1.0 in.) upstream of the exit. The facility was operated for sustained periods of about 10 minutes for each survey across the boundary layer.

Instrumentation

A survey mechanism was used to position the probes both normal to and along the wall. The traversed position of the probes vertical to the nozzle wall was obtained by using a precalibrated potentiometer with an indicated accuracy of 0.0025 centimeter (0.001 in.). A low-voltage contact indicator positioned the probes at the wall surface. Axial location of the probe tip was set before each survey. The data were continuously monitored during each test and were recorded once the pressure and temperature readings reached a constant level for a selected position in the boundary layer.

Sketches of the total-pressure and total-temperature probes are presented in figure 1(b). The pitot pressure probe was a stainless-steel circular tube with an outside diameter of 0.0584 centimeter (0.023 in.) and inside diameter of 0.0381 centimeter (0.015 in.). The leading edge was beveled 10° internally. The total-temperature probe was constructed from a swaged thermocouple silver-soldered into and insulated from a stainless-steel tube of 0.19-centimeter (0.075-in.) outside diameter. Two vent holes (0.0635-cm or 0.025-in. diameter) were located in the side wall of the shield 0.36 centimeter (0.14 in.) from the probe tip. The 30-gage chromel-alumel wires were welded to form a junction which was located about 0.076 centimeter (0.03 in.) downstream of the probe entrance.

DATA REDUCTION

Pressure Data

The pressures were measured with strain-gage-type diaphragm transducers. Nozzle-wall static pressures were measured with transducers having a range of 0 to 6.895×10^3 Pa (0 to 1 psia). The pitot probe was connected to transducers having ranges of 0 to 6.895×10^3 Pa (0 to 1 psia), 0 to 34.48×10^3 Pa (0 to 5 psia), and 0 to 34.48×10^4 Pa (0 to 50 psia). This triple transducer range improved the accuracy of the pressure data since a range nearest to full-scale reading was always used. The accuracy of all transducer readings was 0.25 percent of full scale.

Total-Temperature Data

The total-temperature probe is the same as that used in reference 13, which was calibrated at Mach numbers of 3, 6, and 8.5 for a range of unit Reynolds numbers from 4.72×10^6 to 4.72×10^7 per centimeter (12×10^6 to 12×10^7 per in.) and found to have a recovery factor of nearly 1.0. Calibration points were also obtained with this probe in the present $M = 5$ nozzle and are shown in figure 2 for a range of total pressure. Data are shown with and without settling-chamber screens in place and indicate a recovery factor range of about 0.96 to 0.98 with total pressure in close agreement with previous results (ref. 13). A recovery factor of 1.0 was assumed and used for the present limited temperature data based on the results of figure 2. Actual values for the recovery factor (fig. 2) were found to affect the data by less than 1 percent.

TEST CONDITIONS

A summary of the test conditions for the experimental program is given in table IV. Pitot pressure surveys were obtained at several stations along the nozzle axis (table IV). Total-temperature surveys were obtained from different runs than the pitot surveys but for approximately the same test conditions and at one station only ($x = 48.1$ cm or 18.95 in.). All survey data have been normalized by the appropriate stagnation values, recorded simultaneously with the probe data, to account for any small changes in settling-chamber conditions during the surveys. A representative tabulation of the pitot pressures measured in the boundary layer normalized with their respective settling-chamber values is given in table V. Given in table VI are tabulated profiles of Mach number, velocity, and total temperature.

The free-stream conditions at the various survey stations are also given in table IV and were calculated by assuming isentropic expansion to the measured pitot pressures of an ideal gas with $\gamma = 1.4$. The ideal gas properties of air have been used in all data reduction.

COMPUTED BOUNDARY-LAYER PROFILES

Values of the calculated free-stream static pressures were obtained from the isentropic relation

$$\frac{p_e}{p_{t,1}} = \left(1 + \frac{\gamma - 1}{2} M_e^2 \right)^{-\gamma/\gamma-1} \quad (1)$$

where M_e was obtained from the isentropic relation for the ratio of measured free-stream pitot pressure to settling-chamber pressure given by

$$\frac{p_{t,2}}{p_{t,1}} = \left[\frac{(\gamma + 1)M_e^2}{(\gamma - 1)M_e^2 + 2} \right]^{\gamma/\gamma-1} \left[\frac{\gamma + 1}{2\gamma M_e^2 - (\gamma - 1)} \right]^{1/\gamma-1} \quad (2)$$

The local values of Mach number ($M > 1$) through the boundary layer were obtained from the Rayleigh pitot formula, assuming constant static pressure p_e through the boundary layer as given by

$$\frac{p_{t,2}}{p_e} = \left[\frac{(\gamma + 1)M^2}{2} \right]^{\gamma/\gamma-1} \left[\frac{\gamma + 1}{2\gamma M^2 - (\gamma - 1)} \right]^{1/\gamma-1} \quad (3)$$

The velocity profiles through the boundary layer were obtained by using the Mach number and total-temperature profiles. Assuming an ideal gas ($p = \rho RT$ where R is the gas constant) and constant ratio of specific heats, velocity profiles were then calculated from the expression

$$\frac{u}{u_e} = \frac{M}{M_e} \left(\frac{T}{T_e} \right)^{1/2} \quad (4)$$

where

$$T = T_t \left(1 + \frac{\gamma - 1}{2} M^2 \right)^{-1} \quad (5)$$

and $\gamma = \frac{7}{5}$. Total temperature measured throughout the inviscid flow was always found to be equal to the stagnation temperature regardless of total pressure to within about 5-percent

accuracy. When measured values of T_t in the boundary layer were not available, a quadratic temperature variation across the boundary layer was used to compute velocity profiles.

Displacement and momentum thicknesses were obtained by integrating the density and velocity profiles across the boundary layer according to the following equations (with negligible transverse curvature effects)

$$\delta^* = \int_0^\delta \left(1 - \frac{\rho u}{\rho_e u_e} \right) dy \quad (6)$$

and

$$\theta = \int_0^\delta \frac{\rho u}{\rho_e u_e} \left(1 - \frac{u}{u_e} \right) dy \quad (7)$$

where δ equals the value of y when $u/u_e = 0.995$. Values of θ and δ^* were found to be reduced by about 0.5 percent over most of the nozzle length when transverse curvature effects were included in equations (6) and (7). This effect increases somewhat for small values of nozzle radius.

RESULTS AND DISCUSSION

Nozzle Inviscid Flow

The inviscid flow in the nozzle was measured with pitot-pressure and total-temperature probes. The experimental Mach number distribution at the boundary-layer edge is shown in figure 3 and was determined by using the isentropic flow equation (eq. (2)) with pitot-pressure data for three values of stagnation pressure. Mach number increases from the sonic throat to a value of about 5 at the nozzle exit. By comparing open and filled symbols in figure 3, it is obvious that the free-stream Mach number was little affected by the screen configuration in the settling chamber. Predicted nozzle flow characteristics were obtained from reference 14 for the present nozzle coordinates (see table I for the nozzle coordinates) and, as seen in figure 3, the predicted Mach number distribution is in good agreement with experiment. A more complete analysis of the inviscid flow field is presented in the appendix along with further comparisons between experiment and predictions.

Nozzle Boundary-Layer Profiles

Pitot profiles.- Boundary-layer pitot profiles along the nozzle wall for three total pressures are presented in figure 4. A sketch of the nozzle contour indicating the coordinate system and profile locations is also included. Pitot pressure divided by tunnel stagnation pressure is plotted normal to the center line from the nozzle wall at axial locations from 27.15 centimeters (10.69 in.) to 48.11 centimeters (18.94 in.) from the nozzle throat.

At the most upstream stations ($x = 27.15$ cm and 36.0 cm, 10.69 in. and 14.19 in.), the pitot profiles for $p_{t,1} = 34.48 \times 10^4$ Pa (50 psia) are much different all the way across the boundary layer from the profiles for $p_{t,1} = 172 \times 10^4$ and 344.8×10^4 Pa (250 and 500 psia). At the three downstream stations, the pitot profiles at the lowest stagnation pressure are also different from the other profiles in the outer part of the boundary layer while all the profiles are more nearly similar in shape nearer the wall. The difference in profile shapes at the upstream locations is attributed to transition from the laminar boundary layer present at the lower pressure to turbulent boundary-layer flow for the higher pressures; nozzle-wall boundary-layer transition will be discussed further in a later section.

Temperature profiles.- Boundary-layer temperature profiles are often presented in Crocco variables, $(T_t - T_w)/(T_{t,1} - T_w)$ against u/u_∞ , where the Crocco solution for Prandtl number one and zero pressure gradient is a linear function. Profiles measured in nozzle-wall boundary layers have not, in general, followed the Crocco linear relationship but rather an approximate quadratic variation of $(T_t - T_w)/(T_{t,1} - T_w)$ with u/u_∞ (see refs. 15 and 16, for example). Temperature profiles measured near the exit of the present nozzle are presented in Crocco variables in figure 5 and table VI both with and without settling-chamber screens. The temperature function follows a nearly quadratic relation with velocity ratio at the lower pressure $R_\infty = 0.68 \times 10^5$ per cm (1.74×10^5 per in.) where $\frac{T_w}{T_{t,1}} = 0.8$ to 0.83 ; however, for the higher total pressures and higher wall-to-total temperature ratios there is a significant deviation from the quadratic variation at a value of $\frac{u}{u_e} \approx 0.8$ with a temperature overshoot occurring near the edge of the boundary layer. This overshoot is not uncommon for adiabatic boundary layers both on flat plates and nozzle walls (ref. 16). The settling-chamber screen configuration does not appear to influence the temperature profiles significantly except possibly at $R_\infty = 8.7 \times 10^5$ per centimeter (3.41×10^5 per in.).

Two finite-difference predictions for adiabatic wall conditions $\left(\frac{T_w}{T_{t,1}} = 0.93\right)$ at the lower total pressures are shown in figure 5 for comparison with data. The temperature overshoot is apparent in the predicted profile but occurs through a greater extent of the boundary layer than experiment; the result is poor agreement between prediction and data. Since the wall-temperature distribution down the nozzle contour was not measured, however, adiabatic wall temperatures were assumed for the entire nozzle in the analytical solution $\left(\frac{T_w}{T_{t,1}} = 0.93 \text{ at the nozzle exit}\right)$. Hence, from recent results in a Mach 6 nozzle (ref. 17) for $0.75 \leq \frac{T_w}{T_{t,1}} \leq 1.15$ and in a supersonic half-nozzle (ref. 18) showing that temperature profiles are sensitive to upstream wall-temperature history (settling chamber and throat), the poor agreement between theory and data may be expected. Also, Beckwith (ref. 19) has shown that the Crocco solution is applicable to turbulent boundary-layer flow with constant wall temperature and pressure but depends on the magnitude of the pressure fluctuations.

The temperature-probe design did not allow probing upstream of the nozzle exit ($x = 48.11 \text{ cm, } 18.94 \text{ in.}$); therefore, a quadratic temperature profile (as shown in fig. 5) was used to compute velocity profiles from pitot-pressure data at upstream stations. This assumption, as seen in figure 6, has little effect on calculated velocity profiles at the exit station. Here, both the measured (temperature overshoot) and quadratic profiles were used to calculate velocity from pitot profiles and to calculate the displacement thickness, δ^* (eq. (6)), and momentum thickness, θ (eq. (7)). Whereas displacement thickness is almost independent of the temperature profile, the momentum thickness is significantly larger with the quadratic temperature profile.

Analysis of profiles.- In order to verify that laminar flow did occur along the nozzle contour, boundary-layer profiles (with screens) are compared with laminar, transitional, and turbulent finite-difference predictions (ref. 12) in figures 7 and 8 at $x = 27.15$ and 48.1 centimeters (10.69 and 18.94 in.), respectively. An implicit finite-difference procedure was utilized to predict the boundary-layer characteristics of the nozzle. This finite-difference method (ref. 12) solves the boundary-layer equations for laminar, transitional, and turbulent flows. Turbulent flow is treated by using a two-layer eddy viscosity model and, for the present solutions, a constant turbulent Prandtl number of 0.9 . Transition location for the transition predictions in figure 7(a) was arbitrarily chosen at about 13.97 centimeters (5.5 in.) downstream of the throat. Data are presented first as pitot pressure against y for a direct comparison of data and theory (see fig. 7(a)) and then as pitot pressure, Mach number, and velocity ratios against y/δ^* , a similarity form, which more clearly shows the state of the boundary layer (figs. 7(b), 7(c), and 7(d), respectively).

At the $x = 27.15$ centimeters (10.69 in.) station (fig. 7(a)) the predicted pitot profile for laminar flow agrees with data at the lowest Reynolds number $R_\infty = 6.8 \times 10^4$ per centimeter ($R_\infty = 1.74 \times 10^5$ per in.), and the predicted profile for turbulent flow agrees with the data at the highest Reynolds number $R_\infty = 6.8 \times 10^5$ per centimeter ($R_\infty = 1.73 \times 10^6$ per in.). In figures 7(b), 7(c), and 7(d) the lower Reynolds number data are shown more clearly to be laminar since the shape of the profile is much different from the shapes at the higher Reynolds numbers. The profiles for $R = 0.827 \times 10^5$ per centimeter (2.1×10^5 per in.) agree well with the laminar finite-difference prediction, and the highest local Reynolds number profiles also agree with the turbulent finite-difference prediction for $R = 0.827 \times 10^6$ per centimeter (2.1×10^6 per in.).

Near the exit of the nozzle ($x = 48.1$ centimeters; 18.94 in.) the lowest Reynolds number profile shown in figure 8(a) no longer agrees with the laminar, transitional, or turbulent prediction and has assumed a shape more like the higher Reynolds number profiles but with a smaller thickness. In figures 8(b), 8(c), and 8(d) the profiles for all three Reynolds numbers appear to correlate in similarity variables, except near the wall, and agree with the turbulent prediction. In physical coordinates (fig. 8(a)), the lower Reynolds number profile does not agree with either the calculated laminar or turbulent prediction, indicating that transition or some other flow change occurred along the nozzle contour for $27.18 \text{ centimeters} \leq x \leq 48.1 \text{ centimeters}$ ($10.69 \text{ in.} \leq x \leq 18.94 \text{ in.}$). The highest Reynolds number profile (fig. 8(a)) agrees with the turbulent prediction for the same Reynolds number except near the edge of the boundary layer where the theoretical δ is below experiment; this disagreement is probably related to disturbance waves in the inviscid flow impinging on the boundary layer, as discussed in the appendix.

Boundary-layer thickness parameters.- From profiles presented in the previous section and additional profiles not presented but given in table V, boundary-layer thickness parameters were obtained for each of the three Reynolds numbers and are presented in figures 9, 10, and 11. The parameters δ , δ^* , and θ are plotted against axial distance, x , from the nozzle throat along with finite-difference predictions for laminar, transitional, or turbulent flow. Boundary-layer thickness, δ , was defined as the location where $\frac{u}{u_e} = 0.995$, and experimental values of displacement and momentum thicknesses were found by numerical integration, assuming a quadratic temperature profile. Values of δ obtained from pitot profiles are expected to be larger than values of δ from velocity profiles (for Prandtl number < 1).

At the lowest Reynolds number (fig. 9(a)) the boundary-layer thickness is predicted by laminar theory for about half the nozzle length and then increases toward the transitional prediction. The displacement thickness (fig. 9(b)) agrees with the laminar prediction along the entire nozzle length; this agreement is fortuitous near the nozzle exit since the

profiles at $x = 48.1$ centimeters (18.94 in.) are not laminar (see fig. 8). The momentum thickness (fig. 9(c)) also appears to be predicted by the laminar theory for about the first half of the nozzle and then increases above the laminar value further downstream. Thus, this analysis of the boundary-layer thickness parameters indicates that for $R_\infty = 6.8 \times 10^4$ per centimeter (1.74×10^5 per in.) the nozzle-wall boundary layer is laminar for at least 25.4 to 30.5 centimeters (10 to 12 in.) downstream of the nozzle throat. For the higher Reynolds number cases $R_\infty > 3.41 \times 10^5$ per centimeter (8.7×10^5 per in.) (figs. 10 and 11), the boundary-layer thickness parameters generally agree with the corresponding turbulent predictions except for $x > 35.6$ centimeters (14 in.). Increases in thickness parameters near the nozzle exit over the entire range of R_∞ may be related to inviscid disturbances in the nozzle flow field (see the appendix) or possibly Taylor-Görtler vortices which can also be present in turbulent flow. It should be pointed out that recent results from reference 20 indicate that, if relaminarization occurs along the nozzle wall (downstream of throat), classical mixing-length concepts used in numerical prediction methods must be modified to account for residual transition effects (low Reynolds number effects). For the present nozzle, transition appears to move from downstream near the nozzle exit to upstream of the throat region for only a small increase in Reynolds number (as discussed in a later section); therefore, relaminarization does not occur here and these low Reynolds number effects were not included in the present numerical calculations.

Boundary-Layer Profiles at Intermediate Pressure

Additional pitot-pressure profiles were obtained in the lower Reynolds number range to determine the maximum nozzle transition Reynolds number and are shown in figure 12 for $\frac{T_w}{T_{t,1}} \approx 0.9$. These nozzle-wall boundary-layer profiles with screens (table V) are compared with laminar, transitional, and turbulent predictions (ref. 12) in figure 12(a) through figure 12(f) at $x = 22.1, 27.2, 31.0, 37.34, 42.9$, and 48.1 centimeters ($x = 8.7, 10.69, 12.2, 14.69, 16.9$, and 18.94 in.), respectively. These profiles clearly indicate that the wall boundary layer remains laminar up to a maximum $R_\infty = 10.0 \times 10^4$ per centimeter (2.56×10^5 per in.) for $22.1 \leq x \leq 37.34$ centimeters ($8.7 \leq x \leq 14.7$ in.) before going transitional at the next highest test Reynolds number; the nozzle-wall boundary layer is therefore laminar for about 38.2 centimeters (15 in.) downstream of the nozzle throat for $R_\infty \leq 10.0 \times 10^4$ per centimeter (2.56×10^5 per in.). Recent results obtained by Anders, Stainback, Keefe, and Beckwith (ref. 21) in the same nozzle using a hot-wire and fluctuating pitot probe showed that the wall boundary layer remains laminar up to $R_\infty = 1.31 \times 10^5$ per centimeter (3.34×10^5 per in.) when the wall was polished. These results confirm the earlier results of reference 11. The next increase in Reynolds number to $R_\infty = 11.45 \times 10^4$ per centimeter (2.91×10^5 per in.) causes transition to move abruptly upstream of all survey stations. Similar behavior of the movement of transition

location was observed in part I of reference 11 from measured disturbance levels which originated at acoustical origins near several of the present boundary-layer profile stations. A gradual decrease in boundary-layer thickness is observed with increasing Reynolds number (fig. 12) before transition occurs. The disagreement between data for $R_\infty = 10.1 \times 10^4$ per centimeter (2.56×10^5 per in.) and the laminar profile predictions shown in figures 12(e) and 12(f) near the exit is attributed to the presence of Taylor-Görtler vortices (refs. 9 and 10). These vortices develop in the concave region of the nozzle and would tend to change the laminar boundary-layer profile shapes; the vortices might be expected to increase entrainment of the flow and therefore increase δ .

Additional Factors Affecting Transition

Many factors, such as wall roughness, wall curvature, flow disturbances in upstream piping and valves, and disturbances in nozzle settling chambers due to locally separated regions and high-density screens, may be expected to influence transition on the nozzle side walls. A critical evaluation of such factors has been discussed earlier by Morkovin (ref. 22). Some of the more obvious factors that might affect transition were investigated herein; the shape of pitot profiles was observed for a range of Reynolds numbers at the $x = 27.8$ centimeter (10.69 in.) station for various system changes.

Wall temperature.- Additional tests were made to determine the effects of changes in wall temperature on the location of transition along the nozzle wall. The nozzle wall was heated by strip-type heaters wrapped around the exterior surface of the nozzle. A layer of insulation was then applied to the whole strip heater assembly. Wall temperatures up to about 478 K (860° R) could be obtained. The interior wall temperature was measured at several locations near the exit.

For a nozzle-wall to total-temperature ratio of about 1.4 (fig. 13), boundary-layer pitot profiles at the $x = 27.18$ centimeter (10.69 in.) station indicated that the flow was laminar up to $R_\infty = 12.3 \times 10^4$ per centimeter (3.13×10^5 per in.); at the same station for a wall-to-total temperature ratio of about 0.85, laminar flow was observed only up to a Reynolds number of 10.0×10^6 per centimeter (2.56×10^5 per in.). The calculations (ref. 12) in figure 13 for $\frac{T_w}{T_{t,1}} = 0.93$ are shown for comparison only. Heating the wall increased the transition Reynolds number approximately 20 percent. As expected, the boundary-layer thickness is greater for these heated-wall tests when compared to the cold-wall data at the same longitudinal station and value of R_∞ . Heating the nozzle wall may reduce roughness effects since the boundary-layer thickness increases; however, increases in T_w beyond some limit will probably destabilize the boundary layer. Free-stream disturbance measurements shown in part I of reference 11 also indicate that heating the nozzle wall delayed transition. The effects of heating the nozzle wall on maintaining a laminar wall boundary layer need further investigation.

Two-dimensional steps.- Effects of two-dimensional steps on transition were determined by a systematic misalignment of the nozzle settling-chamber flanges (fig. 1(b)) at a distance of 11.4 centimeters (4.5 in.) upstream of the throat. The flanges were misaligned so that a forward facing step to the flow was located symmetrically at the assembly top side and a rearward step was located at the bottom (see sketch in fig. 14(a)). Step heights were varied from 0 to 0.3124 centimeter (0 to 0.123 in.) compared with the calculated nominal subsonic boundary-layer height (by the method of ref. 12) of 0.254 centimeter (0.10 in.). A sample of the pitot surveys (for the forward facing step) for $h = 0.3124$ centimeter (0.123 in.) at two longitudinal stations in the nozzle is shown in figures 14(a) and 14(b). An analysis of the boundary-layer thickness variation with Reynolds number (fig. 14(c)) indicated that, for the $x = 27.2$ centimeter (10.7 in.) survey station and range of steps tested, no significant change in transition Reynolds number $R_\infty = 10.0 \times 10^4$ per centimeter (2.56×10^5 per in.) was observed compared to previous data shown in figure 12 with no step. An increase in the laminar boundary-layer thickness of about 50 percent maximum for $R_\infty < 3.5 \times 10^6$ and about 41 percent for $R_\infty > 3.5 \times 10^6$ (turbulent boundary layer) was observed with step-height increase for the Reynolds number range tested, as shown in figure 14(c).

Screen configuration.- High-pressure drop screens tend to produce jets or wakes downstream of the screen causing turbulence. Stainback and Wagner (ref. 23) and Stainback and Anders (pt. I of ref. 11) have reported the effects of interchanging various screen configurations in the present nozzle settling chamber on free-stream disturbance levels in the nozzle. Screen configurations 1, 2, 3, and 4 of table III were used for the present study to evaluate their effects on transition as indicated by the nozzle-wall boundary layer at the station $x = 27.2$ centimeters (10.7 in.). Screen configurations 1 and 2 are low Δp screens and 3 and 4 are high Δp screens. Pitot profiles for screen configurations 2 and 4 are shown in figure 15 for a range of test Reynolds numbers. The mean pitot pressure profiles indicated no change in transition Reynolds number (10.0×10^4 per centimeter, 2.56×10^5 per in.) for the various screen configurations. Free-stream disturbance measurements reported in reference 23 indicate that boundary-layer transition is affected by the settling-chamber screen configuration, whereas the measured free-stream root-mean-square disturbance levels reported in part I of reference 11 show little effect of screens; therefore, it is possible that the screens are changing the spectra of the free-stream disturbances but not the nozzle-wall boundary layer. In reference 11, the beginning of transition occurred at $6.42 \times 10^4 < R_\infty$ per centimeter $< 6.93 \times 10^4$ ($1.63 \times 10^5 < R_\infty$ per in. $< 1.76 \times 10^5$) for all screens.

Upstream piping and flow control valve.- Some portion of the free-stream disturbances found in the supersonic test section of a nozzle may be traceable to upstream piping and control valves (refs. 8 and 11). If the magnitude of these disturbances is sufficiently large, then it is possible for such disturbances to affect boundary-layer stability and transition. The incoming air to the present nozzle may be supplied through two different routes of different pipe diameter and control valves (see sketch in fig. 16). Pitot profiles were obtained at the same longitudinal station as before, $x = 27.2$ centimeters (10.69 in.), to evaluate possible changes in transition Reynolds number due to change in upstream valving and pipe size. Normal operation is to control the flow through the 10 centimeter (4 in.) valve. This method of control was used for all of the previous tests. Tests were made by directing the air supply through one pipe-valve system while the other passage remained isolated. Also, tests were made by allowing a constant mass flow to pass through one pipe-valve system at 48.4 MPa (7 psia) while at the same time the nozzle air supply through the second pipe-valve system was controlled so that the desired settling-chamber pressure could be achieved. The mean pitot-pressure profiles (fig. 16) indicated no change in transition Reynolds number from that found in the other tests with normal flow control (see fig. 12). Furthermore, essentially no change in boundary-layer thickness was observed. The valve size in the air supply line significantly affected the vorticity fluctuations and fluctuating pitot-pressure levels in the settling chamber as well as the pressure fluctuation in the nozzle free stream (ref. 11) at the higher test Reynolds numbers but apparently did not affect transition downstream in the nozzle as indicated by mean profile measurements. Reference 22 suggests that upstream disturbances in supersonic wind tunnels may be attenuated downstream and not strongly influence the nozzle-wall boundary layer.

Roughness.- There are various forms of roughness that might exist on nozzle walls or approach sections with sufficient height relative to the local boundary layer or displacement thickness to induce turbulence in the flow. Aside from purposely installing roughness elements locally to produce turbulence, some of the disturbances propagating into the supersonic test section may be caused by machining irregularities along the nozzle-wall contour (waviness) (ref. 9), wall-probe interference, and/or contaminants in the flow that become irregularly deposited roughness on the nozzle-wall surface. Of course, the tripping effectiveness of these possible disturbances is dependent on their location and whether the local flow is subsonic or supersonic. Inspection of the present nozzle clearly revealed a very fine, nonuniform, powder-like deposit of alumina oxide on the wall surface of the subsonic approach section. It was determined that the alumina oxide deposit originated in the air dryer system and was small enough to pass through the screen configurations. Tests were made without disturbing the deposit and with the deposit removed from the approach section; no change in transition Reynolds number was found for these tests.

When the surface deposit in the approach region was randomly scribed (prior to removal of deposit) with a pencil point, resulting in the roughness pattern shown in the insert of figure 17, a change in pitot profile shape occurred at $x = 27.2$ centimeters (10.69 in.) for $R_\infty = 7.1 \times 10^4$ per centimeter (1.81×10^5 per in.). Previous tests showed no change from the profile shape up to $R_\infty = 1.01 \times 10^5$ per centimeter (2.56×10^5 per in.) at the same station. The profile shapes change with increasing Reynolds number (fig. 17) and approach agreement with turbulent theory at the highest R_∞ for turbulent flow. The roughness pattern is confined to a circumferential region of about 7.62 centimeters (3 in.) upstream of the throat minimum. Microscopic examination of the random three-dimensional "clumps" of alumina oxide particles formed by scraping through the deposit indicated the average deposit thickness to be of the order of 0.00254 centimeter (0.001 in.). Calculated values of the laminar boundary-layer thickness and displacement thicknesses (by the method of ref. 12) at a distance of 2.54 centimeters (1 in.) upstream of the throat are 0.0889 centimeter (0.035 in.) and 0.00711 centimeter (0.0028 in.), respectively. The corresponding ratios of three-dimensional roughness height to boundary-layer thicknesses are about 0.03 and 0.333, respectively.

It is therefore apparent that very small three-dimensional roughness located in the subsonic flow region of a supersonic nozzle can promote nozzle-wall transition. Furthermore, the often observed gradual movement of transition with Reynolds number on a nozzle wall of a tunnel may possibly be partly due to the effects of roughness. Transition has been shown herein (fig. 12) to occur abruptly throughout the entire nozzle over a small Reynolds number range with nominal roughness rather than to change gradually from laminar to turbulent flow as usually observed. Results from the present experiments indicate that three-dimensional type roughness located in the subsonic approach near the throat influences transition while two-dimensional step-type roughness located at the beginning of the subsonic approach (caused by nozzle settling-chamber flange misalignment) does not. Preliminary results presented in reference 11 indicate that polishing the nozzle wall delays transition significantly.

Comparison With Other Results

One of the main purposes of a quiet tunnel is to simulate as closely as possible the acoustic environment of flight (ref. 9). As pointed out in reference 9, the nozzle size is an important factor in attempts to simulate flight conditions for transition in a wind tunnel. Small nozzles may allow higher unit Reynolds numbers at the same Mach number than larger nozzles, but the maximum model length determines the maximum test Reynolds number. The present experimental results have therefore been compared to similar results from other nozzles and to flight-transition correlations to evaluate Reynolds number requirements for wind-tunnel flight simulation with quiet test conditions.

The pitot-pressure profiles indicate that laminar boundary-layer flow on the Mach 5 nozzle wall was achieved for a higher value of $R_{\infty,D} = 1.316 \times 10^6$ than previously reported. A comparison of values of $R_{\infty,D}$ for laminar or transitional flow in several nozzles $\frac{T_w}{T_{t,1}} < 1$ is listed in the following table, and a review and analysis of these nozzles are given in reference 10:

Tunnel (ref. 10)	M_∞	R_∞		Nozzle exit diameter, D		$R_{\infty,D}$	Comments
		per m	per ft	m	ft		
20-inch Jet Propulsion Lab.	4.6	1.9×10^6	0.6×10^6	0.509	1.67	1.002×10^6	Laminar to nozzle exit, $x \approx 355$ cm (140 in.)
Contoured nozzle Univ. of Michigan	8.0	1.5	.5	.202	.66	.080	Laminar to nozzle exit, $x \approx 86$ cm (34 in.)
22-in. helium Langley Res. Center	16.2	.05	.02	.559	1.835	.0367	Transitional at $x \approx 353$ cm (139 in.)
4-in. (present) Langley Res. Center	5.0	11.48	3.76	.107	.35	1.316	Transitional at $x \approx 48$ cm (19 in.); $\frac{T_w}{T_{t,1}} \approx 1.4$

Figure 18 shows a comparison of the maximum unit Reynolds number obtained while maintaining a laminar side-wall boundary layer for several different nozzles. The unit Reynolds number is plotted against a Reynolds number based on a length, L , which approximates the maximum possible length of a model that can be tested in each tunnel. This maximum model length, L (see sketch in fig. 18), was computed from the enclosed inviscid test rhombus (dashed lines in sketch) formed by the intersection of Mach lines from the exit diameter with the tunnel axis and corresponds to a model at zero angle of attack. The expression for model length is then

$$L_{\max} = \frac{2r}{\tan \phi}$$

where $r = \frac{D}{2}$.

The solid flagged symbols in figure 18 represent hot-wire and fluctuating pitot results from part I of reference 11 for various factors affecting transition. The solid flagged symbol for $R_{\infty,L} = 7.25 \times 10^6$ and $R_{\infty} = 1.6 \times 10^7$ per meter (4.6×10^6 per ft) was recently obtained by Anders, Stainback, Keefe, and Beckwith (ref. 21) with the nozzle polished. The faired lines are based on correlations (ref. 24) of flight data for local transition Reynolds number and local "mean" unit Reynolds numbers on sharp cones at $M_e = 4$ and 8. Values of L_{max} for the flight data are based on distance to transition. The present results show that a laminar nozzle-wall boundary layer was maintained at $M = 5$ for higher Reynolds numbers than previously reported. The maximum Reynolds numbers are based on an optimistic length and represent the beginning of transition. Higher maximum Reynolds numbers are therefore required before a fully developed turbulent boundary layer can be obtained on models. Possible studies of the beginning of transition on test models in the present $M = 5$ conventional nozzle can be made, however, under quiet conditions that approach the lower range of flight simulation.

Recommendations for the Development of a Laminar Flow Nozzle

The obvious need for a "quiet" tunnel, having laminar rather than turbulent boundary layers on the nozzle side walls and high unit Reynolds number operation capability, has been suggested by Beckwith and Bertram (ref. 24). A quiet tunnel would be essential for transition-related studies and for the study of turbulent boundary layers or free shear-layer development in the absence of noise radiation from the turbulent nozzle-wall boundary layer. Concepts are currently being considered and developed to specify design criteria of a supersonic/hypersonic quiet tunnel at the Langley Research Center as reported by Beckwith in reference 9. Experimental results obtained at $M_{\infty} = 4.6$ in the Jet Propulsion Laboratory 20-inch tunnel (ref. 1) and at $M_{\infty} = 5$ in a conventional nozzle (refs. 10 and 11) having a 10.67-centimeter (4.2-in.) exit diameter have shown that free-stream disturbance levels are reduced by an order of magnitude when the side-wall boundary layer is laminar. Thus, one of the principal design requirements for a quiet tunnel would be to maintain a laminar boundary layer on the nozzle side walls and test section for sufficiently high Reynolds numbers. This requirement allows the "natural" transition process to be completed in a model boundary layer or shear layer. Consequently, basic information regarding the transition process on a supersonic nozzle wall and factors affecting transition is required for the design and development of a "quiet" tunnel.

Based on the several factors investigated herein, roughness appears to be the dominant factor affecting transition on the nozzle wall. Results shown in figure 18 (flagged symbols from ref. 11) show that polishing the nozzle throat region increased the transition Reynolds number by about 30 percent greater than that for the unpolished nozzle at the same wall temperature. Results from the present study and from reference 11 show that a nozzle should be highly polished (mirror finish) to achieve laminar flow along the nozzle

walls and thus the maximum "quiet" test Reynolds number. The turbulent boundary layer approaching the sonic throat may be removed through a bleed system as reported in references 9 and 11. Once a quiet tunnel is developed, then pressure disturbances, entropy fluctuations, and vorticity generated upstream of the sonic throat may be greatly reduced by the proper selection and design of settling-chamber screens and mufflers, length-to-diameter ratio, inlet valves and piping, and elimination of steps along the settling chamber and nozzle contour.

The present results and those of references 9 and 11 indicate that, with sufficient care given to the identifiable factors affecting transition, a laminar-flow nozzle-wall boundary layer can be maintained at Mach 5 to higher Reynolds numbers than previously reported for conventional nozzles. When transition occurs along the nozzle wall at higher operating Reynolds numbers, however, test models can be effectively shielded from free-stream disturbances, as reported in reference 25.

CONCLUDING REMARKS

Measurements of wall boundary-layer profiles and thicknesses in a Mach 5 nozzle for a range of wall temperatures have been made. During the first series of tests the wall temperature was maintained in the range of $0.8 < \frac{T_w}{T_t} < 0.9$. The nozzle-wall boundary layer was found to be laminar downstream of the throat to within about 10 centimeters (4 in.) of the exit for the lower test Reynolds number of 10.1×10^5 per centimeter (2.56×10^5 per in.). The boundary layer was turbulent throughout the nozzle for $R_\infty = 1.45 \times 10^5$ per centimeter (2.91×10^5 per in.). In general, the implicit finite-difference theoretical method gave acceptable predictions of the experimental pitot pressure, Mach number, and velocity profiles and was used to confirm the presence of laminar or turbulent flow on the nozzle wall. The nozzle-wall boundary layer appeared to change abruptly from laminar to transitional throughout the nozzle as Reynolds number was increased. The disagreement between the measured and theoretical profiles near the exit may be attributed to free-stream disturbances and/or the presence of Taylor-Görtler vortices that develop in the concave region of the nozzle.

The total-temperature profiles at the nozzle exit followed a nearly quadratic variation with velocity at the lowest test Reynolds number and wall-to-total temperature ratio of less than 0.85. For higher test Reynolds numbers and for wall-to-total temperature ratios greater than 0.85, however, there is a temperature "overshoot" that occurs near the edge of the boundary layer.

When the nozzle wall was heated to a wall-to-total temperature ratio of approximately 1.4, the boundary layer over most of the nozzle was laminar for a high Reynolds

number of about 12.3×10^5 per centimeter (3.1×10^5 per in.) compared to 1.01×10^5 per centimeter (2.56×10^5 per in.) at the lower wall temperatures. Effects of two-dimensional-type steps in the nozzle settling chamber, disturbances from various changes in settling-chamber screen configurations, and disturbances from inlet-air-supply piping and control valves over the range of Reynolds numbers caused no apparent change in transition onset; however, changes in boundary-layer thickness were observed. Three-dimensional-type roughness generated in the nozzle subsonic approach section by randomly crosshatching a powder deposit of alumina oxide caused transition to occur at a lower exit Reynolds number of 0.7×10^5 per centimeter (1.8×10^5 per in.).

The measured mean boundary-layer profiles indicate that, with sufficient care given to the identified factors affecting transition, a laminar nozzle-wall boundary layer can be maintained at Mach 5 up to higher Reynolds numbers than previously reported. Furthermore, possible transition studies on test models in the same conventional nozzle can be made under relatively quiet conditions (laminar nozzle-wall boundary layers) that approach flight conditions.

Langley Research Center
National Aeronautics and Space Administration
Hampton, Va. 23665
August 1, 1975

APPENDIX

MACH 5 NOZZLE FLOW-FIELD CHARACTERISTICS

William D. Harvey and Aubrey M. Cary, Jr.
Langley Research Center

The normalized temperature parameter at a single station near the nozzle exit has been shown herein to follow a quadratic relation with velocity (fig. 5) at the lower Reynolds number and $\frac{T_w}{T_t} = 0.8$ to 0.83, but this parameter overshoots the general Crocco linear relationship for the higher Reynolds number and temperature ratio. Reference 16 has shown that nozzle-wall turbulent boundary layers may be different from flat-plate boundary layers at similar local conditions. These differences are attributed to the effects of upstream temperature and pressure gradients along and normal to the wall that would not generally exist for uniform flow over flat plates. Also, if upstream disturbances that may have resulted from an overexpansion at the throat are present, then these individual disturbances would have some influence on the boundary-layer profiles (ref. 15). In particular, the profile data across the inviscid flow core would be affected by waves crossing the nozzle center line upstream of the survey station. Furthermore, noise generated in supersonic nozzle flows originates in regions where the flow becomes subsonic along center-line shock reflections or wave systems (ref. 26).

In order to determine if the present Mach 5 nozzle has such a wave system or disturbances in the inviscid flow field, pitot-pressure measurements were made across a portion of the nozzle at several stations; these results are shown in figure 19. The wavy distributions in the inviscid flow region near the nozzle center line clearly indicate that significant disturbances are present. Also, included at the top of figure 19 is the resulting Mach number distribution along the center line and nozzle wall calculated by a method of characteristics as applied to nozzle flows in reference 14. The original specified nozzle coordinates (table I) were used along with a starting line at the sonic throat to calculate the flow field. Experimental Mach number values obtained from the pitot surveys at the center line (fig. 19) are compared to the theory for five stations. With the exception of station $x = 38.842$ centimeters (15.7 in.) the experimental Mach number values and theory agree very well and indicate that disturbances are present on the inviscid-flow center line. Calculations from reference 14 give indications of weak shocks present in the flow field supporting the present results. These disturbances apparently are caused primarily by poor nozzle design in that a slight overexpansion may have occurred near the inflection point.

APPENDIX

The upstream origins of possible disturbances were crudely estimated by extending a straight dashed line on the nozzle scale drawing representing the Mach wave angle for Mach 5. Then, by extrapolating pitot-pressure peak values back to their corresponding longitudinal measuring stations at $x = 32.22$ centimeters (12.7 in.) and $x = 39.84$ centimeters (15.7 in.), Mach lines drawn parallel to the Mach 5 wave angles were found to connect the extrapolated Y-axis intersections. The approximate Mach lines from either side of the center line were found to cross on the nozzle axis at about $x = 37.5$ centimeters (14.7 in.) (fig. 19). Considering the region just downstream of station $x = 32.22$ centimeters (12.7 in.) bounded by the Mach lines, the Mach number obtained from pitot-pressure profiles is high and agrees with the theory. By traversing Mach lines in the lateral direction it may be noted that the increase in pitot-pressure level also indicates a compression wave. Traversing downstream to station $x = 39.84$ centimeters (15.7 in.) shows that the Mach number is lower in the faired Mach line inner region, further indicating that a possible recompression has occurred. It is thus concluded that disturbances are present in the inviscid flow field of this nozzle.

REFERENCES

1. Laufer, John: Aerodynamic Noise in Supersonic Wind Tunnels. J. Aerosp. Sci., vol. 28, no. 9, Sept. 1961, pp. 685-692.
2. Wagner, R. D., Jr.; Maddalon, D. V.; and Weinstein, L. M.: Influence of Measured Freestream Disturbances on Hypersonic Boundary-Layer Transition. AIAA J., vol. 8, no. 9, Sept. 1970, pp. 1664-1670.
3. Stainback, P. C.; Fischer, M. C.; and Wagner, R. D.: Effects of Wind-Tunnel Disturbances on Hypersonic Boundary-Layer Transition. Parts I and II. AIAA Paper No. 72-181, Jan. 1972.
4. Morkovin, Mark V.: Critical Evaluation of Transition From Laminar to Turbulent Shear Layers With Emphasis on Hypersonically Traveling Bodies. AFFDL-TR-68-149, U.S. Air Force, Mar. 1969. (Available from DDC as AD 686 178.)
5. Mack, Leslie M.: On the Application of Linear Stability Theory to the Problem of Supersonic Boundary-Layer Transition. AIAA Paper No. 74-134, Jan.-Feb. 1974.
6. Kendall, J. M.: Wind Tunnel Experiments Relating to Supersonic and Hypersonic Boundary Layer Transition. AIAA Paper No. 74-133, Jan.-Feb. 1974.
7. Pate, S. R.; and Schueler, C. J.: Radiated Aerodynamic Noise Effects On Boundary-Layer Transition in Supersonic and Hypersonic Wind Tunnels. AIAA J., vol. 7, no. 3, Mar. 1969, pp. 450-457.
8. Stainback, P. Calvin; Wagner, Richard D.; Owen, F. Kevin; and Horstman, Clifford C.: Experimental Studies of Hypersonic Boundary-Layer Transition and Effects of Wind-Tunnel Disturbances. NASA TN D-7453, 1974.
9. Beckwith, I. E.: Development of a High Reynolds Number Quiet Tunnel for Transition Research. AIAA Paper No. 74-135, Jan.-Feb. 1974.
10. Beckwith, Ivan E.; Harvey, William D.; Harris, Julius E.; and Holley, Barbara B.: Control of Supersonic Wind-Tunnel Noise by Laminarization of Nozzle-Wall Boundary Layers. NASA TM X-2879, 1973.
11. Stainback, P. C.; Anders, J. B.; Harvey, W. D.; Cary, A. M.; and Harris, J. E.: An Investigation of Boundary-Layer Transition on the Wall of a Mach 5 Nozzle. AIAA Paper No. 74-136, Jan.-Feb. 1974.
12. Harris, Julius E.: Numerical Solution of the Equations for Compressible Laminar, Transitional, and Turbulent Boundary Layers and Comparisons With Experimental Data. NASA TR R-368, 1971.

13. Stone, David R.; and Cary, Aubrey M., Jr.: Discrete Sonic Jets Used as Boundary-Layer Trips at Mach Numbers of 6 and 8.5. NASA TN D-6802, 1972.
14. Prozan, R. J.: Solution of Non-Isoenergetic Supersonic Flows by Method of Characteristics. LMSC-HREC D162220-III-A (Contract NAS 7-761), Lockheed Missiles & Space Co., July 1971. (Available as NASA CR-132274.)
15. Beckwith, Ivan E.; Harvey, William D.; and Clark, Frank L. (With appendix A by Ivan E. Beckwith, William D. Harvey, and Christine M. Darden and appendix B by William D. Harvey, Lemuel E. Forrest, and Frank L. Clark): Comparisons of Turbulent-Boundary-Layer Measurements at Mach Number 19.5 With Theory and an Assessment of Probe Errors. NASA TN D-6192, 1971.
16. Bushnell, Dennis M.; Johnson, Charles B.; Harvey, William D.; and Feller, William V.: Comparison of Prediction Methods and Studies of Relaxation in Hypersonic Turbulent Nozzle-Wall Boundary Layers. NASA TN D-5433, 1969.
17. Feller, William V.: Effects of Upstream Wall Temperatures on Hypersonic Tunnel Wall Boundary-Layer Profile Measurements. AIAA J., vol. 11, no. 4, Apr. 1973, pp. 556-558.
18. Gates, D. F.; and Allen, R. W.: Experimental Measurements of Upstream History Effects in Turbulent Supersonic Flow. Proceedings of the 1974 Heat Transfer and Fluid Mechanics Institute, Lorin R. Davis and Robert E. Wilson, eds., Stanford Univ. Press, 1974, pp. 330-347.
19. Beckwith, Ivan E.: Comments on Crocco's Solution and the Independence Principle for Compressible Turbulent Boundary Layers. AIAA J., vol. 12, no. 2, Feb. 1974, pp. 245-247.
20. Bushnell, D. M.; Cary, A. M., Jr.; and Holley, B. B.: Mixing Length in Low Reynolds Number Compressible Turbulent Boundary Layers. AIAA J., vol. 13, no. 8, Aug. 1975.
21. Anders, J. B.; Stainback, P. C.; Keefe, L. R.; and Beckwith, I. E.: Sound and Fluctuating Disturbance Measurements in the Settling Chamber and Test Section of a Small, Mach 5 Wind Tunnel. ICIASF '75 Record, IEEE Publ. 75 CHO 993-6 AES, pp. 329-340.
22. Morkovin, M. V.: On Supersonic Wind Tunnels With Low Free-Stream Disturbances. Trans. ASME, Ser. E: J. Appl. Mech., vol. 26, no. 3, Sept. 1959, pp. 319-323.
23. Stainback, P. C.; and Wagner, R. D.: A Comparison of Disturbance Levels Measured in Hypersonic Tunnels Using a Hot-Wire Anemometer and a Pitot Pressure Probe. AIAA Paper No. 72-1003, Sept. 1972.
24. Beckwith, Ivan E.; and Bertram, Mitchel H.: A Survey of NASA Langley Studies on High-Speed Transition and the Quiet Tunnel. NASA TM X-2566, 1972.

25. Harvey, W. D.; Berger, M. H.; and Stainback, P. C.: Experimental and Theoretical Investigation of a Slotted Noise Shield Model for Wind Tunnel Walls. AIAA Paper No. 74-624, July 1974.
26. Back, Lloyd H.; and Cuffel, Robert F.: Viscous Slipstream Flow Downstream of a Centerline Mach Reflection. AIAA J., vol. 9, no. 10, Oct. 1971, pp. 2107-2109.

TABLE I.- MEASURED NOZZLE COORDINATES

x		r		M _e (ref. 13)	x		r		M _e (ref. 13)
cm	in.	cm	in.		cm	in.	cm	in.	
-11.5316	-4.537	6.9921	2.7528	0.0121	3.58648	1.412	1.2624	0.4970	1.9196
-11.0998	-4.370	6.9449	2.7342	.0122	4.21386	1.659	1.3528	.5326	2.0822
-10.2616	-4.040	6.6266	2.6089	.0134	4.84378	1.907	1.4519	.5716	2.2391
-9.3980	-3.700	5.8364	2.2978	.0168	5.47116	2.154	1.5532	.6115	2.3877
-8.5344	-3.360	4.5872	1.806	.0273	6.0960	2.400	1.6584	.6529	2.5310
-7.6835	-3.025	3.6962	1.4552	.0424	6.72338	2.647	1.7703	.6969	2.6663
-6.7818	-2.670	2.9692	1.1690	.0658	7.34822	2.893	1.8824	.7411	2.7950
-5.9817	-2.355	2.4511	.9650	.0977	7.97306	3.139	1.9949	.7854	2.9163
-5.1308	-2.020	2.0295	.7990	.1417	8.6004	3.386	2.1059	.8291	3.0310
-4.2672	-1.680	1.6993	.6690	.2053	9.2253	3.632	2.2174	.8730	3.1418
-3.4112	-1.340	1.4407	.5672	.2934	9.8501	3.878	2.3305	.9175	3.2480
-2.5654	-1.010	1.2486	.4916	.4073	10.4750	4.124	2.4455	.9628	3.3493
-1.70688	-.672	1.1018	.4338	.58103	11.1023	4.371	2.5616	1.0085	3.4465
-.85344	-.336	1.0231	.4028	.7826	11.7272	4.617	2.6734	1.0525	3.5383
0	0	1.0053	.3958	1.0000	12.3520	4.863	2.7833	1.0958	3.6265
.02540	.010	1.0053	.3958	1.0078	12.9794	5.110	2.8903	1.1379	3.7083
.10414	.041	1.0053	.3958	1.0110	13.6068	5.357	2.9949	1.1791	3.7855
.26416	.104	1.0056	.3959	1.0794	14.2342	5.604	3.0983	1.2198	3.8593
.42164	.166	1.0076	.3967	1.1133	14.8615	5.851	3.1989	1.2594	3.9290
.58166	.229	1.0109	.3980	1.1619	15.4889	6.098	3.2949	1.2972	3.9937
.73914	.291	1.0160	.4000	1.2000	16.1184	6.346	3.3894	1.3344	4.0565
1.05664	.416	1.0295	.4053	1.2751	16.7488	6.594	3.4811	1.3705	4.1153
1.69164	.666	1.0658	.4196	1.4355	17.3787	6.842	3.5697	1.4054	4.1710
2.32410	.915	1.1173	.4399	1.5936	18.0086	7.090	3.6495	1.4368	4.2228
2.95402	1.163	1.1831	.4658	1.7490	18.6385	7.338	3.7275	1.4675	4.2640

TABLE I.- Concluded

x		r		M _e (ref. 13)	x		r		M _e (ref. 13)
cm	in.	cm	in.		cm	in.	cm	in.	
19.2684	7.586	3.8026	1.4971	4.3203	35.1003	13.819	5.0018	1.9692	4.9800
19.8984	7.834	3.8760	1.5260	4.3660	35.7353	14.069	5.0259	1.9787	4.9923
20.5308	8.083	3.9474	1.5541	4.4088	36.3703	14.319	5.0483	1.9875	5.0027
21.1633	8.332	4.0163	1.5812	4.4505	37.0053	14.569	5.0691	1.9957	5.0143
21.7932	8.580	4.0833	1.6076	4.4887	37.6403	14.819	5.0894	2.0037	5.0247
22.4257	8.829	4.1481	1.6331	4.5250	38.1000	15.000	5.1031	2.0091	5.0303
23.0581	9.078	4.2103	1.6576	4.5613	38.2753	15.069	5.1079	2.0110	5.0327
23.6906	9.327	4.2687	1.6806	4.5940	38.9103	15.319	5.1272	2.0186	5.0423
24.3230	9.576	4.3251	1.7028	4.6267	39.5453	15.569	5.1445	2.0254	5.0497
24.9580	9.826	4.3807	1.7247	4.6560	40.1803	15.819	5.1618	2.0322	5.0583
25.5905	10.075	4.4366	1.7467	4.6853	40.8153	16.069	5.1778	2.0385	5.0647
26.2230	10.324	4.4899	1.7677	4.7140	41.4503	16.319	5.1928	2.0444	5.0723
26.8580	10.574	4.5410	1.7878	4.7388	42.0853	16.569	5.2060	2.0496	5.0767
27.4904	10.823	4.5883	1.8064	4.7640	42.7203	16.819	5.2189	2.0547	5.0842
28.1229	11.072	4.6330	1.824	4.7883	43.3553	17.069	5.2306	2.0593	5.0887
28.7579	11.322	4.6761	1.8410	4.8085	43.9903	17.319	5.2415	2.0636	5.0943
29.3929	11.572	4.7165	1.8569	4.8307	44.6227	17.568	5.2502	2.0670	5.0967
30.0253	11.821	4.7539	1.8716	4.8520	45.2577	17.818	5.2583	2.0702	5.1023
30.6603	12.071	4.7871	1.8847	4.8693	45.8927	18.068	5.2669	2.0736	5.1037
31.2953	12.321	4.8224	1.8986	4.8885	46.5277	18.318	5.2743	2.0765	5.1083
31.9278	12.570	4.8552	1.9115	4.9067	47.1627	18.568	5.2822	2.0796	5.1087
32.5628	12.820	4.8867	1.9239	4.9210	47.7977	18.818	5.28955	2.0825	5.1103
33.1978	13.070	4.9169	1.9358	4.9377	48.4073	19.068	5.3033	2.0879	5.1147
33.8328	13.320	4.9464	1.9474	4.9530	49.0677	19.318	5.3129	2.0917	5.1147
34.4653	13.569	4.9743	1.9584	4.9657	49.7027	19.568	5.3246	2.0963	5.1193
					50.0024	19.686	5.3398	2.1023	5.1193

TABLE II.- SETTLING-CHAMBER PARTS FOR
NOZZLE TEST CHAMBER

Part no.	Name	Description
1	Entrance cone	One 50-mesh screen, 0.794-cm (0.316 in.) holes One 50-mesh screen, and one 4-mesh screen
2	Honeycomb	1.905-cm (0.75 in.) long, 0.476-cm (0.1874 in.) honeycomb
3	Screen	One 50-mesh screen, 1.509-cm (0.5941 in.) long
4	Screen	One 50-mesh screen, 1.509-cm (0.5941 in.) long
6	Inlet adapter	7.62-cm (0.30 in.) long, 10.15-cm (3.996 in.) ID ^a × 13.96-cm (5.496 in.) ID
8	Screen	One 50-mesh screen, 1.509-cm (0.5941 in.) long
12	Rigimesh	5.08-cm (2.0 in.) long, 0.3175-cm (1.25 in.) thick, 12 × 64 mesh
13	Rigimesh	3.175-cm (1.25 in.) long (2), 0.1588-cm (0.06252 in.) thick (each) 12 × 64 mesh (can be used separately)

^aID — inside diameter.

TABLE III.- SCREEN CONFIGURATIONS TESTED

[Screen configurations 1 and 2 are low Δp screens; configurations 3 and 4 are high Δp screens.]

Screen Configurations											
1			2			3			4		
Part no.	Name	Length, cm (in.)	Part no.	Name	Length, cm (in.)	Part no.	Name	Length, cm (in.)	Part no.	Name	Length, cm (in.)
6	Inlet adapter	7.62 (3.00)	6	Inlet adapter	7.62 (3.00)	6	Inlet adapter	7.62 (3.00)	6	Inlet adapter	7.62 (3.00)
1	Entrance cone	1.27 (0.50)	1	Entrance cone	1.27 (0.50)	1	Entrance cone	1.27 (0.50)	12	Rigimesh	5.08 (2.00)
13	Rigimesh	.159 (0.626)	2	Honeycomb	1.905 (0.75)	3	Screen	1.509 (0.5941)	13	Rigimesh	.159 (0.0626)
2	Honeycomb	1.905 (0.75)	13	Rigimesh	3.175* (1.25)	4	Screen	1.509 (0.5941)		Spacer	1.27 (0.50)
3	Screen	1.509 (0.5941)	3	Screen	1.509 (0.5941)	13	Rigimesh	3.175* (1.25)	13	Rigimesh	.159 (0.0626)
4	Screen	1.509 (0.5941)	4	Screen	1.509 (0.5941)	12	Rigimesh	5.08 (2.00)	3	Screen	1.509 (0.5941)
	Spacers	16.528 (6.507)	8	Screen	1.509 (0.5941)		Spacers	10.337 (4.07)	4	Screen	1.509 (0.5941)
				Spacers	12.003 (4.726)				8	Screen	1.509 (0.5941)
										Spacers	11.685 (4.60)
	Total	30.50 (11.83)		Total	30.50 (11.83)		Total	30.50 (11.83)		Total	30.50 (11.83)

*Two pieces.

TABLE IV.- STAGNATION AND TEST CONDITIONS

(a) Pitot surveys with screens

Survey station, x		T_w		T_t		$P_{t,1}$		$\frac{P_{t,2,e}}{P_{t,1}}$	M_e	$(R_\infty)_{exit}$	
cm	in.	K	$^{\circ}R$	K	$^{\circ}R$	MPa	psi			per cm	per in.
9.36	3.675	300	540	378	680	345	50	0.3200	3.031	0.68×10^5	1.74×10^5
9.36	3.675	300	540	378	680	345	50	.3283	3.000	.68	1.74
19.50	7.650	300	540	378	680	345	50	.1265	4.111	.68	1.74
19.50	7.650	300	540	378	680	1722	250	.1234	4.140	3.41	8.70
19.50	7.650	300	540	378	680	3450	500	.1244	4.130	6.81	17.30
27.18	10.69	300	540	320	575	207	30	.0888	4.535	.54	1.37
27.18	10.69	300	540	322	580	276	40	.0899	4.532	.71	1.81
27.18	10.69	300	540	327	590	345	50	.0894	4.531	.86	2.20
27.18	10.69	300	540	378	680	345	50	.0853	4.591	.68	1.74
27.18	10.69	300	540	334	600	415	60	.0904	4.520	1.01	2.56
27.18	10.69	300	540	340	610	485	70	.0878	4.555	1.15	2.91
27.18	10.69	300	540	345	620	551	80	.0877	4.558	1.27	3.23
27.18	10.69	300	540	347	635	690	100	.0878	4.555	1.66	4.20
27.18	10.69	300	540	378	680	1722	250	.0864	4.572	3.41	8.70
27.18	10.69	300	540	378	680	3450	500	.0838	4.613	6.81	17.30
32.20	12.70	300	540	378	680	345	50	.0853	4.591	.68	1.74
32.20	12.70	300	540	378	680	1722	250	.0864	4.572	3.41	8.70
32.20	12.70	300	540	378	680	3450	500	.0838	4.613	6.81	17.30
36.00	14.2	300	540	378	680	345	50	.07157	4.811	.68	1.74
36.00	14.2	300	540	378	680	1722	250	.07243	4.795	3.41	8.70
36.00	14.2	300	540	378	680	3450	500	.07157	4.8105	6.81	17.30
37.40	14.69	300	540	322	580	276	40	.0705	4.831	.71	1.81
37.40	14.69	300	540	327	590	345	50	.0704	4.831	.86	2.20
37.40	14.69	300	540	334	600	415	60	.0700	4.840	1.01	2.56
37.40	14.69	300	540	340	610	485	70	.0708	4.827	1.15	2.91
37.40	14.69	300	540	345	620	551	80	.0709	4.824	1.27	3.23
39.80	15.65	300	540	378	680	345	50	.06567	4.922	.68	1.74
39.80	15.65	300	540	378	680	1722	250	.06801	4.872	3.41	8.70
39.80	15.65	300	540	378	680	3450	500	.06722	4.890	6.81	17.30
44.10	17.35	300	540	378	680	1722	250	.0667	4.9055	3.41	8.70
44.10	17.35	300	540	378	680	3450	500	.0637	4.9625	6.81	17.30
48.10	18.95	300	540	322	580	276	40	.0620	4.995	.71	1.81
48.10	18.95	300	540	327	590	345	50	.0618	4.997	.86	2.20
48.10	18.95	300	540	367	660	345	50	.0627	4.998	.68	1.74
48.10	18.95	300	540	334	600	415	60	.0617	5.000	1.01	2.56
48.10	18.95	300	540	340	610	485	70	.0647	4.936	1.15	2.91
48.10	18.95	300	540	345	620	551	80	.0648	4.935	1.27	3.23
48.10	18.95	300	540	389	700	1722	250	.0632	4.9705	3.41	8.70
48.10	18.95	300	540	383	690	3450	500	.0627	4.9805	6.81	17.30

TABLE IV.- Continued
(b) Pitot surveys without screens

Survey station, x		T _w		T _t		P _{t,1}		P _{t,2,e}	M _e	(R _∞) _{exit}	
cm	in.	K	°R	K	°R	MPa	psi	P _{t,1}		per cm	per in.
9.36	3.675	300	540	395	710	345	50	0.2960	3.120	0.68 × 10 ⁵	1.74 × 10 ⁵
19.50	7.650	300	540	395	710	345	50	.1152	4.223	.68	1.74
19.50	7.650	300	540	403	725	1722	250	.1227	4.1475	3.41	8.70
19.50	7.650	300	540	389	700	3450	500	.1173	4.200	6.81	17.4
31.20	12.30	300	540	386	695	345	50	.0766	4.7255	.68	1.74
31.20	12.30	300	540	392	705	1722	250	.0803	4.6645	3.41	8.70
31.20	12.30	300	540	395	710	3450	500	.0797	4.6745	6.81	17.30
32.20	12.70	300	540	383	690	345	50	.0781	4.6985	.68	1.74
32.20	12.70	300	540	383	690	1722	250	.0800	4.6735	3.41	8.70
32.20	12.70	300	540	389	700	3450	500	.0793	4.6815	6.81	17.30
36.00	14.20	300	540	378	680	345	50	.0699	4.8445	.68	1.74
36.00	14.20	300	540	403	725	1722	250	.0727	4.7875	3.41	8.70
36.00	14.20	300	540	402	722	3450	500	.0721	4.799	6.81	17.30
44.10	17.35	300	540	404	726	345	50	.0603	5.0305	.68	1.74
44.10	17.35	300	540	393	706	1722	250	.0642	4.9465	3.41	8.70
44.10	17.35	300	540	394	710	3450	500	.0636	4.9575	6.81	17.30
48.10	18.95	300	540	383	690	345	50	.0601	5.035	.68	1.74
48.10	18.95	300	540	403	725	1722	250	.0594	5.050	3.41	8.70
48.10	18.95	300	540	402	722	3450	500	.0572	5.100	6.81	17.30

TABLE IV.- Concluded

(c) Total temperature surveys with screens

Survey station, x		T_w		T_t		$P_{t,1}$		$\frac{T_{t,e}}{T_{t,1}}$	M_e	$(R_\infty)_{exit}$	
cm	in.	K	°R	K	°R	MPa	psi			per cm	per in.
48.1	18.95	304	546	364	655	345	50	0.971	5.0	0.68×10^5	1.74×10^5
48.1	18.95	329	592	387	696	1722	250	.981	5.0	3.41	8.70
48.1	18.95	333	600	383	690	3450	500	.980	5.0	6.81	17.30

(d) Total temperature surveys without screens

Survey station, x		T_w		T_t		$P_{t,1}$		$\frac{T_{t,e}}{T_{t,1}}$	M_e	$(R_\infty)_{exit}$	
cm	in.	K	°R	K	°R	MPa	psi			per cm	per in.
48.1	18.95	316	569	395	710	345	50	0.966	5.0	0.68×10^5	1.74×10^5
48.1	18.95	338	608	404	725	1722	250	.987	5.0	3.41	8.70
48.1	18.95	346	624	335	694	3450	500	.987	5.0	6.81	17.30

(e) Pitot surveys with screens and heated wall

Survey station, x		T_w		T_t		$P_{t,1}$		$\left(\frac{P_{t,2}}{P_{t,1}}\right)_e$	M_e	$(R_\infty)_{exit}$	
cm	in.	K	°R	K	°R	MPa	psi			per cm	per in.
27.18	10.69	485	872	363	652	207	30	0.08735	4.56	0.54×10^5	1.37×10^5
27.18	10.69	484	871	359	645	276	40	.08665	4.57	.71	1.81
27.18	10.69	473	850	342	615	345	50	.08596	4.58	.86	2.20
27.18	10.69	454	817	329	591	415	60	.08527	4.59	1.01	2.56
27.18	10.69	452	814	360	646	485	70	.08391	4.61	1.15	2.91
27.18	10.69	432	778	353	635	551	80	.08735	4.56	1.27	3.23

(f) Pitot surveys with screens and roughness

Survey station, x		T_w		T_t		$P_{t,1}$		$\left(\frac{P_{t,2}}{P_{t,1}}\right)_e$	M_e	$(R_\infty)_{exit}$	
cm	in.	K	°R	K	°R	MPa	psi			per cm	per in.
27.18	10.69	300	540	320	575	207	30	0.0859	4.578	0.54×10^5	1.37×10^5
27.18	10.69	300	540	322	580	276	40	.0873	4.560	.71	1.81
27.18	10.69	300	540	327	590	345	50	.0873	4.558	.86	2.20
27.18	10.69	300	540	334	600	415	60	.0880	4.551	1.01	2.56
27.18	10.69	300	540	340	610	485	70	.0880	4.551	1.15	2.91
27.18	10.69	300	540	345	620	551	80	.0873	4.558	1.27	3.23

TABLE V.- EXPERIMENTAL PITOT PROFILES

(a) At $x = 22.1$ cm (8.7 in.)

$R_\infty = 5.41 \times 10^4/\text{cm}$ ($1.37 \times 10^5/\text{in.}$), $M_e = 4.53$			$R_\infty = 8.64 \times 10^4/\text{cm}$ ($2.2 \times 10^5/\text{in.}$), $M_e = 4.53$			$R_\infty = 12.7 \times 10^4/\text{cm}$ ($3.23 \times 10^5/\text{in.}$), $M_e = 4.54$		
y, cm	y, in.	$\frac{P_{t,2}}{P_{t,1}}$	y, cm	y, in.	$\frac{P_{t,2}}{P_{t,1}}$	y, cm	y, in.	$\frac{P_{t,2}}{P_{t,1}}$
0.02794	0.011	0.42×10^{-2}	0.02794	0.011	0.54×10^{-2}	0.02794	0.011	1.49×10^{-2}
.0330	.013	.55	.0356	.014	1.00	.0484	.019	2.37
.0534	.021	.76	.0585	.023	1.65	.0585	.023	2.70
.0786	.031	1.37	.0711	.028	2.38	.0814	.032	3.10
.0965	.038	1.70	.094	.037	2.90	.1015	.040	3.36
.1120	.044	2.16	.109	.043	3.50	.150	.059	4.09
.1270	.050	3.25	.122	.048	5.04	.1905	.075	4.49
.1371	.054	4.10	.1295	.051	6.77	.224	.088	4.89
.1575	.062	5.50	.137	.054	8.25	.249	.098	5.09
.1700	.067	6.62	.1525	.060	8.73	.262	.103	5.37
.1905	.075	8.04	.175	.067	8.98	.280	.110	5.73
.2160	.085	8.94	.198	.078	8.88	.313	.123	6.39
.2285	.090	8.95	.226	.088	8.83	.350	.138	7.05
.2465	.097	8.95	.249	.098	8.77	.379	.149	7.37
.2660	.1045	8.94	.274	.108	8.70	.401	.158	7.80
.2950	.116	8.83	.308	.121	8.68	.419	.165	8.12
.3180	.125	8.78	.358	.141	8.66	.445	.175	8.38
.3380	.133	8.76	.384	.151	8.65	.495	.195	8.68
.379	.149	8.74	.422	.166	8.60	.524	.206	8.74
.419	.165	8.70	.455	.179	8.59	.556	.219	8.85
.452	.178	8.68	.514	.202	8.55	.512	.233	8.88
.494	.194	8.60	.539	.212	8.55	.615	.242	8.88
.529	.208	8.62	.570	.224	8.56	.659	.259	8.87
.570	.224	8.57	.640	.252	8.54	.678	.267	8.87
.613	.241	8.60	.745	.293	8.54	.710	.279	8.84
.650	.256	8.58				.747	.294	8.85
.694	.273	8.57						
.745	.293	8.54						

TABLE V.- Continued

(b) At $x = 27.2$ cm (10.7 in.)

$R_{\infty} = 5.41 \times 10^4/\text{cm}$ ($1.37 \times 10^5/\text{in.}$), $M_e = 4.54$			$R_{\infty} = 8.64 \times 10^4/\text{cm}$ ($2.2 \times 10^5/\text{in.}$), $M_e = 4.53$			$R_{\infty} = 12.7 \times 10^4/\text{cm}$ ($3.23 \times 10^5/\text{in.}$), $M_e = 4.56$		
y, cm	y, in.	$\frac{p_{t,2}}{p_{t,1}}$	y, cm	y, in.	$\frac{p_{t,2}}{p_{t,1}}$	y, cm	y, in.	$\frac{p_{t,2}}{p_{t,1}}$
0.02794	0.011	0.47×10^{-2}	0.02794	0.011	0.55×10^{-2}	0.02794	0.011	1.45×10^{-2}
.033	.013	.60	.0381	.015	1.05	.0356	.014	2.36
.0534	.021	.80	.0585	.023	1.70	.0560	.022	2.82
.099	.039	1.72	.0736	.029	2.42	.0736	.029	3.12
.112	.044	2.18	.094	.037	2.92	.1015	.040	3.25
.127	.050	3.25	.109	.043	3.55	.1170	.046	3.29
.137	.054	4.12	.122	.048	5.03	.142	.056	3.50
.1575	.062	5.49	.1295	.051	6.76	.1750	.069	4.30
.170	.067	6.57	.137	.054	8.20	.198	.078	4.61
.188	.074	7.99	.1525	.060	8.42	.231	.091	4.85
.213	.084	8.88	.1675	.066	8.94	.246	.097	4.97
.2285	.090	8.89	.1955	.077	8.84	.279	.111	5.72
.246	.097	8.88	.221	.087	8.80	.312	.123	6.35
.264	.104	8.89	.246	.097	8.74	.336	.132	6.52
.289	.114	8.79	.272	.107	8.66	.364	.143	6.90
.315	.124	8.75	.305	.120	8.63	.389	.153	7.32
.335	.132	8.75	.325	.128	8.71	.430	.169	8.30
.373	.147	8.72	.356	.140	8.62	.463	.182	8.55
.414	.163	8.70	.381	.150	8.62	.506	.199	8.68
.446	.176	8.63	.432	.170	8.58	.536	.211	8.80
.487	.192	8.62	.460	.181	8.57	.570	.224	8.82
.524	.206	8.60	.508	.200	8.51	.607	.239	8.83
.566	.223	8.56	.536	.211	8.51	.640	.252	8.85
.606	.239	8.57	.555	.218	8.51	.666	.262	8.84
			.575	.226	8.55	.700	.276	8.80
			.635	.250	8.53	.740	.291	8.81
			.740	.291	8.50			

TABLE V.- Continued

(c) At $x = 31.0$ cm (12.2 in.)

$R_\infty = 5.41 \times 10^4/\text{cm}$ ($1.37 \times 10^5/\text{in.}$), $M_e = 4.66$			$R_\infty = 8.64 \times 10^4/\text{cm}$ ($2.2 \times 10^5/\text{in.}$), $M_e = 4.65$			$R_\infty = 12.7 \times 10^4/\text{cm}$ ($3.23 \times 10^5/\text{in.}$), $M_e = 4.67$		
y, cm	y, in.	$\frac{P_{t,2}}{P_{t,1}}$	y, cm	y, in.	$\frac{P_{t,2}}{P_{t,1}}$	y, cm	y, in.	$\frac{P_{t,2}}{P_{t,1}}$
0.0279	0.011	0.41×10^{-2}	0.0305	0.012	0.51×10^{-2}	0.0279	0.011	1.24×10^{-2}
.0381	.015	.44	.0610	.024	1.05	.0456	.018	1.53
.0458	.018	.49	.0763	.030	1.37	.0559	.022	1.90
.0509	.020	.55	.094	.037	2.03	.066	.026	2.18
.0635	.025	.65	.112	.044	2.80	.1145	.045	2.56
.0711	.028	.73	.1345	.053	3.85	.145	.057	2.89
.0762	.030	.86	.160	.063	5.01	.165	.065	3.18
.1015	.040	1.17	.170	.067	6.53	.186	.073	3.45
.1142	.045	1.44	.198	.078	7.74	.203	.080	3.62
.122	.048	1.73	.214	.084	8.00	.229	.090	3.90
.1372	.054	2.04	.236	.093	8.09	.249	.098	4.07
.1475	.058	2.36	.262	.103	8.09	.274	.108	4.35
.1675	.066	3.18	.320	.126	8.00	.300	.118	4.65
.1805	.071	3.63	.353	.139	7.99	.325	.128	4.99
.1905	.075	4.27	.384	.151	7.96	.356	.140	5.39
.198	.078	4.72	.406	.160	7.95	.391	.154	5.85
.2135	.084	5.19	.445	.175	7.93	.432	.170	6.40
.226	.089	5.75	.470	.185	7.89	.465	.183	6.85
.239	.094	6.52	.503	.198	7.84	.490	.193	7.27
.2515	.099	7.00	.549	.216	7.80	.524	.206	7.56
.264	.104	7.66	.590	.232	7.75	.561	.221	7.80
.277	.109	7.85	.620	.244	7.71	.595	.234	7.91
.292	.115	8.00	.655	.258	7.68	.632	.249	7.99
.305	.120	8.06	.689	.271	7.67	.669	.259	7.98
.325	.128	8.09	.721	.284	7.66	.689	.271	7.96
.340	.134	8.09	.751	.296	7.63	.714	.281	7.95
.371	.146	8.08				.746	.294	7.92
.405	.159	8.07						
.422	.166	8.02						
.453	.178	8.00						
.480	.189	7.94						
.504	.198	7.90						
.531	.209	7.90						
.562	.221	7.87						
.591	.233	7.85						
.640	.252	7.77						
.670	.264	7.76						
.700	.276	7.73						
.745	.293	7.69						

TABLE V.- Continued
(d) At $x = 37.4$ cm (14.7 in.)

$R_{\infty} = 7.11 \times 10^4/\text{cm}$ ($1.81 \times 10^5/\text{in.}$), $M_e = 4.83$			$R_{\infty} = 8.64 \times 10^4/\text{cm}$ ($2.2 \times 10^5/\text{in.}$), $M_e = 4.83$			$R_{\infty} = 12.7 \times 10^4/\text{cm}$ ($3.23 \times 10^5/\text{in.}$), $M_e = 4.82$		
y, cm	y, in.	$\frac{P_{t,2}}{P_{t,1}}$	y, cm	y, in.	$\frac{P_{t,2}}{P_{t,1}}$	y, cm	y, in.	$\frac{P_{t,2}}{P_{t,1}}$
0.0305	0.012	0.35×10^{-2}	0.0305	0.012	0.45×10^{-2}	0.0279	0.011	0.87×10^{-2}
.0431	.017	.39	.0431	.017	.80	.0305	.012	1.40
.0685	.027	1.01	.0585	.025	1.27	.0431	.017	1.68
.0813	.032	1.20	.0814	.032	1.62	.061	.025	1.80
.1015	.040	1.55	.1015	.040	2.04	.0761	.030	1.90
.140	.055	2.30	.112	.044	2.40	.094	.037	2.04
.165	.065	2.72	.132	.052	3.08	.165	.042	2.12
.175	.069	3.12	.150	.059	3.40	.1245	.049	2.18
.201	.079	4.06	.178	.070	4.09	.155	.061	2.38
.234	.092	5.13	.208	.082	5.01	.173	.068	2.50
.274	.108	6.42	.247	.097	6.25	.1905	.075	2.65
.298	.117	6.69	.274	.108	6.64	.206	.081	2.72
.338	.133	6.90	.300	.118	6.86	.224	.088	2.85
.394	.155	7.04	.323	.127	7.00	.244	.096	3.04
.427	.168	7.04	.356	.140	7.03	.269	.106	3.24
.458	.180	7.01	.386	.152	7.00	.287	.113	3.36
.500	.197	6.98	.424	.167	7.00	.328	.129	3.42
.541	.213	6.96	.445	.175	7.02	.350	.138	3.89
.571	.225	6.94	.485	.191	6.95	.371	.146	4.09
.649	.255	6.90	.531	.209	6.92	.396	.156	4.31
.686	.270	6.85	.565	.222	6.90	.430	.169	4.60
.716	.282	6.85	.610	.240	6.85	.450	.177	4.85
.750	.295	6.84	.660	.260	6.80	.480	.189	5.19
.795	.313	6.80	.686	.270	6.80	.514	.202	5.44
.839	.330	6.80	.730	.287	6.80	.541	.213	5.72
.885	.348	6.79	.772	.304	6.76	.572	.225	5.94
.922	.363	6.75	.814	.320	6.75	.605	.238	6.19
.965	.380	6.75	.850	.335	6.74	.635	.250	6.47
1.015	.399	6.74	.910	.358	6.73	.669	.263	6.69
1.050	.414	6.73	.949	.373	6.72	.694	.274	6.85
1.091	.430	6.70	1.000	.393	6.66	.745	.293	7.01
			1.049	.412	6.65	.762	.300	7.04
			1.105	.435	6.64	.795	.313	7.07
						.825	.325	7.08
						.880	.346	7.10
						.915	.360	7.05
						1.001	.395	7.06
						1.12	.440	7.06

TABLE V.- Continued

(e) At $x = 42.9$ cm (16.9 in.)

$R_\infty = 5.41 \times 10^4/\text{cm}$ ($1.37 \times 10^5/\text{in.}$), $M_e = 4.95$			$R_\infty = 8.64 \times 10^4/\text{cm}$ ($2.2 \times 10^5/\text{in.}$), $M_e = 4.94$			$R_\infty = 12.7 \times 10^4/\text{cm}$ ($3.23 \times 10^5/\text{in.}$), $M_e = 4.93$		
y, cm	y, in.	$\frac{P_{t,2}}{P_{t,1}}$	y, cm	y, in.	$\frac{P_{t,2}}{P_{t,1}}$	y, cm	y, in.	$\frac{P_{t,2}}{P_{t,1}}$
0.0279	0.011	0.26×10^{-2}	0.0279	0.011	0.37×10^{-2}	0.0279	0.011	0.70×10^{-2}
.0381	.015	.27	.0356	.014	.40	.0381	.015	.74
.0508	.020	.30	.0508	.020	.59	.056	.022	1.17
.0585	.023	.37	.0635	.025	1.01	.0763	.030	1.37
.0711	.028	.64	.0761	.030	1.34	.089	.035	1.50
.0890	.035	.90	.0965	.038	1.63	.1015	.040	1.60
.104	.041	1.10	.1141	.045	1.95	.1295	.051	1.73
.117	.046	1.25	.1345	.053	2.31	.1525	.060	1.81
.1345	.053	1.38	.1525	.060	2.65	.165	.065	1.92
.150	.059	1.50	.173	.068	3.06	.1955	.077	2.06
.165	.065	1.68	.1905	.075	3.32	.216	.085	2.21
.178	.070	1.86	.2180	.086	3.91	.234	.092	2.27
.1905	.075	2.00	.2415	.095	4.39	.246	.097	2.35
.203	.080	2.20	.262	.103	4.71	.267	.105	2.45
.221	.086	2.40	.282	.111	5.01	.284	.112	2.52
.236	.093	2.77	.300	.118	5.35	.343	.135	2.86
.256	.101	3.10	.312	.123	5.60	.361	.142	3.00
.274	.108	3.55	.336	.132	5.87	.384	.151	3.12
.295	.116	4.05	.364	.143	6.05	.404	.159	3.25
.312	.123	4.32	.381	.150	6.16	.435	.171	3.46
.330	.130	4.73	.399	.157	6.29	.450	.177	3.55
.356	.140	5.23	.426	.168	6.36	.470	.185	3.70
.381	.150	5.60	.470	.185	6.93	.490	.193	3.87
.409	.161	5.88	.495	.195	6.43	.549	.216	4.34
.421	.166	6.00	.541	.213	6.44	.590	.232	4.60
.452	.178	6.19	.560	.220	6.43	.625	.246	4.85
.478	.188	6.26	.587	.231	6.41	.663	.261	5.07
.514	.202	6.30	.610	.240	6.41	.699	.275	5.39
.536	.211	6.39	.635	.250	6.39	.741	.292	5.70
.565	.222	6.38	.660	.260	6.37	.793	.312	5.94
.605	.238	6.39	.686	.270	6.36	.807	.318	6.03
.644	.253	6.38	.774	.304	6.36	.846	.333	6.20
.681	.270	6.38	.877	.345	6.36	.892	.351	6.38
.773	.304	6.36	.904	.355	6.36	.931	.367	6.45
.839	.330	6.35				.942	.371	6.50
.880	.346	6.35				.979	.385	6.50
.965	.380	6.35				1.027	.404	6.51
						1.071	.422	6.53
						1.130	.445	6.53
						1.142	.450	6.53

TABLE V.- Continued
(f) At $x = 48.1$ cm (18.94 in.)

$R_{\infty} = 7.11 \times 10^4/\text{cm} (1.81 \times 10^5/\text{in.}), M_e = 5.00$			$R_{\infty} = 8.64 \times 10^4/\text{cm} (2.2 \times 10^5/\text{in.}), M_e = 5.00$			$R_{\infty} = 12.7 \times 10^4/\text{cm} (3.23 \times 10^5/\text{in.}), M_e = 4.94$		
y, cm	y, in.	$\frac{P_{t,2}}{P_{t,1}}$	y, cm	y, in.	$\frac{P_{t,2}}{P_{t,1}}$	y, cm	y, in.	$\frac{P_{t,2}}{P_{t,1}}$
0.0381	0.015	0.33×10^{-2}	0.0279	0.011	0.30×10^{-2}	0.0279	0.011	0.56×10^{-2}
.0560	.022	.80	.0381	.015	.51	.0685	.027	1.90
.0788	.031	1.15	.0559	.022	.66	.1140	.045	1.42
.0991	.039	1.39	.0686	.027	1.30	.140	.055	1.50
.117	.046	1.61	.0787	.031	1.64	.173	.068	1.60
.140	.055	1.85	.1015	.040	1.90	.216	.085	1.82
.155	.061	2.01	.1191	.047	2.09	.254	.099	1.97
.175	.069	2.22	.142	.056	2.30	.274	.108	2.05
.193	.076	2.49	.1675	.066	2.52	.315	.124	2.26
.216	.085	2.70	.198	.078	2.99	.356	.140	2.50
.236	.093	2.99	.228	.090	3.36	.396	.156	2.67
.254	.100	3.20	.254	.100	3.54	.440	.173	2.95
.269	.106	3.40	.287	.113	4.03	.478	.188	3.22
.294	.116	3.77	.305	.120	4.35	.505	.199	3.34
.320	.126	4.16	.320	.126	4.52	.539	.212	3.50
.348	.137	4.51	.348	.137	4.64	.571	.225	3.80
.368	.145	4.86	.376	.148	5.18	.626	.247	4.11
.383	.151	5.11	.406	.160	5.44	.660	.260	4.30
.419	.165	5.40	.445	.175	5.70	.704	.277	4.75
.457	.180	5.70	.477	.188	5.82	.761	.300	5.07
.473	.186	5.75	.520	.205	5.95	.795	.313	5.34
.505	.199	5.89	.555	.218	6.03	.839	.330	5.60
.534	.210	6.00	.605	.238	6.08	.871	.343	5.75
.566	.223	6.06	.635	.250	6.10	.915	.360	5.98
.673	.265	6.11	.685	.270	6.10	.952	.375	6.16
.686	.270	6.09	.741	.292	6.10	1.009	.397	6.39
.709	.279	6.12	.790	.311	6.15	1.550	.415	6.50
.745	.293	6.15	.865	.340	6.17			
.761	.300	6.18	.910	.358	6.17			
.844	.332	6.20	1.041	.410	6.17			
.882	.347	6.20						
.935	.368	6.19						
.965	.380	6.20						

TABLE V.- Continued

(g) At $x = 27.2$ cm (10.7 in.) with heated nozzle wall (see fig. 11)

$R_\infty = 5.4 \times 10^4/\text{cm}$ ($1.35 \times 10^5/\text{in.}$), $M_e = 4.56$, $\frac{T_w}{T_t} = 1.39$			$R_\infty = 8.64 \times 10^4/\text{cm}$ ($2.45 \times 10^5/\text{in.}$), $M_e = 4.58$, $\frac{T_w}{T_t} = 1.38$			$R_\infty = 12.7 \times 10^4/\text{cm}$ ($3.62 \times 10^5/\text{in.}$), $M_e = 4.56$, $\frac{T_w}{T_t} = 1.22$		
y, cm	y, in.	$\frac{P_{t,2}}{P_{t,1}}$	y, cm	y, in.	$\frac{P_{t,2}}{P_{t,1}}$	y, cm	y, in.	$\frac{P_{t,2}}{P_{t,1}}$
0.0279	0.011	0.44×10^{-2}	0.0279	0.011	0.46×10^{-2}	0.0279	0.011	1.00×10^{-2}
.0457	.018	.44	.0483	.019	.46	.0407	.016	1.28
.0660	.026	.46	.0585	.023	.59	.0535	.021	1.60
.0865	.034	.49	.0787	.031	.90	.0663	.026	1.95
.1120	.044	.60	.0965	.038	1.22	.0840	.033	2.16
.132	.052	.75	.114	.045	1.45	.0994	.039	2.40
.150	.059	1.05	.142	.056	2.50	.1170	.046	2.55
.175	.069	1.52	.160	.063	3.35	.1348	.053	2.75
.193	.076	1.96	.1805	.071	4.46	.1525	.060	3.01
.214	.084	2.64	.2005	.079	6.00	.1752	.069	3.25
.238	.094	3.89	.218	.086	8.19	.1880	.074	3.55
.264	.104	5.30	.244	.096	8.95	.2060	.081	3.88
.284	.112	6.75	.257	.101	9.02	.2260	.089	4.09
.302	.119	8.45	.270	.106	9.00	.2740	.108	4.69
.323	.127	8.80	.280	.110	8.99	.2945	.116	4.98
.348	.137	9.10	.302	.119	8.94	.3080	.121	5.28
.379	.149	9.15	.315	.124	8.92	.3280	.129	5.51
.406	.160	9.10	.325	.128	8.91	.3460	.136	5.82
.425	.167	9.08	.358	.141	8.89	.3710	.146	6.10
.450	.177	9.02	.397	.156	8.86	.3940	.155	6.35
.470	.185	8.99	.416	.164	8.83	.4090	.161	6.63
.495	.195	8.89	.437	.172	8.79	.4340	.171	7.00
.516	.203	8.96	.460	.181	8.76	.4550	.179	7.40
.534	.210	8.92	.480	.189	8.75	.4830	.190	7.77
.560	.220	8.90	.506	.199	8.70	.4980	.196	8.04
.585	.230	8.88	.531	.209	8.72	.5240	.206	8.30
.610	.240	8.85	.550	.216	8.69	.5440	.214	8.50
.635	.250	8.84	.577	.227	8.66	.5640	.222	8.55
.660	.260	8.83	.598	.235	8.66	.5900	.232	8.64
.686	.270	8.81	.615	.242	8.65	.6200	.244	8.69
.716	.282	8.79	.651	.256	8.61	.6535	.257	8.71
.750	.295	8.78	.679	.267	8.60	.6890	.271	8.68
.775	.305	8.77	.700	.276	8.60	.7140	.281	8.68
			.721	.284	8.60	.7410	.292	8.66
			.741	.292	8.60			

TABLE V.- Concluded

(h) At $x = 27.2$ cm (10.69 in.) with roughness in subsonic approach section (see fig. 17)

$R_\infty = 5.41 \times 10^4/\text{cm}$ ($1.37 \times 10^5/\text{in.}$), $M_e = 4.58$			$R_\infty = 8.64 \times 10^4/\text{cm}$ ($2.2 \times 10^5/\text{in.}$), $M_e = 4.56$			$R_\infty = 12.7 \times 10^4/\text{cm}$ ($3.84 \times 10^5/\text{in.}$), $M_e = 4.56$		
y, cm	y, in.	$\frac{P_{t,2}}{P_{t,1}}$	y, cm	y, in.	$\frac{P_{t,2}}{P_{t,1}}$	y, cm	y, in.	$\frac{P_{t,2}}{P_{t,1}}$
0.0279	0.011	0.50×10^{-2}	0.0279	0.011	1.5×10^{-2}	0.0279	0.011	1.50×10^{-2}
.0381	.015	.51	.0330	.013	1.84	.0585	.023	2.00
.0509	.020	.55	.0457	.018	2.31	.0686	.027	2.35
.0635	.025	.71	.0585	.023	2.76	.0915	.036	2.69
.0768	.030	.93	.0711	.028	3.14	.109	.043	3.00
.094	.037	1.25	.084	.033	3.50	.127	.050	3.22
.1091	.043	1.56	.099	.039	3.80	.150	.059	3.57
.1245	.049	2.00	.1145	.045	4.01	.1725	.068	3.93
.1345	.053	2.72	.127	.050	4.29	.1985	.078	4.30
.142	.056	3.40	.140	.055	4.50	.221	.087	4.71
.155	.061	4.10	.155	.061	4.76	.244	.096	5.14
.168	.066	4.81	.168	.066	5.04	.267	.105	5.46
.1805	.071	5.64	.1805	.071	5.39	.292	.115	5.85
.198	.078	6.90	.193	.076	5.65	.313	.123	6.15
.211	.083	7.88	.211	.083	5.96	.335	.132	6.47
.224	.088	8.49	.224	.088	6.20	.350	.138	6.69
.241	.095	8.60	.244	.096	6.50	.369	.145	6.92
.254	.100	8.62	.262	.103	6.76	.389	.153	7.19
.269	.106	8.60	.282	.111	6.96	.415	.163	7.52
.287	.113	8.60	.300	.118	7.20	.435	.171	7.82
.310	.122	8.56	.320	.126	7.44	.452	.178	8.09
.325	.128	8.57	.346	.136	7.70	.478	.188	8.30
.338	.133	8.60	.372	.146	7.99	.500	.197	8.55
.358	.141	8.62	.405	.159	8.26	.530	.208	8.70
.389	.153	8.61	.435	.171	8.49	.550	.216	8.75
.414	.163	8.60	.455	.179	8.62	.566	.223	8.75
.446	.176	8.60	.485	.191	8.73	.592	.233	8.76
.490	.193	8.57	.516	.203	8.76	.618	.243	8.76
.529	.208	8.52	.556	.219	8.76	.640	.252	8.76
.566	.223	8.52	.613	.241	8.76	.669	.263	8.75
.605	.238	8.50	.659	.259	8.77	.700	.275	8.75
.645	.254	8.50	.700	.275	8.76	.727	.286	8.75
.694	.273	8.49	.752	.296	8.75	.760	.299	8.75
.745	.293	8.46						

TABLE VI.- MACH NUMBER, TEMPERATURE, AND VELOCITY PROFILES,

x = 48.11 cm (18.94 in.)

(a) With screens

$R_\infty = 0.68 \times 10^5/\text{cm} \ (1.74 \times 10^5/\text{in.}), \quad \frac{T_w}{T_{t,1}} = 0.83$				
$\frac{y}{\delta}$	$\frac{M}{M_\infty}$	$\frac{T_t}{T_{t,\infty}}$	$\frac{T_t - T_w}{T_{t,\infty} - T_w}$	$\frac{u}{u_\infty}$
0.0349	0.233	0.869	0.2294	0.4709
.0569	.319	.888	.3412	.5982
.0760	.386	.902	.4235	.6789
.0884	.441	.911	.4765	.7325
.10562	.483	.922	.5412	.7701
.1440	.531	.937	.6312	.8110
.1750	.563	.944	.6676	.8315
.2110	.594	.949	.6988	.8511
.2430	.621	.953	.7259	.8677
.2775	.647	.958	.7518	.8808
.3180	.680	.963	.7829	.8971
.3475	.706	.966	.7988	.9081
.3790	.735	.970	.8259	.9218
.4660	.803	.979	.8747	.9460
.5175	.854	.982	.8953	.9620
.5910	.899	.986	.9165	.9729
.6560	.932	.987	.9271	.9821
.7310	.968	.988	.9300	.9883
.7910	.984	.988	.9294	.9912
.8600	.993	.987	.9276	.9924
.9290	.998	.987	.9253	.9926
1.000	1.00	.987	.9253	.9936

TABLE VI.- Continued

(a) Continued

$R_{\infty} = 3.41 \times 10^5/\text{cm} \ (8.7 \times 10^5/\text{in.}), \quad \frac{T_w}{T_{t,1}} = 0.84$				
$\frac{y}{\delta}$	$\frac{M}{M_{\infty}}$	$\frac{T_t}{T_{t,\infty}}$	$\frac{T_t - T_w}{T_{t,\infty} - T_w}$	$\frac{u}{u_{\infty}}$
0.0222	0.3381	0.907	0.3800	0.6280
.0385	.3888	.913	.4200	.6860
.0491	.4298	.921	.4740	.7276
.0600	.4516	.927	.5130	.7490
.0687	.4638	.934	.5570	.7605
.0774	.4689	.938	.5860	.7663
.0894	.4823	.944	.6253	.7784
.1035	.4904	.952	.6787	.7879
.1109	.4968	.955	.7000	.7942
.1349	.5188	.964	.7587	.8130
.1590	.5471	.970	.8000	.8341
.1815	.5658	.974	.8253	.8473
.2100	.5783	.978	.8560	.8561
.2295	.5984	.981	.8760	.8682
.2410	.6117	.983	.8887	.8761
.2630	.6334	.987	.9107	.8875
.2845	.6507	.990	.9333	.8974
.3058	.6699	.993	.9500	.9070
.3290	.6932	.995	.9680	.9174
.3502	.7135	.997	.9813	.9260
.3760	.7312	.999	.9967	.9336
.3980	.7548	1.0012	1.008	.9424
.4220	.7735	1.0029	1.019	.9490
.4420	.7896	1.0042	1.028	.9548
.4660	.8085	1.0057	1.038	.9611
.5080	.8423	1.0079	1.053	.9712
.5460	.8809	1.0097	1.065	.9813
.5910	.9145	1.011	1.073	.9891
.6340	.9437	1.0104	1.069	.9949
.6850	.9684	1.0085	1.057	.9984
.7240	.9807	1.0064	1.043	.9999
.7640	.9911	1.0046	1.031	1.0008
.8550	.9968	1.0009	1.006	.9997
.8940	.9976	1.0001	1.001	.9996
1.000	1.00	1.00	1.00	1.00

TABLE VI.- Continued

(a) Concluded

$R_{\infty} = 6.80 \times 10^5/\text{cm} \quad (1.73 \times 10^6/\text{in.}), \quad \frac{T_w}{T_{t,1}} = 0.87$				
$\frac{y}{\delta}$	$\frac{M}{M_{\infty}}$	$\frac{T_t}{T_{t,\infty}}$	$\frac{T_t - T_w}{T_{t,\infty} - T_w}$	$\frac{u}{u_{\infty}}$
0.0283	0.3563	0.9125	0.3269	0.6508
.0435	.3868	.9262	.4323	.6886
.0586	.4362	.9362	.5092	.7391
.0866	.4822	.9470	.5923	.7887
.1140	.5021	.9573	.6715	.7996
.1470	.5288	.9675	.7500	.8217
.1845	.5601	.9752	.8092	.8445
.1985	.5685	.9767	.8208	.8500
.2300	.5964	.9791	.8392	.8665
.2610	.6203	.9816	.8585	.8795
.2858	.6372	.9841	.8777	.8888
.3240	.6681	.9882	.9092	.9043
.3480	.6850	.9905	.9269	.9124
.3780	.7059	.9930	.9462	.9215
.4260	.7362	.9968	.9754	.9344
.4740	.7727	1.000	1.00	.9479
.5320	.8115	1.0030	1.023	.9006
.6100	.8486	1.0055	1.0423	.9717
.6950	.8886	1.0084	1.065	.9824
.7540	.9111	1.0097	1.075	.9877
.8300	.9408	1.0109	1.084	.9943
.8760	.9771	1.010	1.077	1.0009
.9380	.9886	1.0085	1.065	1.0022
.950	.9968	1.006	1.046	1.0023
1.000	1.00	1.0035	1.027	1.0017
1.030	1.00	1.0027	1.021	1.0013
1.159	1.00	1.000	1.00	1.000

TABLE VI.- Continued

(b) Without screens

$R_{\infty} = 0.68 \times 10^5/\text{cm} \ (1.74 \times 10^5/\text{in.}), \quad \frac{T_w}{T_{t,1}} = 0.80$				
$\frac{y}{\delta}$	$\frac{M}{M_{\infty}}$	$\frac{T_t}{T_{t,\infty}}$	$\frac{T_t - T_w}{T_{t,\infty} - T_w}$	$\frac{u}{u_{\infty}}$
0.0214	0.232	0.859	0.326	0.468
.0409	.282	.890	.476	.552
.0556	.362	.905	.548	.656
.0659	.444	.912	.581	.737
.0911	.538	.930	.662	.813
.1120	.572	.939	.706	.836
.1328	.602	.947	.744	.857
.1540	.635	.951	.758	.874
.1745	.659	.956	.783	.886
.1990	.689	.961	.805	.901
.2175	.712	.962	.810	.911
.2185	.732	.966	.831	.919
.2600	.755	.968	.838	.928
.2790	.776	.970	.848	.936
.3000	.807	.974	.868	.946
.3275	.827	.976	.878	.952
.3460	.854	.979	.894	.961
.3760	.869	.982	.906	.966
.4040	.896	.984	.918	.977
.4260	.921	.986	.930	.980
.4490	.922	.988	.940	.981
.4700	.936	.989	.947	.985
.4950	.941	.992	.959	.986
.5160	.950	.992	.960	.987
.5340	.945	----	----	----
.5510	.956	.995	.974	.990
.6070	.967	.996	.979	.994
.6580	.976	.998	.989	.996
.7660	.986	.999	.995	.998
.7560	.990	1.000	1.000	.999
.8340	.995	1.000	1.000	.999
1.000	1.000	1.000	1.000	1.000
1.091	1.000	1.000	1.000	1.000
1.280	1.000	1.000	1.000	1.000
1.472	1.000	1.000	1.000	1.000

TABLE VI.- Continued

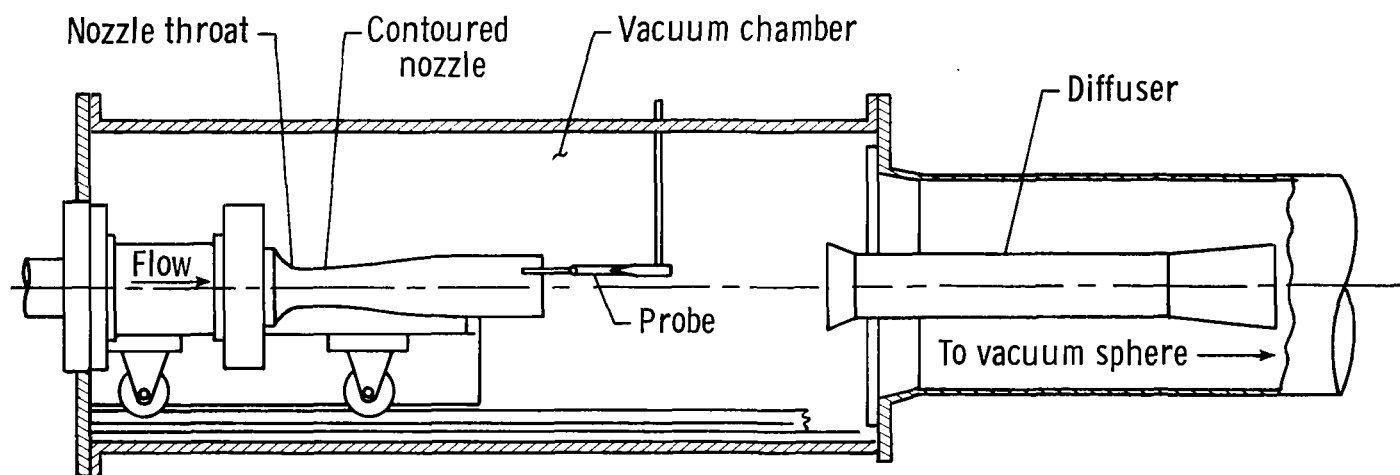
(b) Continued

$R_{\infty} = 3.41 \times 10^5/\text{cm} \ (8.7 \times 10^5/\text{in.}), \quad \frac{T_w}{T_{t,1}} = 0.84$				
$\frac{y}{\delta}$	$\frac{M}{M_{\infty}}$	$\frac{T_t}{T_{t,\infty}}$	$\frac{T_t - T_w}{T_{t,\infty} - T_w}$	$\frac{u}{u_{\infty}}$
0.0268	0.3239	0.900	0.471	0.614
.0464	.4092	.914	.545	.710
.0568	.4364	.917	.559	.736
.0865	.4745	.929	.606	.772
.1120	.4942	.937	.640	.790
.1420	.5160	.948	.691	.808
.1680	.5358	.955	.728	.825
.1930	.5600	.959	.754	.840
.2140	.5795	.962	.767	.854
.2430	.6000	.966	.791	.867
.2719	.6226	.970	.814	.878
.2960	.6376	.973	.832	.888
.3210	.6580	.976	.851	.897
.3520	.6786	.978	.861	.906
.3775	.7017	.980	.878	.916
.4050	.7192	.983	.897	.924
.4260	.7398	.986	.914	.932
.4510	.7581	.990	.935	.940
.4790	.7751	.993	.955	.948
.5090	.7941	.995	.969	.954
.544	.8164	.998	.987	.962
.5820	.8435	1.000	1.002	.970
.6100	.8650	1.0016	1.010	.974
.6460	.8919	1.002	1.013	.982
.6890	.9138	1.004	1.032	.988
.7240	.9360	1.005	1.034	.992
.7660	.9540	1.006	----	----
.8210	.9740	1.008	1.057	1.001
.850	.9847	1.006	1.042	1.002
.8950	.9943	1.004	1.032	1.001
.9475	.9981	1.002	1.013	1.000
1.00	1.00	1.002	1.012	1.000
1.050	1.00	1.001	----	1.000
1.080	1.00	1.000	----	1.000
1.360	1.00	.999	1.000	1.000

TABLE VI.- Concluded

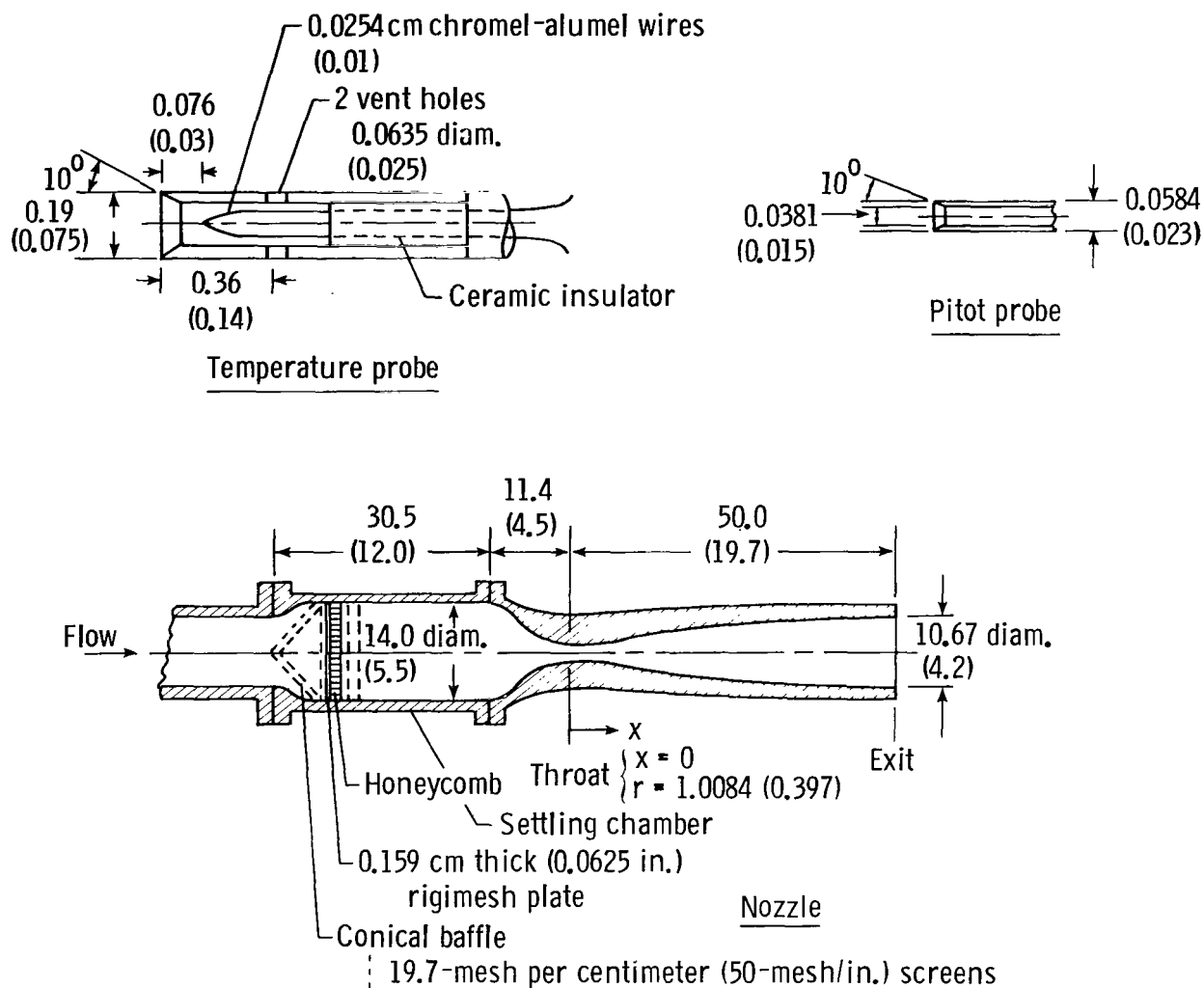
(b) Concluded

$R_{\infty} = 6.80 \times 10^5/\text{cm} \quad (1.73 \times 10^6/\text{in.}), \quad \frac{T_w}{T_{t,1}} = 0.90$				
$\frac{y}{\delta}$	$\frac{M}{M_{\infty}}$	$\frac{T_t}{T_{t,\infty}}$	$\frac{T_t - T_w}{T_{t,\infty} - T_w}$	$\frac{u}{u_{\infty}}$
0.0290	0.360	0.940	0.412	0.6724
.0529	.414	.958	.590	.7335
.0660	.456	.966	.665	.7736
.1110	.509	.982	.818	.8202
.148	.538	.990	.902	.8420
.1798	.565	.994	.942	.8617
.2085	.586	.992	.917	.8718
.2380	.606	.994	.942	.8830
.2640	.626	.994	.942	.8920
.2930	.646	.993	.932	.9010
.3220	.664	.996	.961	.9100
.3770	.702	.998	.984	.9258
.4330	.738	1.003	1.029	.9400
.483	.774	1.004	1.038	.9535
.540	.814	1.007	1.068	.9650
.5990	.850	1.009	1.088	.9760
.660	.887	1.009	1.088	.9830
.716	.919	1.009	1.088	.9915
.772	.944	1.009	1.088	.9960
.825	.964	1.009	1.088	1.000
.886	.983	1.009	1.088	1.001
.950	.996	1.006	1.058	1.002
1.00	1.00	1.004	1.038	1.002
1.06	1.00	1.002	1.020	1.001
1.165	1.00	1.000	1.000	1.000



(a) Schematic sketch of apparatus.

Figure 1.- Nozzle test chamber and Mach 5 nozzle.



(b) Details of survey probes, settling chamber, and nozzle. (Dimensions are in centimeters; values in parentheses are in inches.)

Figure 1.- Concluded.

$p_{t,1}$		R_∞/cm	$R_\infty/\text{in.}$
MPa	psia		
345	50	0.68×10^5	1.74×10^5
1722	250	3.41	8.70
3450	500	6.80	17.3

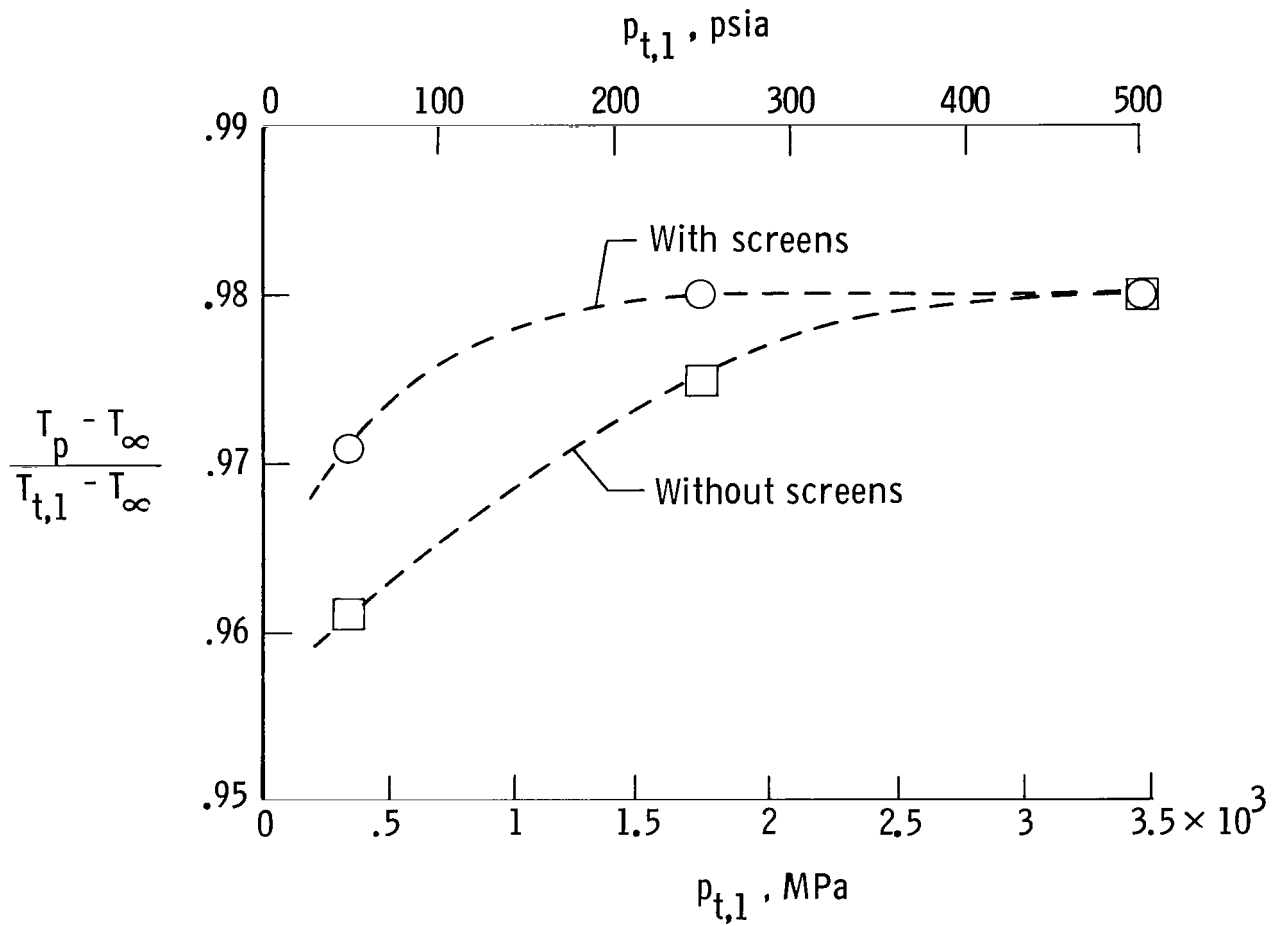


Figure 2.- Total temperature probe calibration in $M = 5$ nozzle. $0.83 \leq \frac{T_w}{T_{t,\infty}} \leq 0.87$.

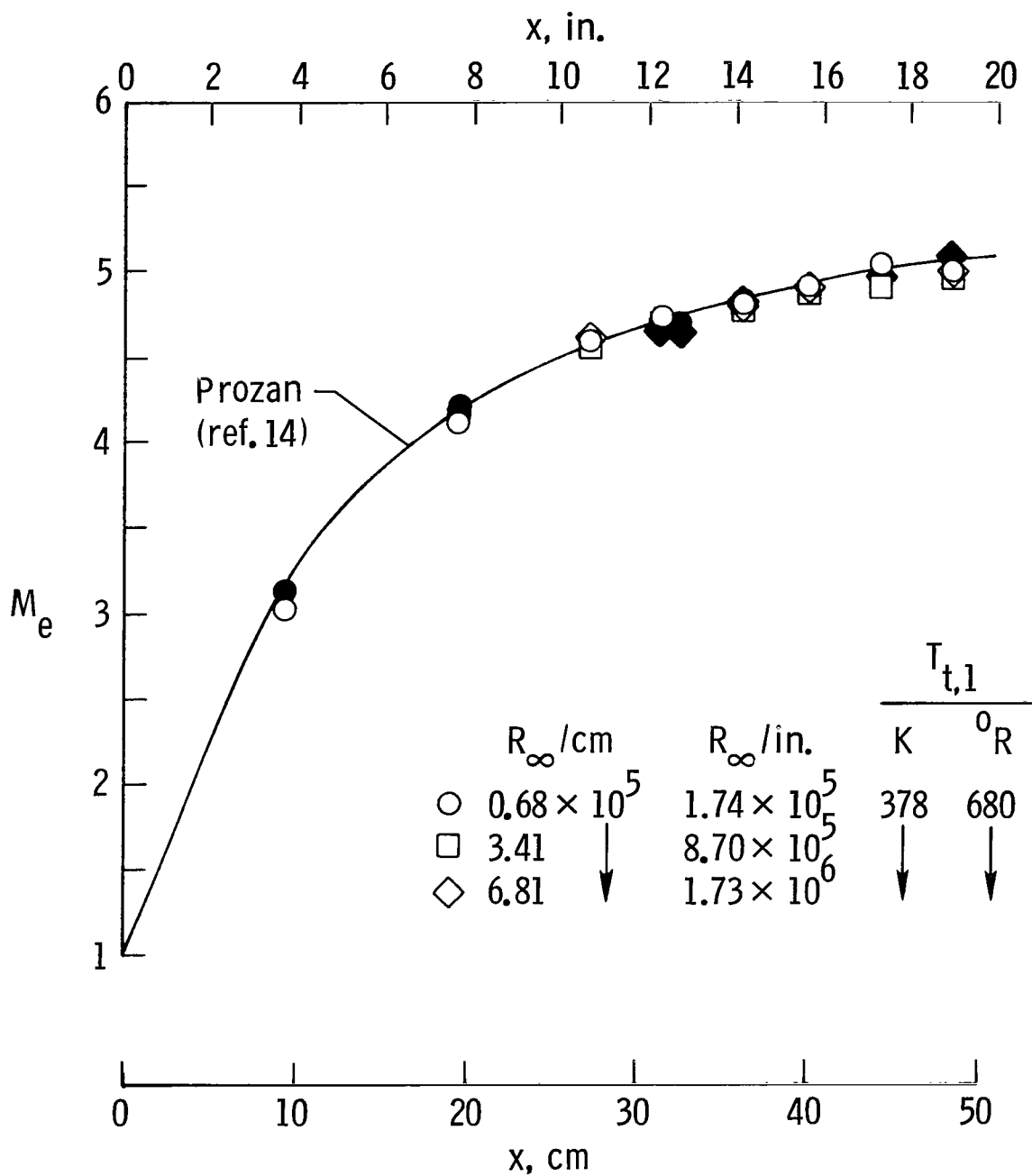


Figure 3.- Mach number distribution at boundary-layer edge along the nozzle wall.
(Open symbols represent screens in settling chamber; filled symbols represent no screens.)

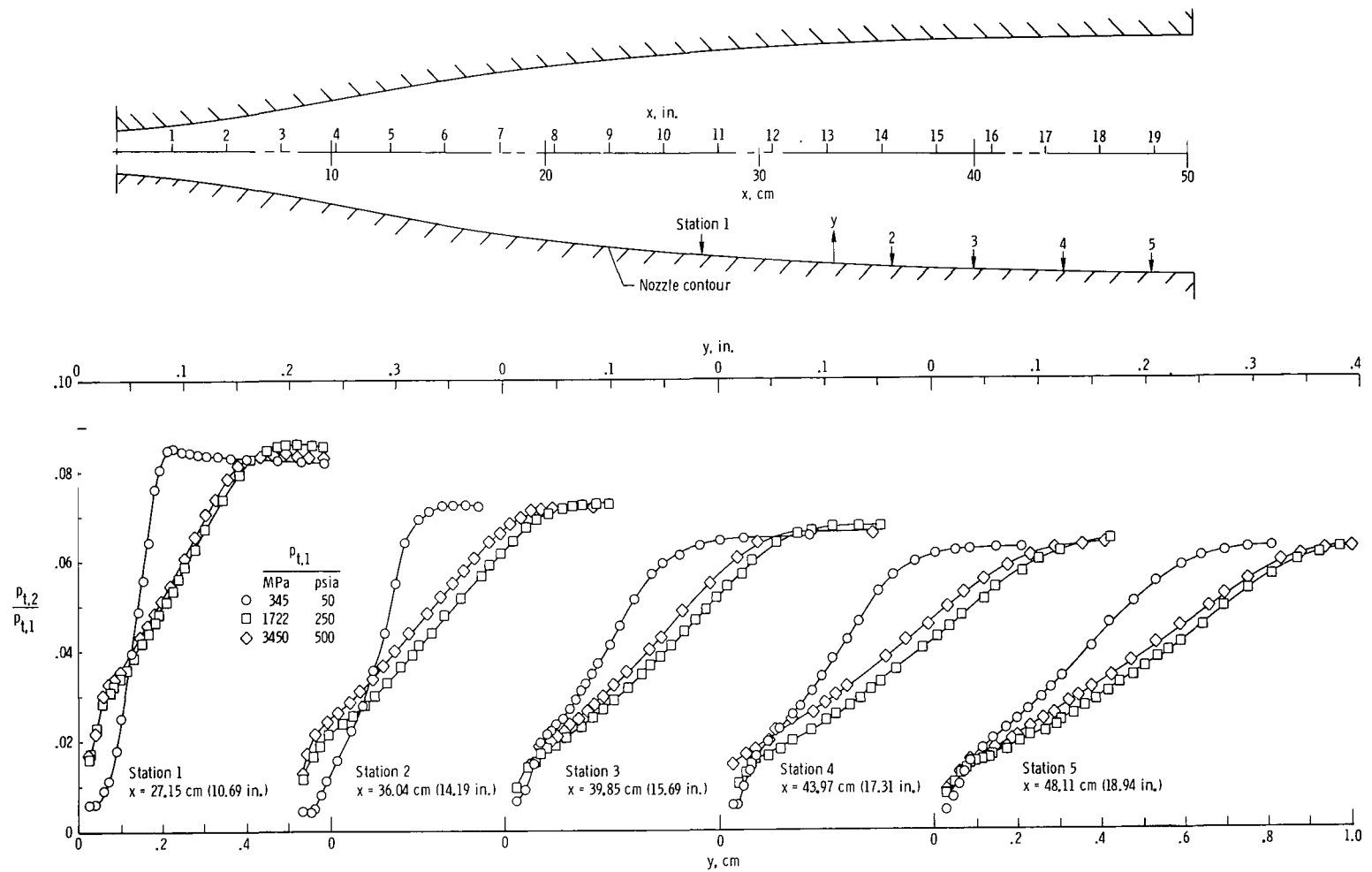


Figure 4.- Boundary-layer pitot profiles along the nozzle wall.

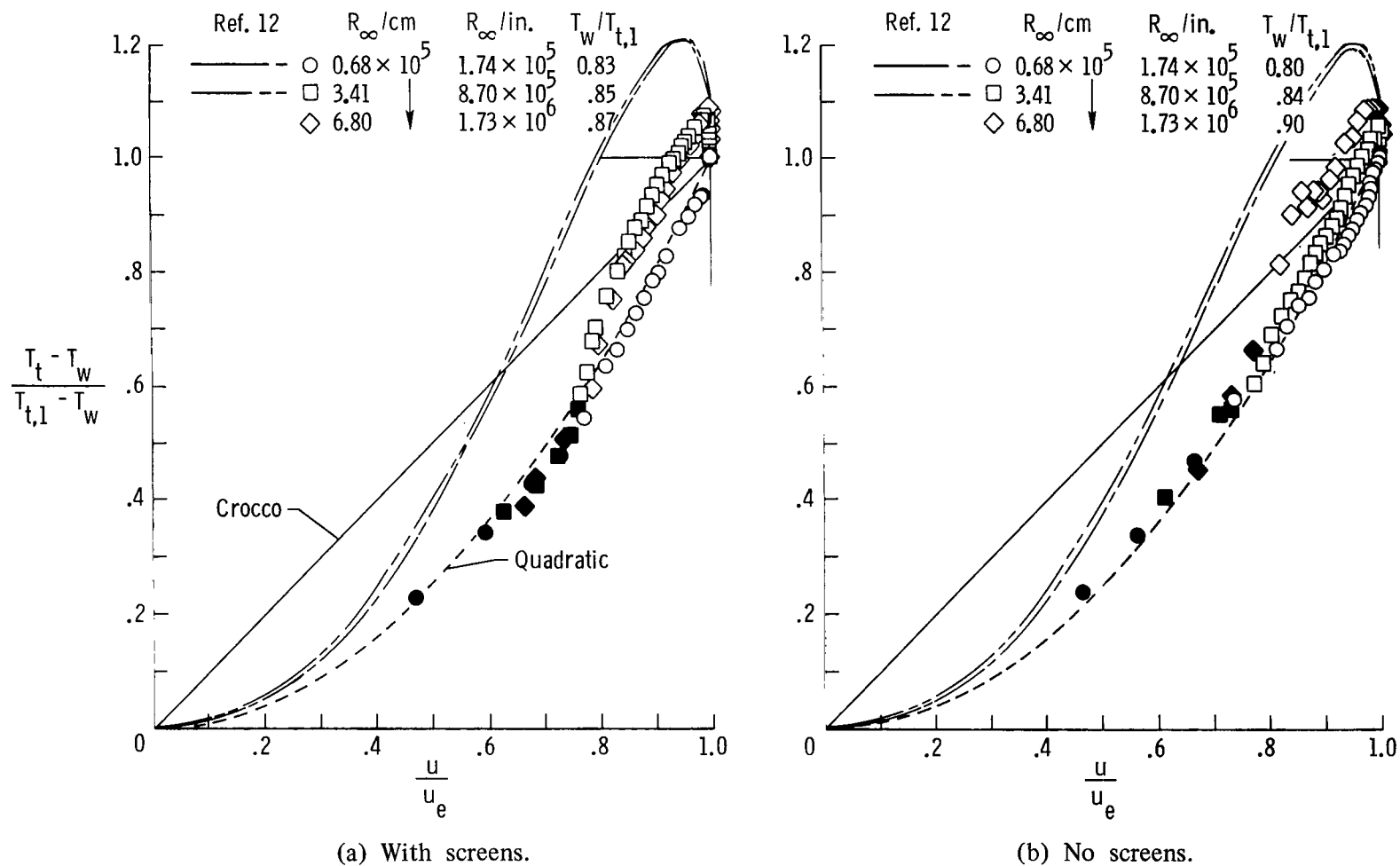


Figure 5.- Temperature-velocity profiles near the nozzle exit. $x = 48.11$ cm (18.94 in.).
(Filled symbols represent extrapolated temperatures.)

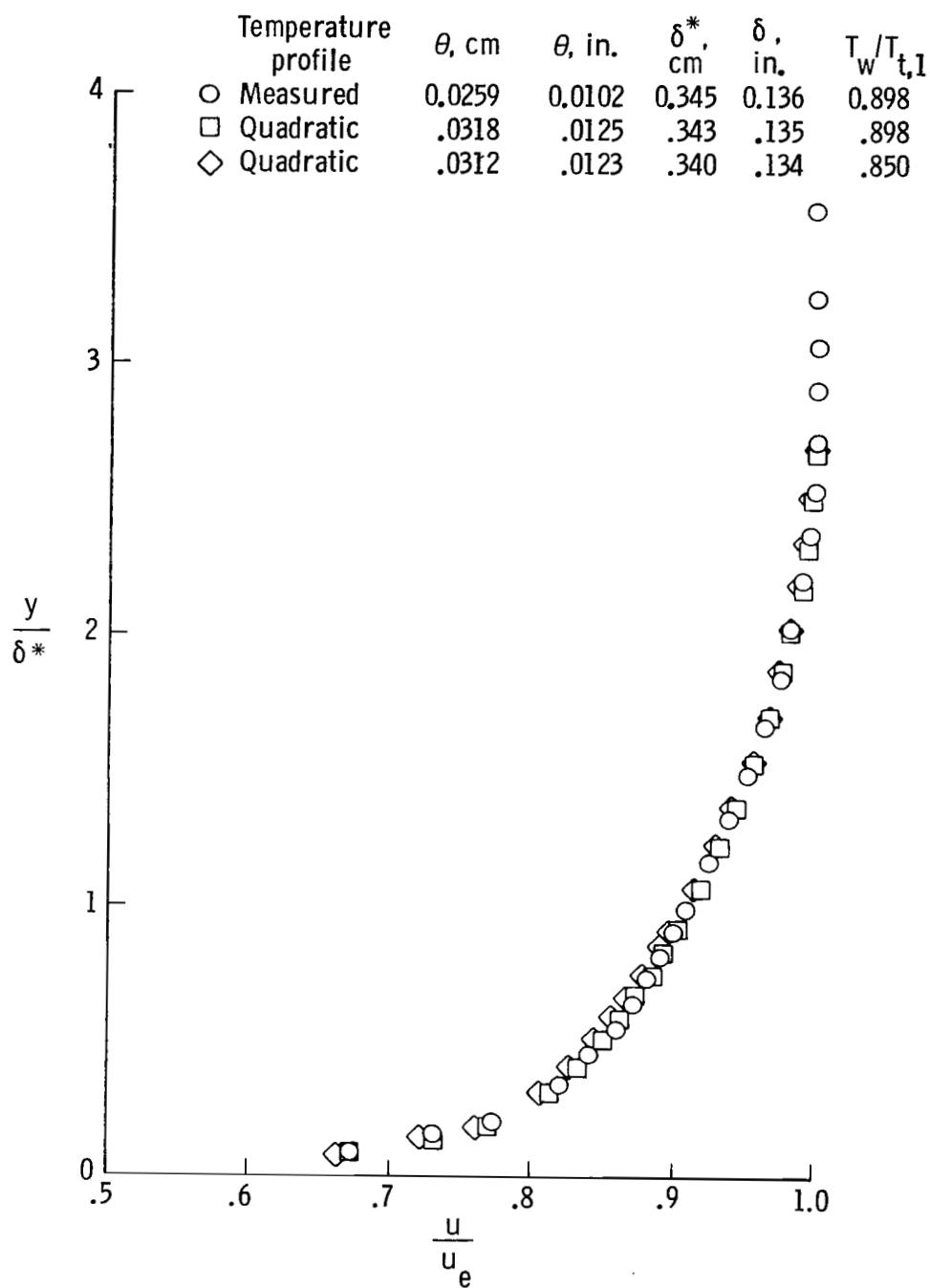
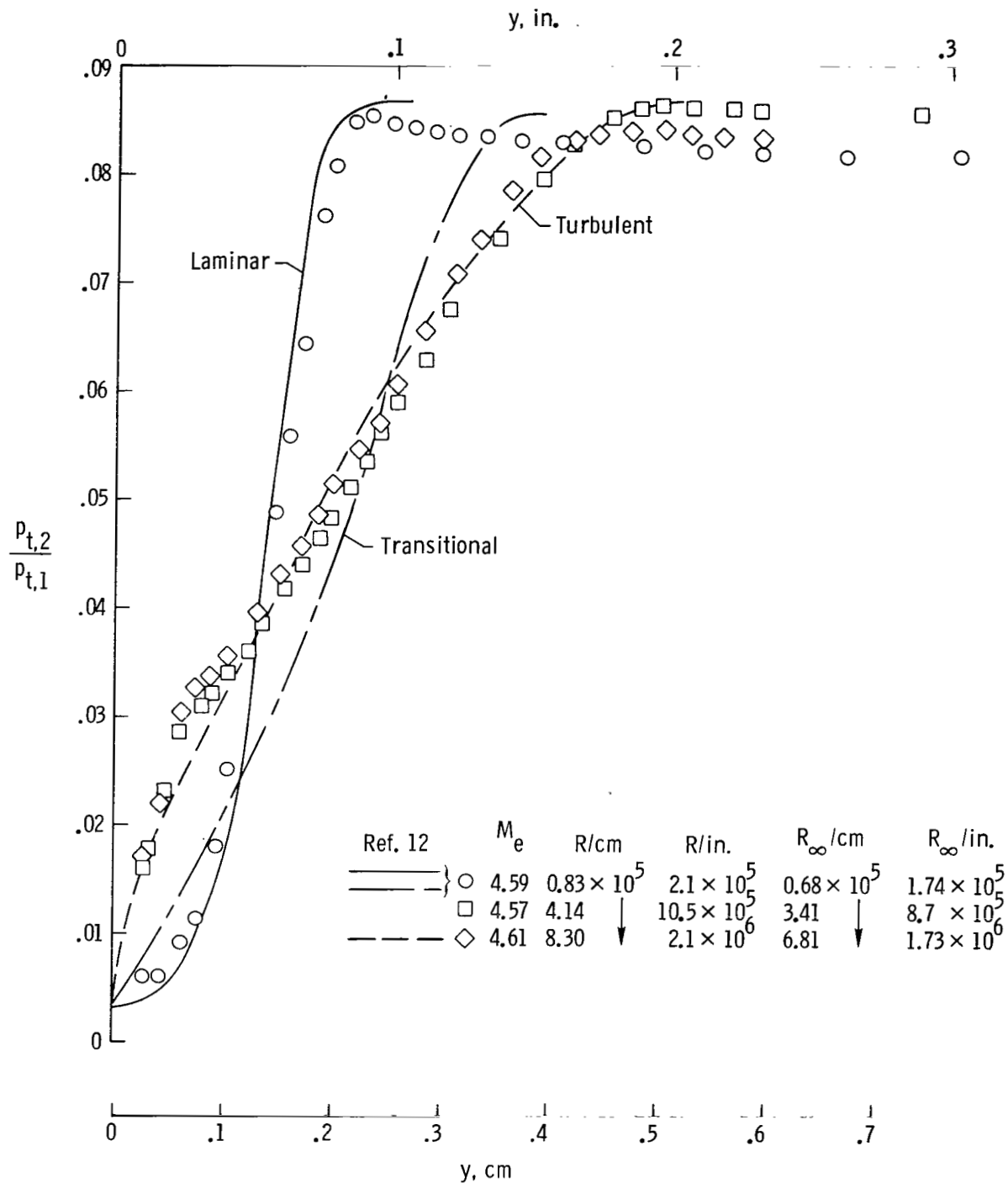
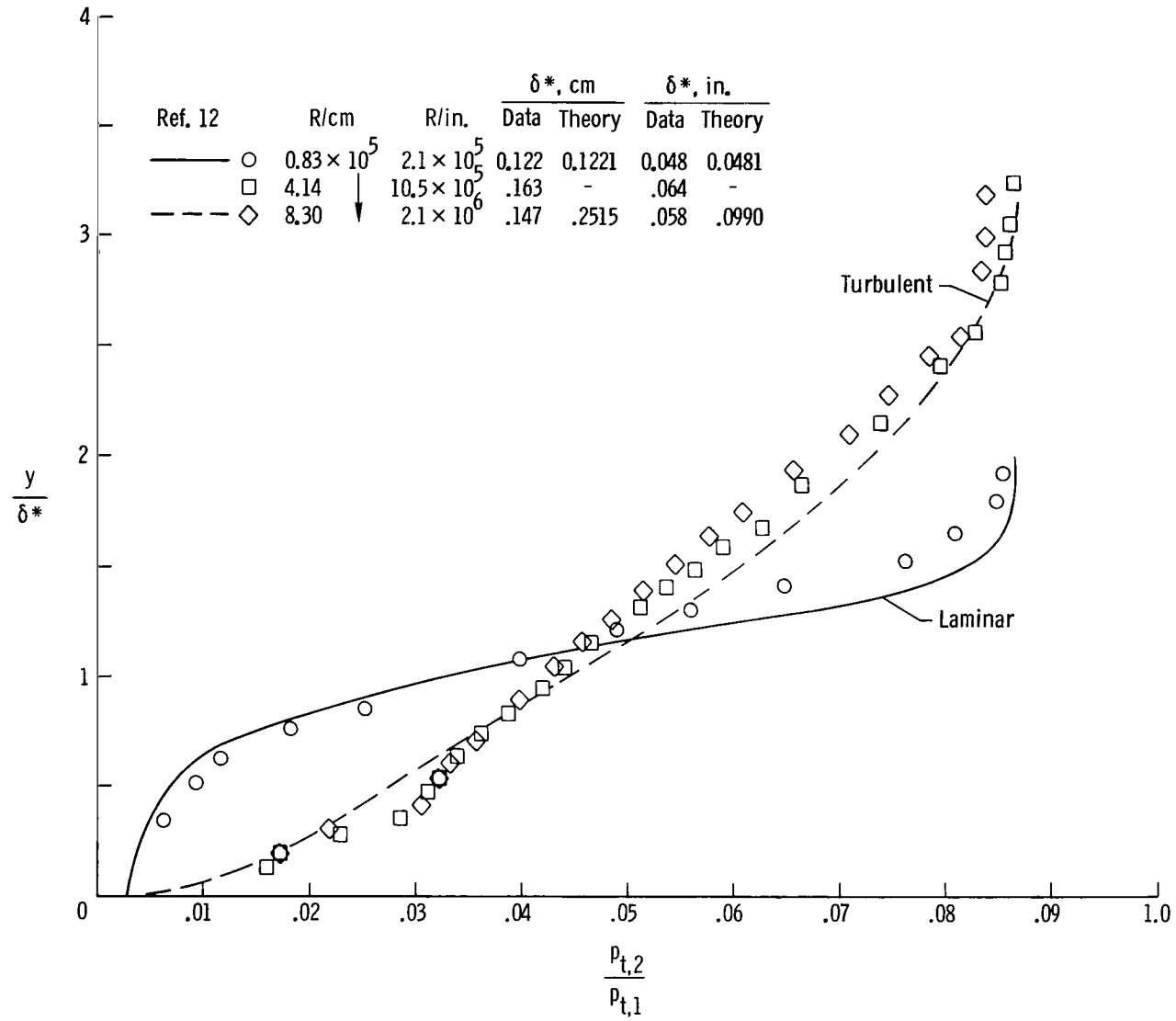


Figure 6.- Effect of temperature profile on calculated velocity profile. No screens,
 $R_\infty = 6.81 \times 10^5$ per centimeter (1.73×10^6 in.), $x = 48.11$ centimeters (18.94 in.).



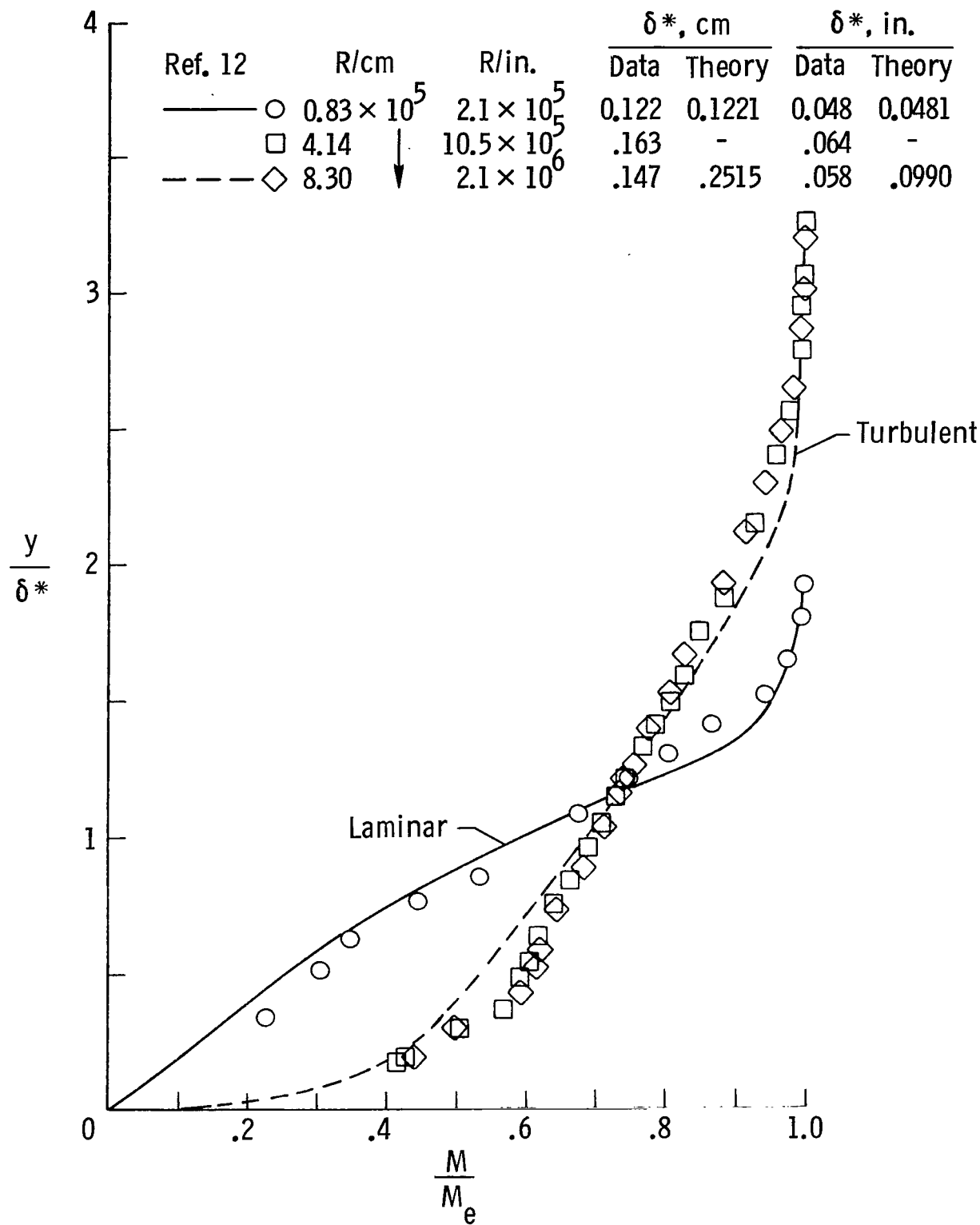
(a) Pitot profiles in physical coordinates.

Figure 7.- Comparison of boundary-layer profiles at $x = 27.15$ centimeters (10.69 in.) with finite-difference method predictions (with settling-chamber screens). $\frac{T_w}{T_{t,1}} = 0.9$.



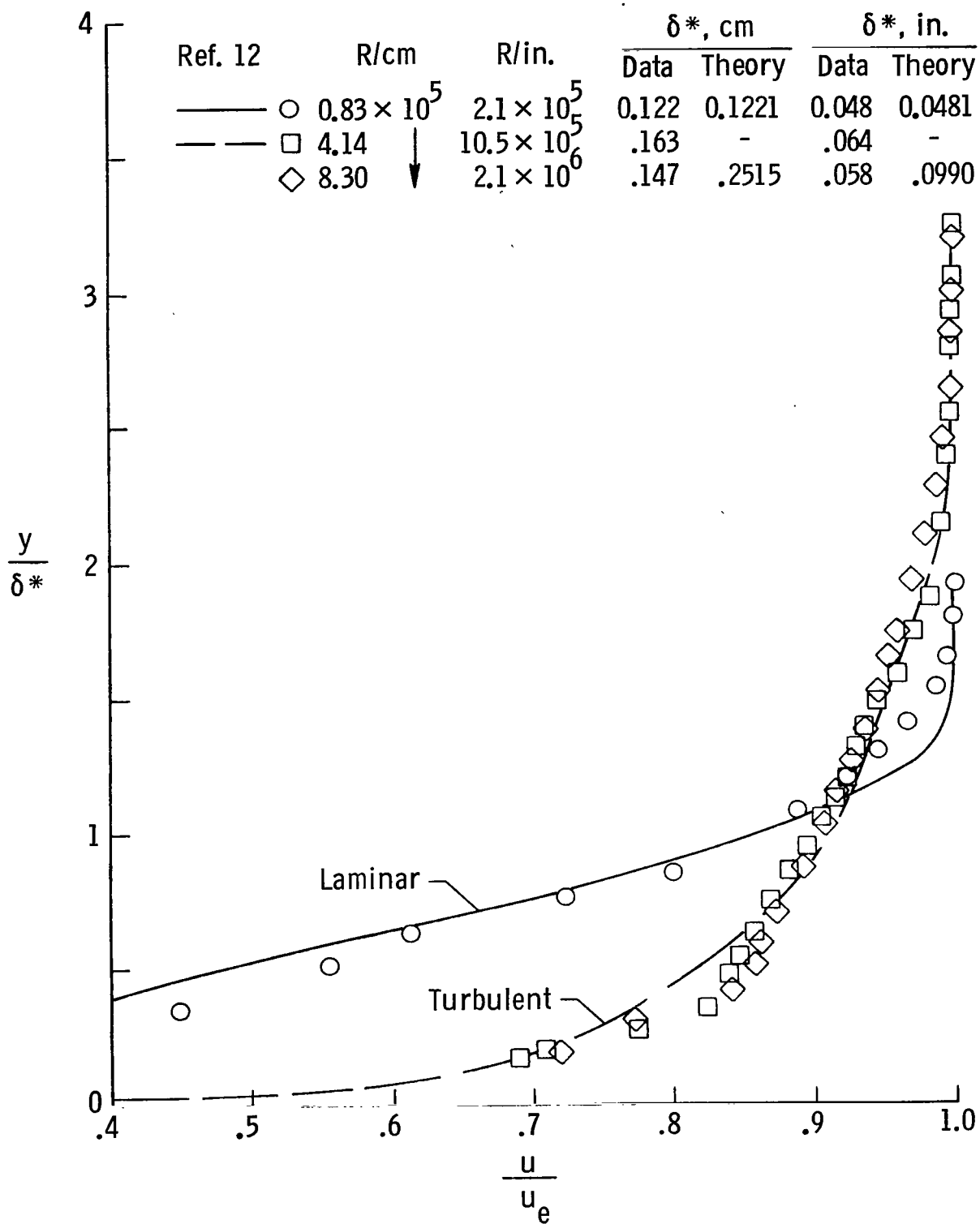
(b) Pitot profiles in similarity coordinates.

Figure 7.- Continued.



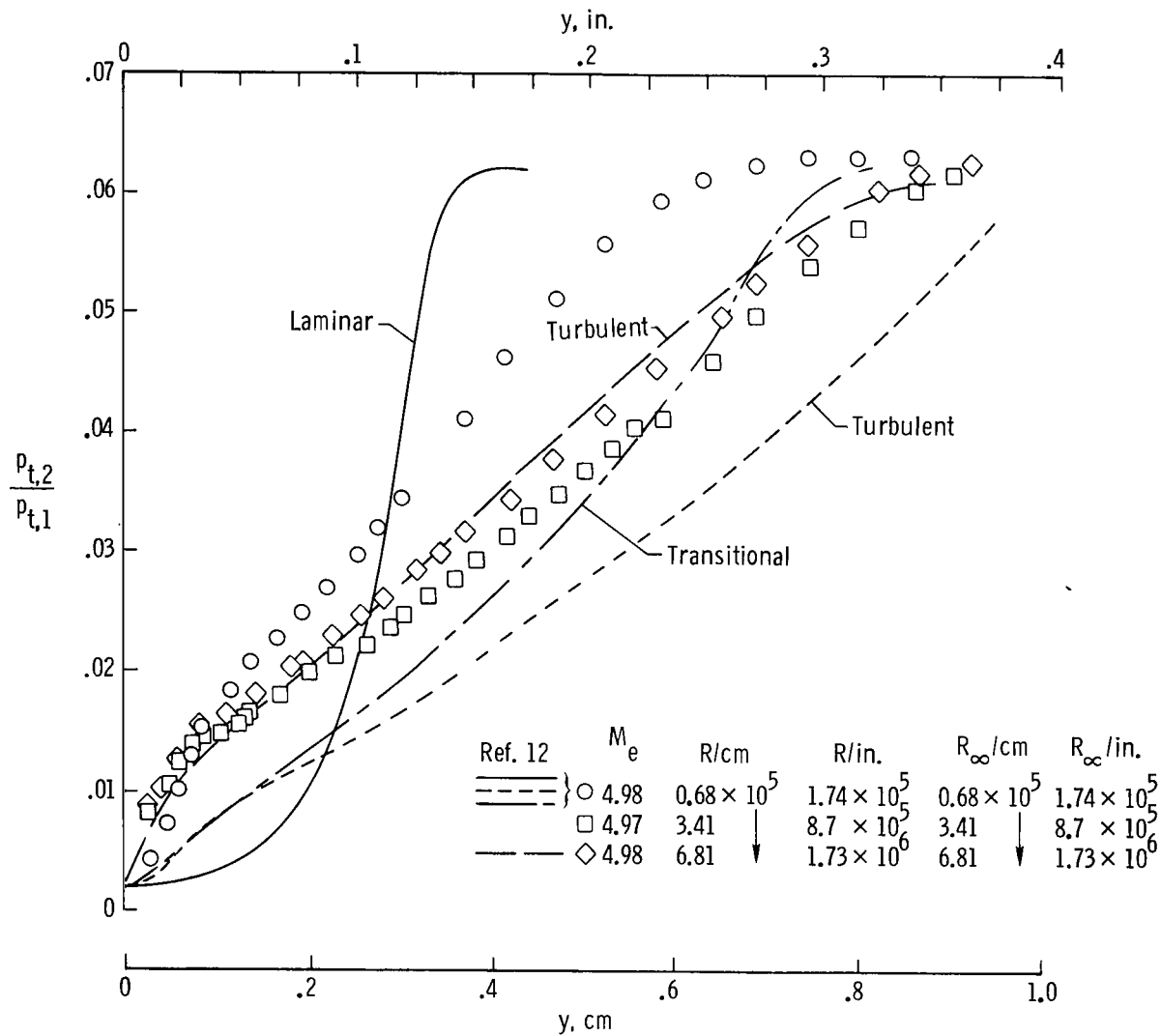
(c) Mach number profiles in similarity coordinates.

Figure 7.- Continued.



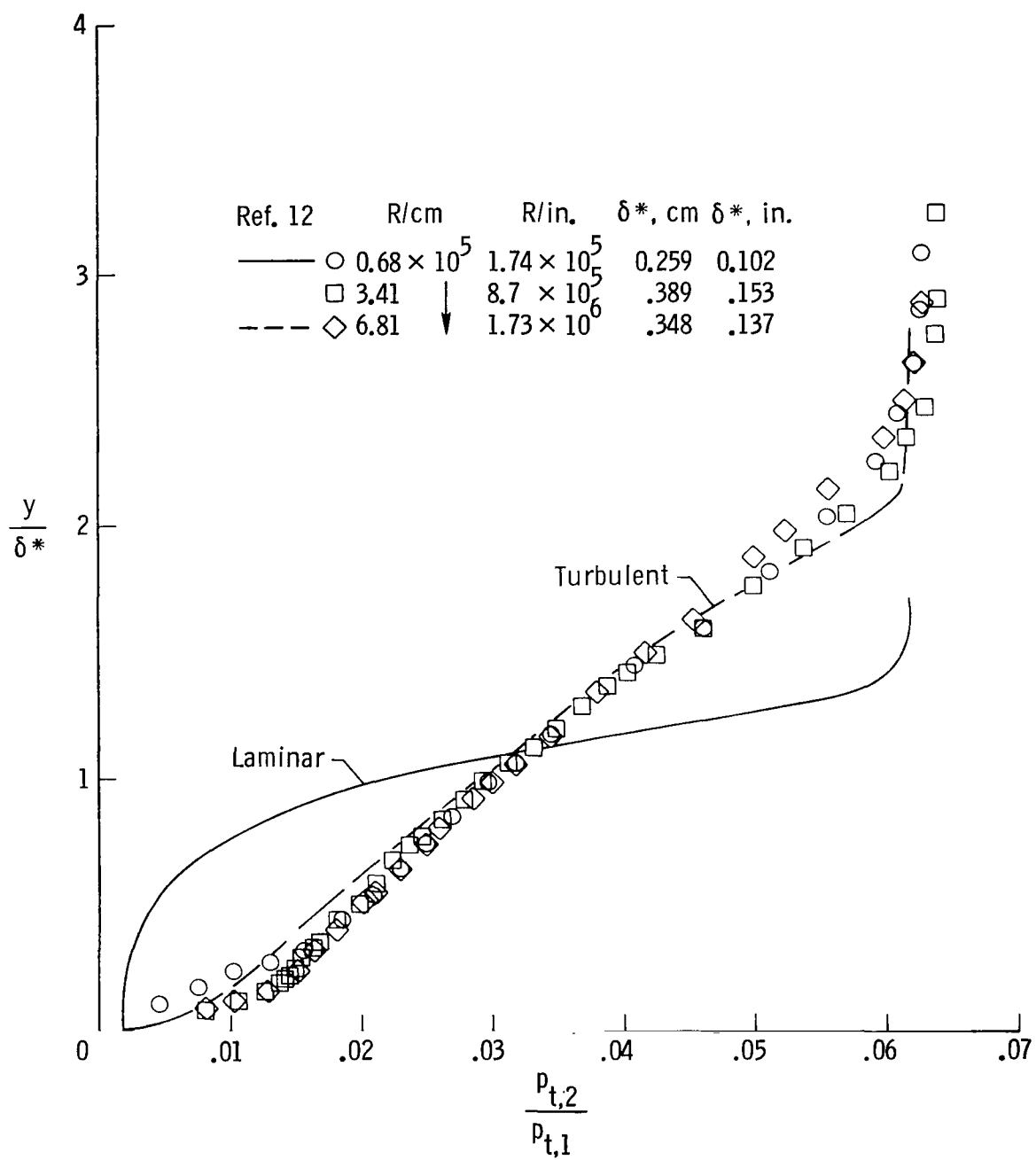
(d) Velocity profiles in similarity coordinates.

Figure 7.- Concluded.



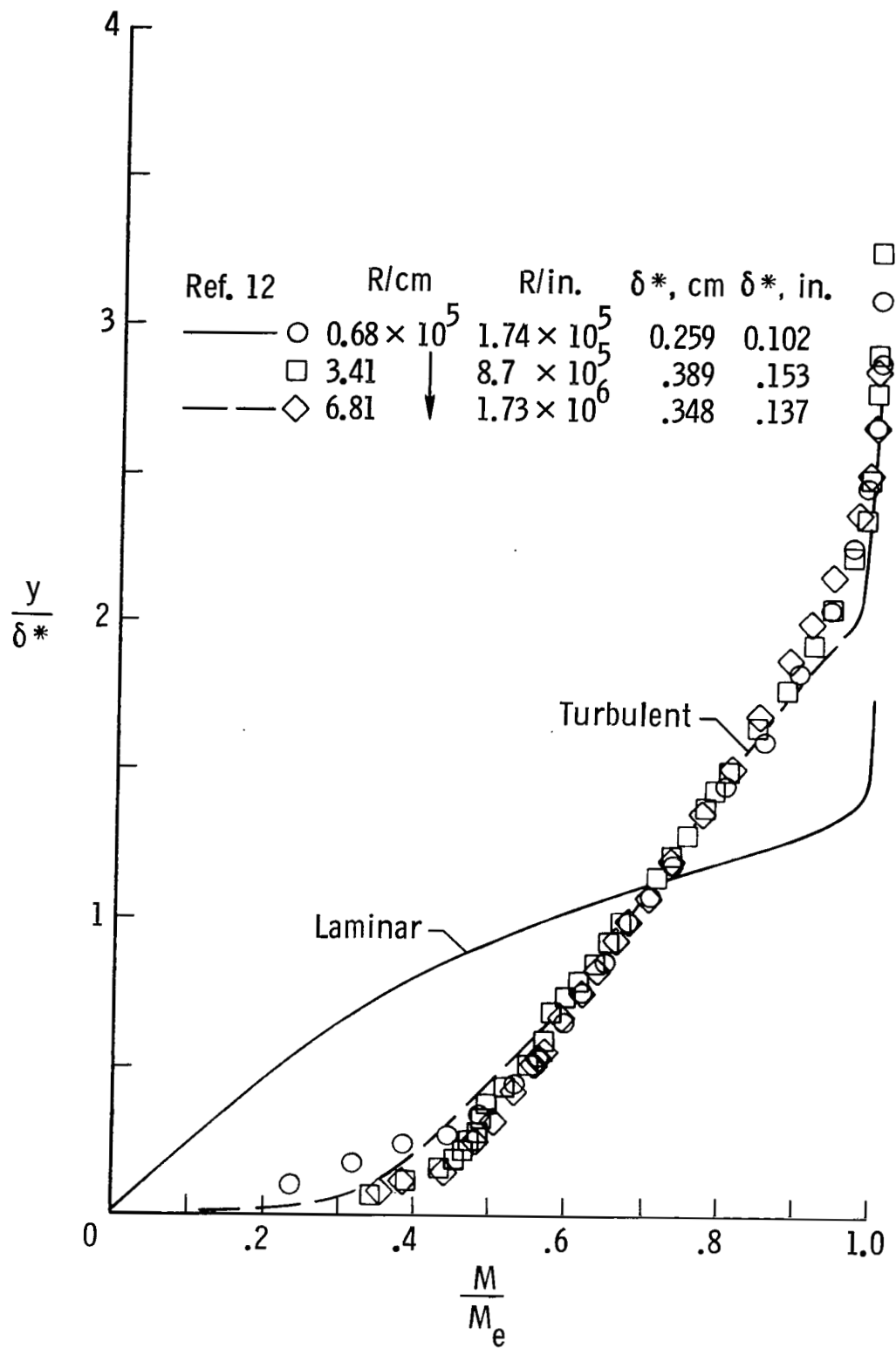
(a) Pitot profiles in physical coordinates.

Figure 8.- Comparison of boundary-layer profiles at $x = 48.1$ centimeters (18.94 in.) with finite-difference method predictions (with settling-chamber screens). $\frac{T_w}{T_{t,1}} = 0.9$.



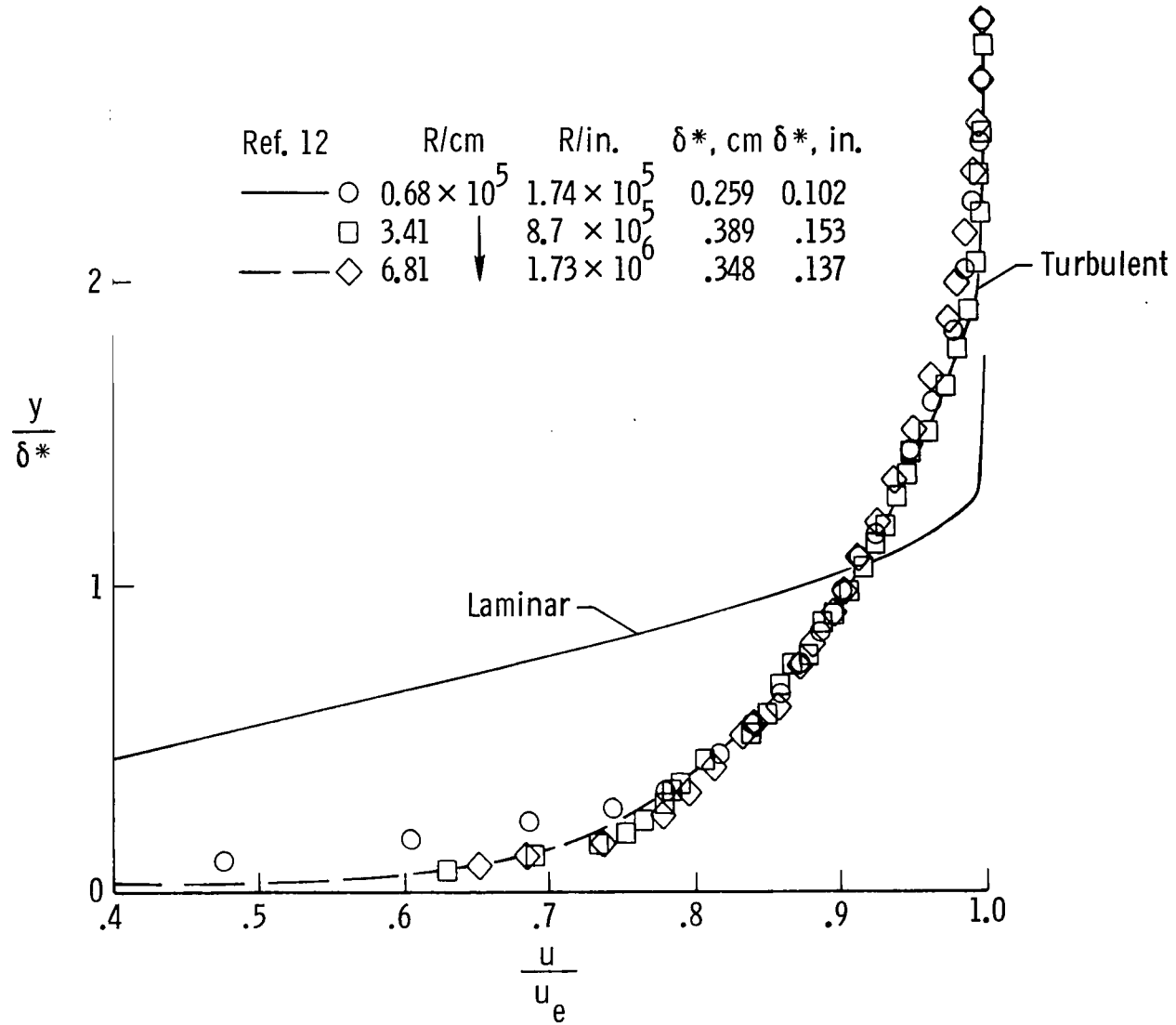
(b) Pitot profiles in similarity coordinates.

Figure 8.- Continued.



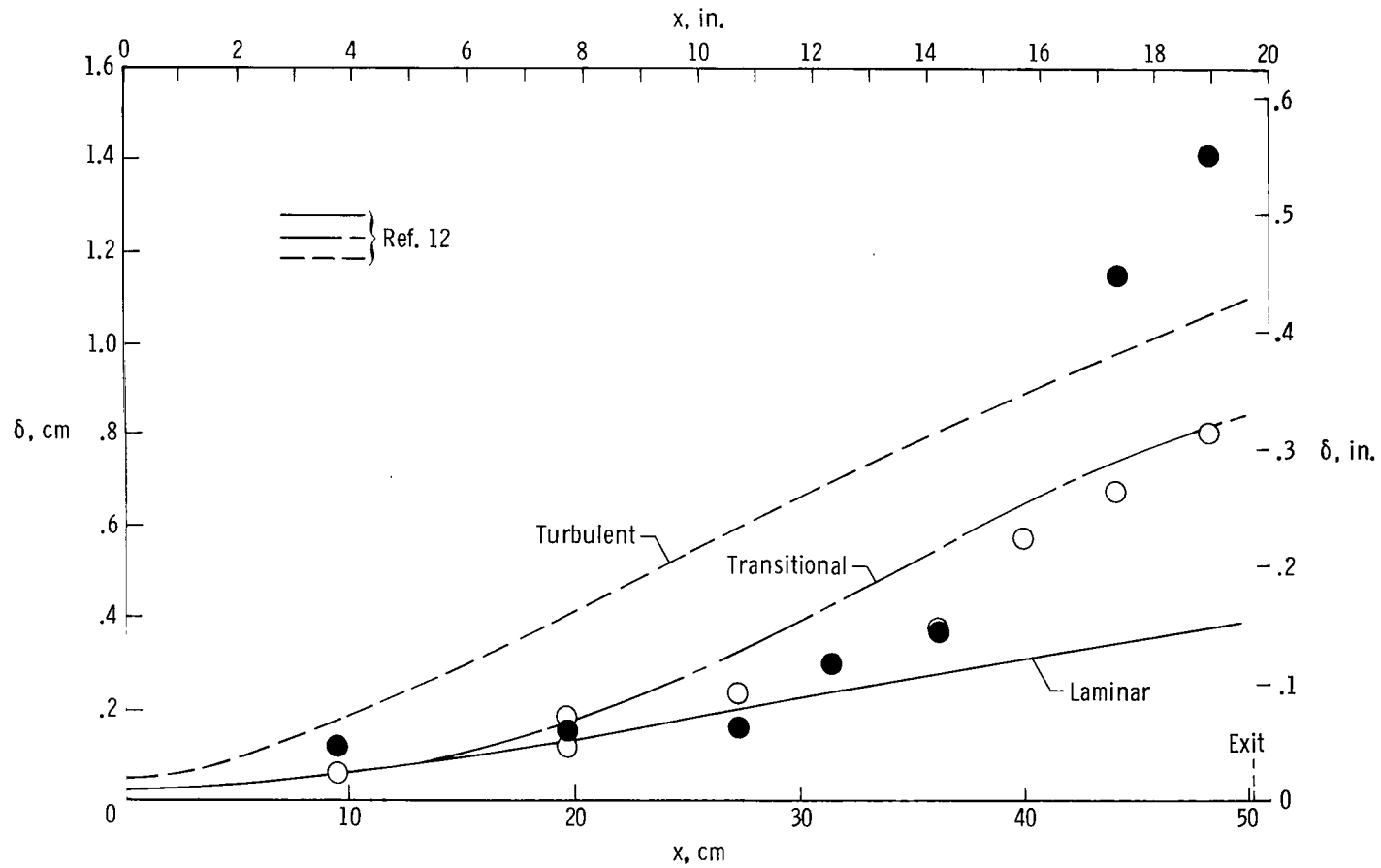
(c) Mach number profiles in similarity coordinates.

Figure 8.- Continued.



(d) Velocity profiles in similarity coordinates.

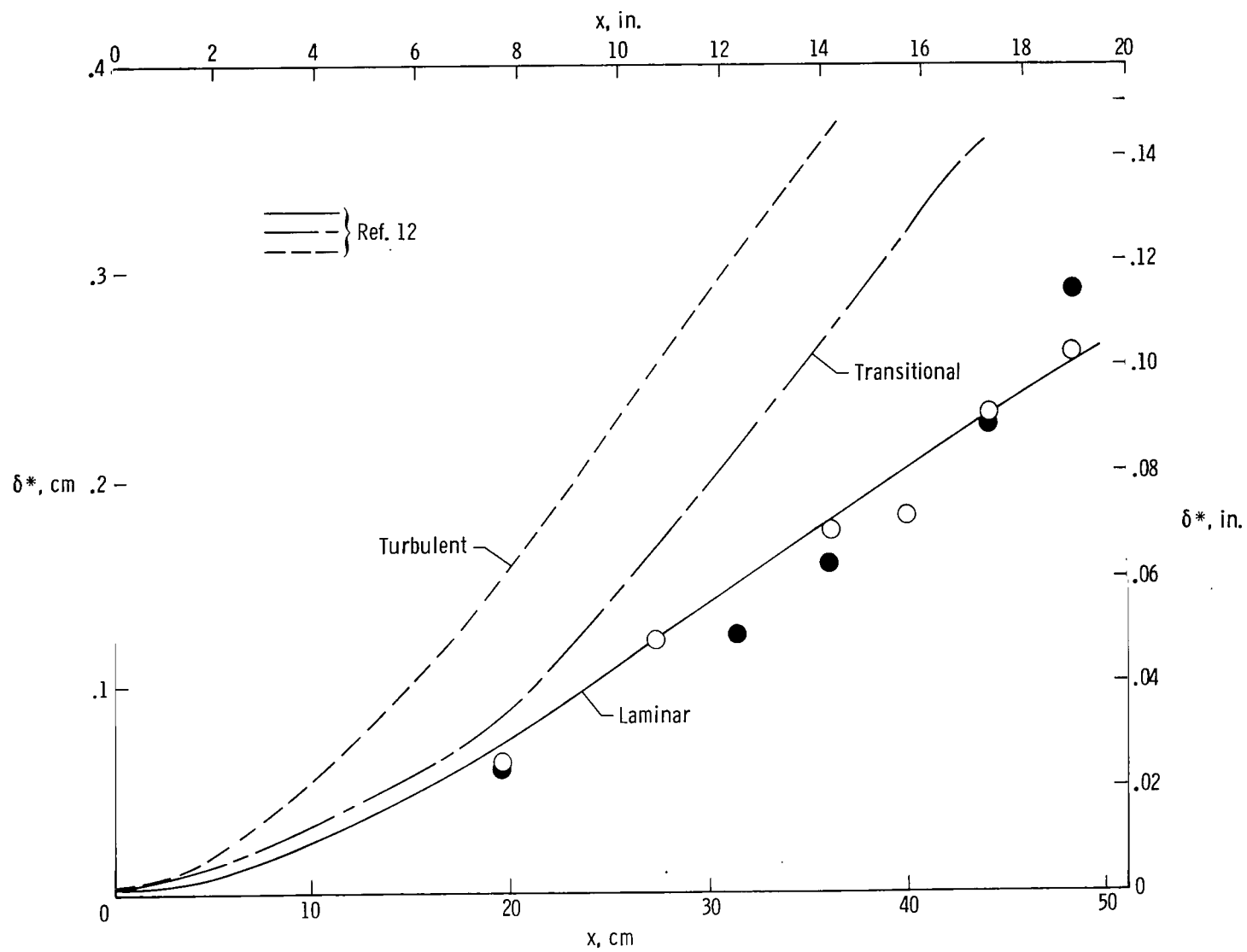
Figure 8.- Concluded.



(a) Boundary-layer thickness.

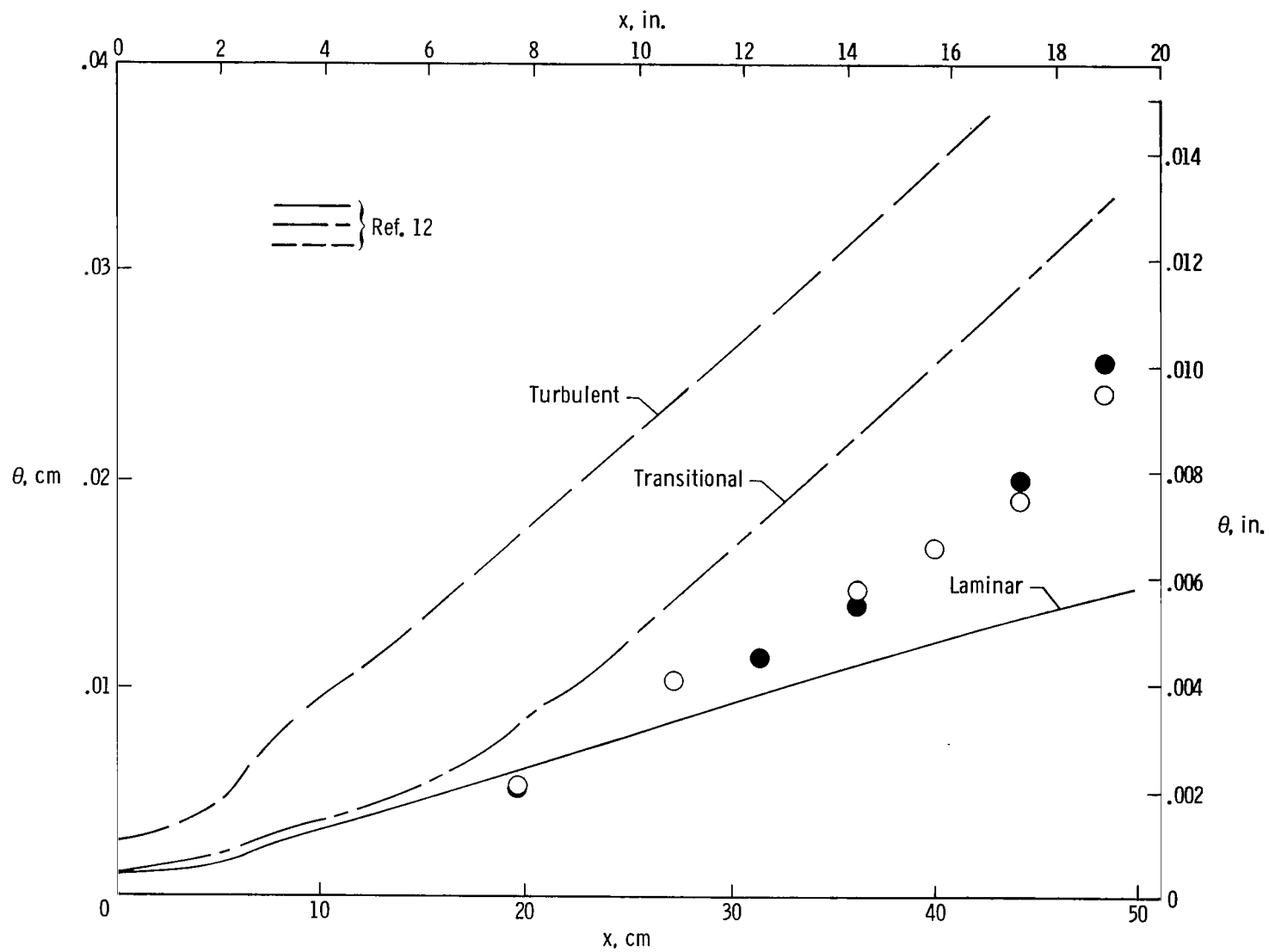
Figure 9.- Boundary-layer thickness and integral parameters along the nozzle wall.

$R_{\infty} = 0.68 \times 10^5$ per centimeter ($1.73 \times 10^5/\text{in.}$). (Filled symbols, no screens.)



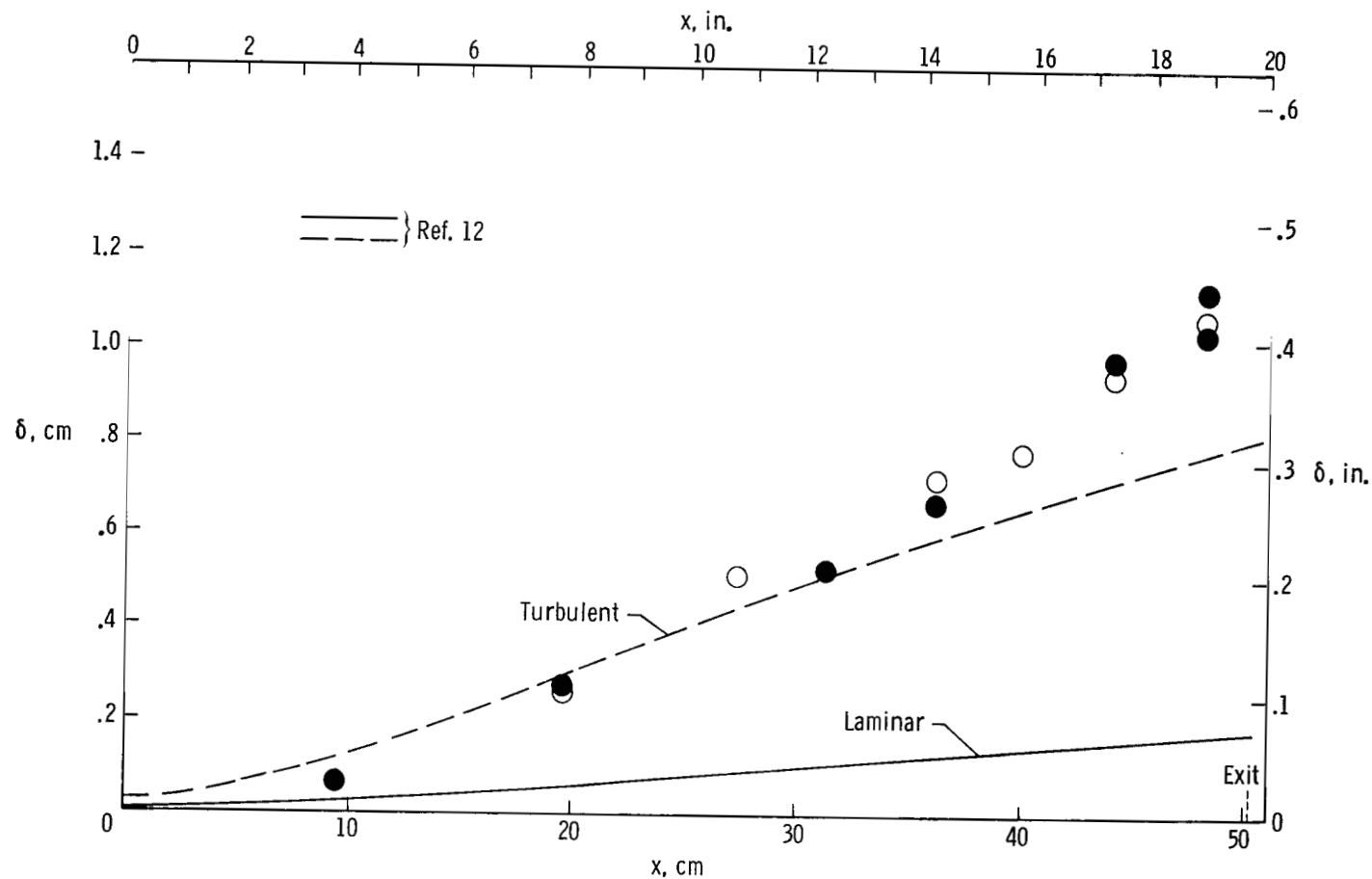
(b) Displacement thickness.

Figure 9.- Continued.



(c) Momentum thickness.

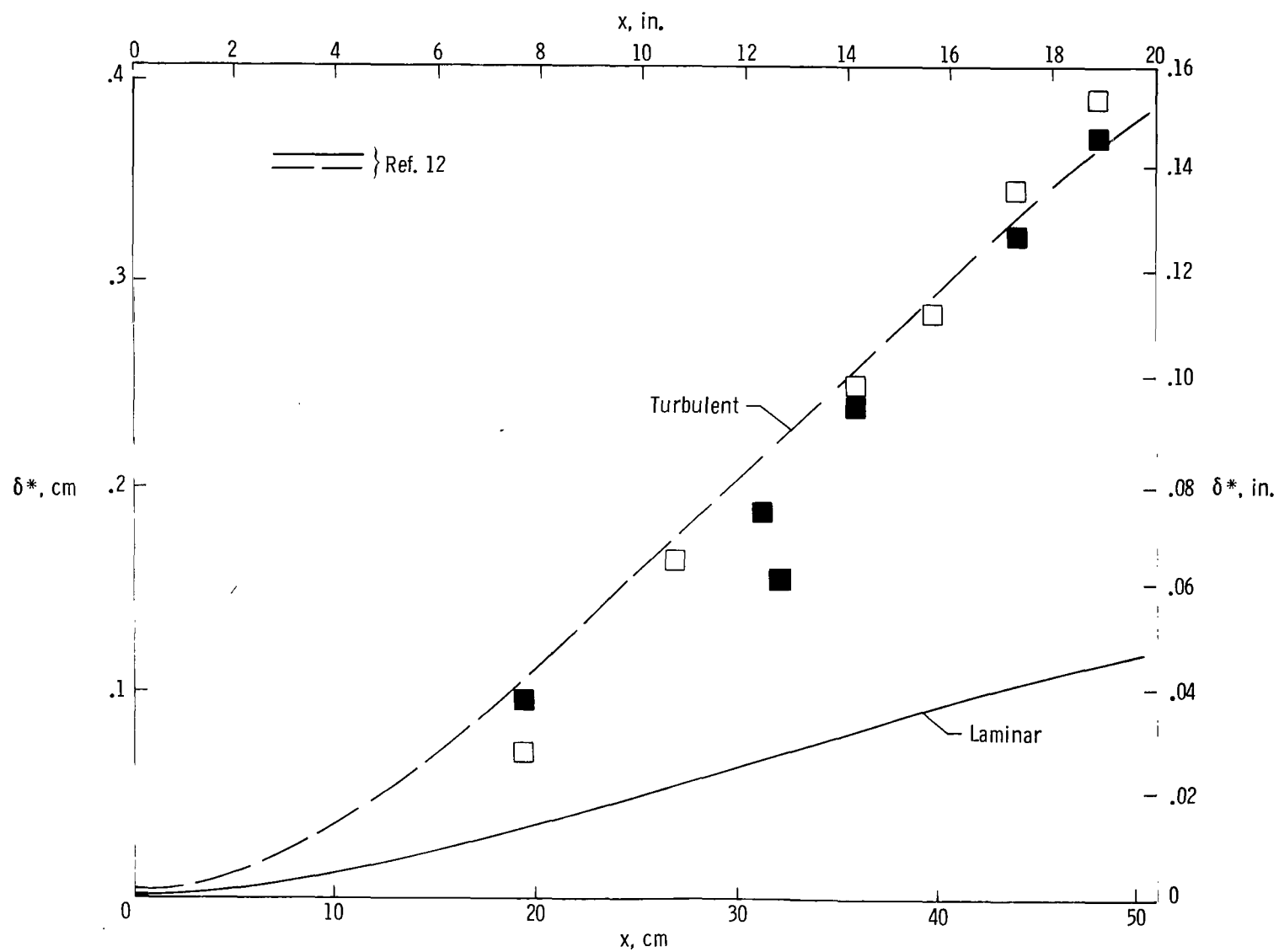
Figure 9.- Concluded.



(a) Boundary-layer thickness.

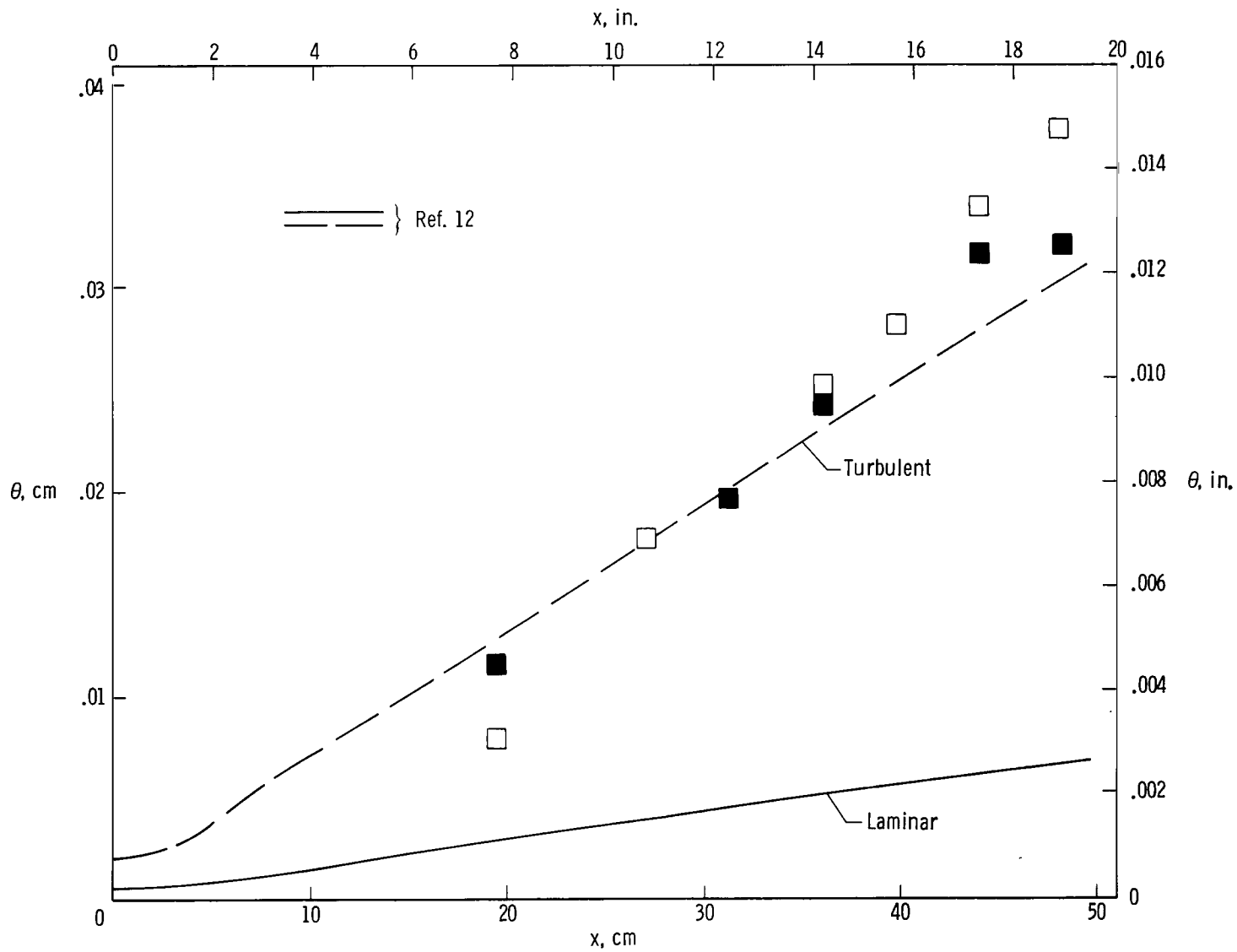
Figure 10.- Boundary-layer thickness and integral parameters along the nozzle wall.

$R_{\infty} = 3.41 \times 10^5$ per centimeter (8.7×10^5 /in.). (Filled symbols, no screens.)



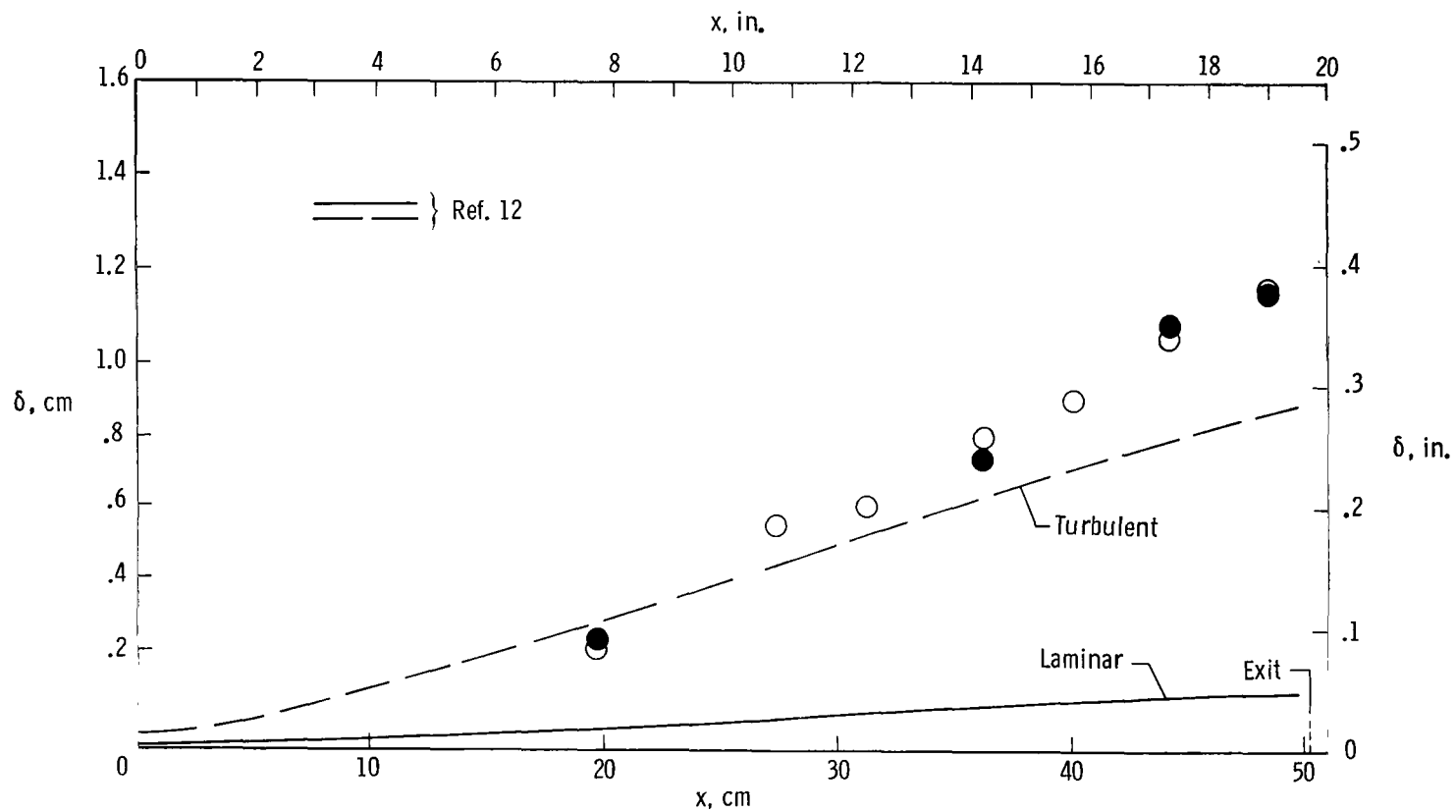
(b) Displacement thickness.

Figure 10.- Continued.



(c) Momentum thickness.

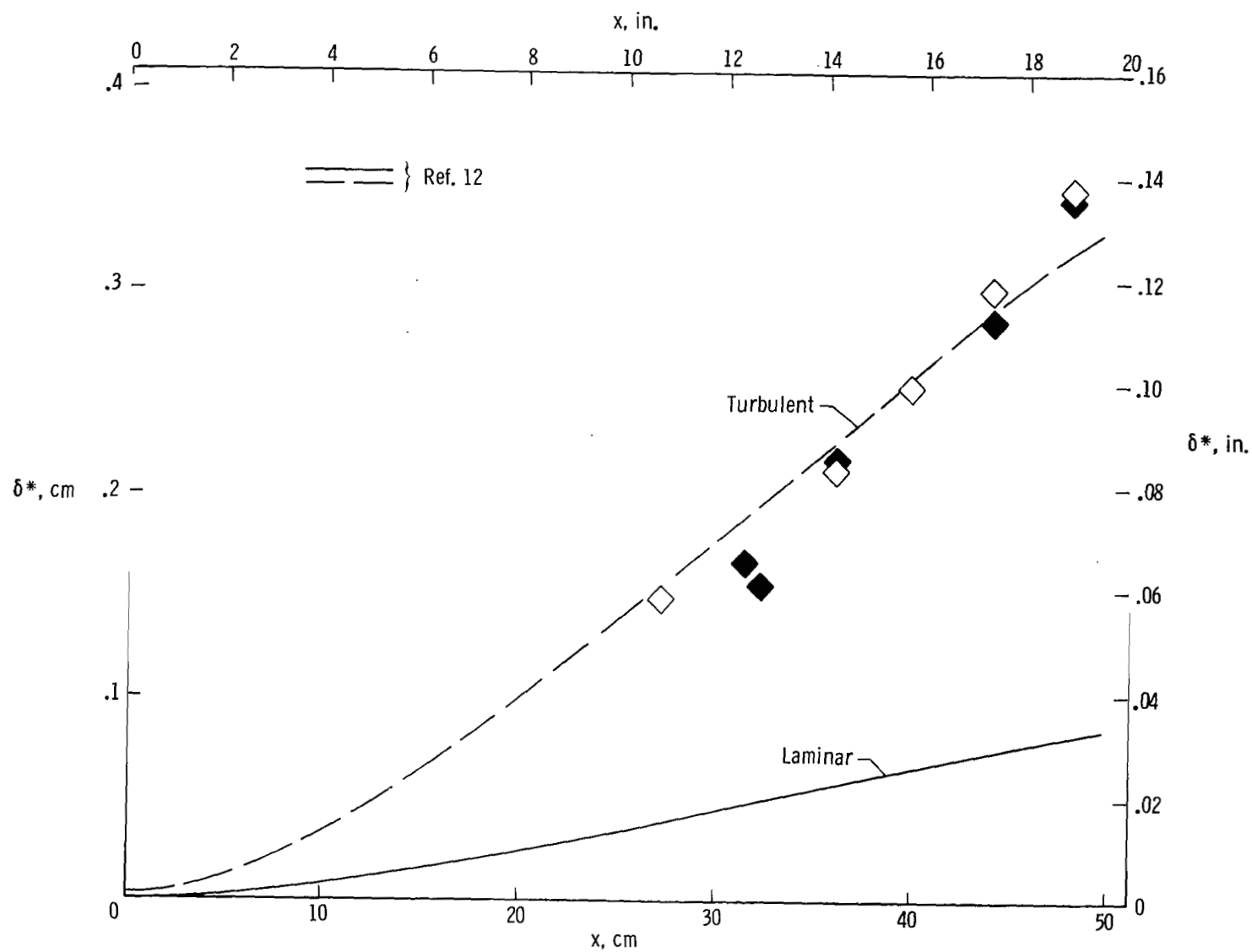
Figure 10.- Concluded.



(a) Boundary-layer thickness.

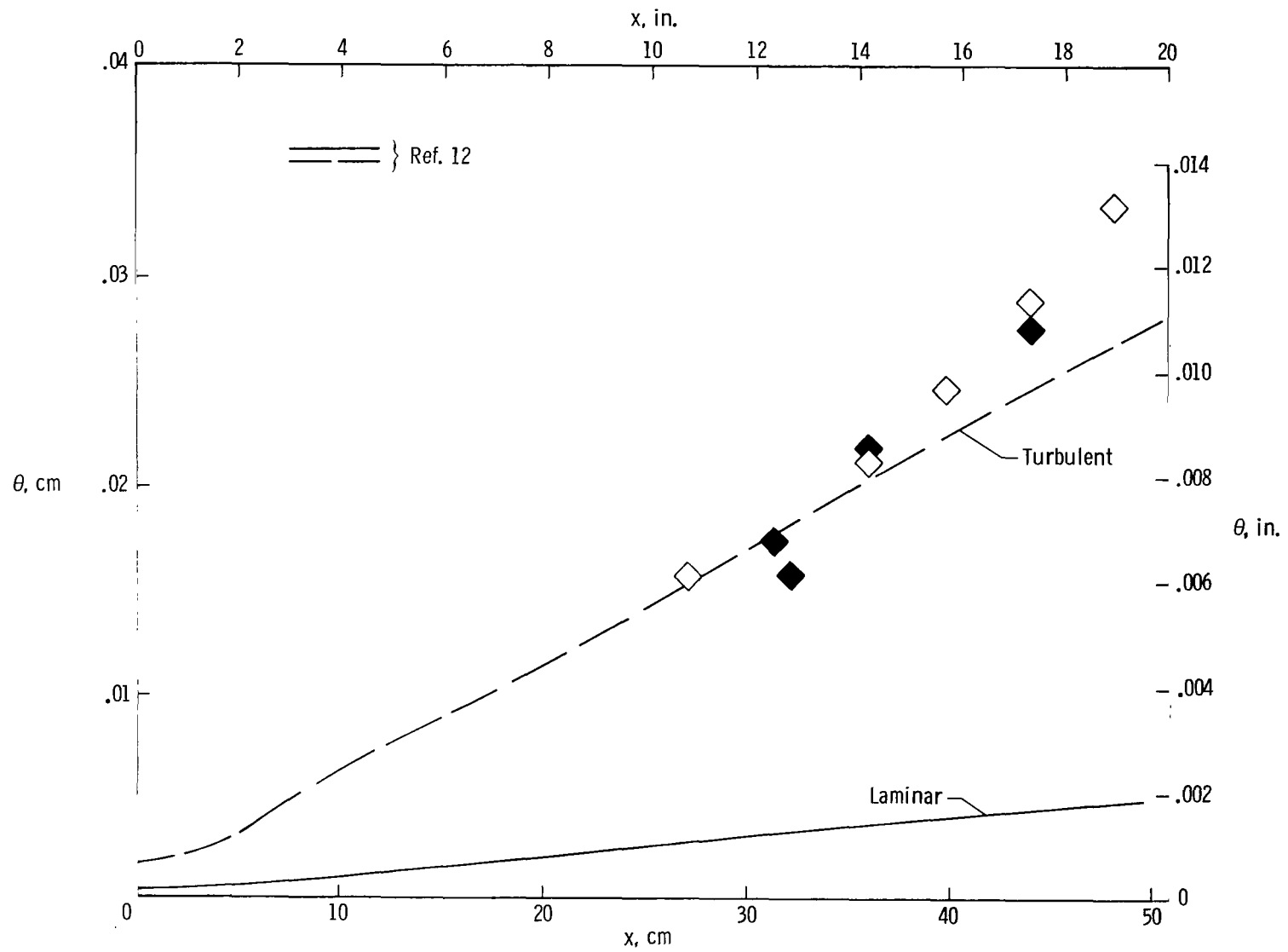
Figure 11.- Boundary-layer thickness and integral parameters along the nozzle wall.

$R_{\infty} = 6.81 \times 10^5$ per centimeter (1.73×10^6 /in.). (Filled symbols, no screens.)



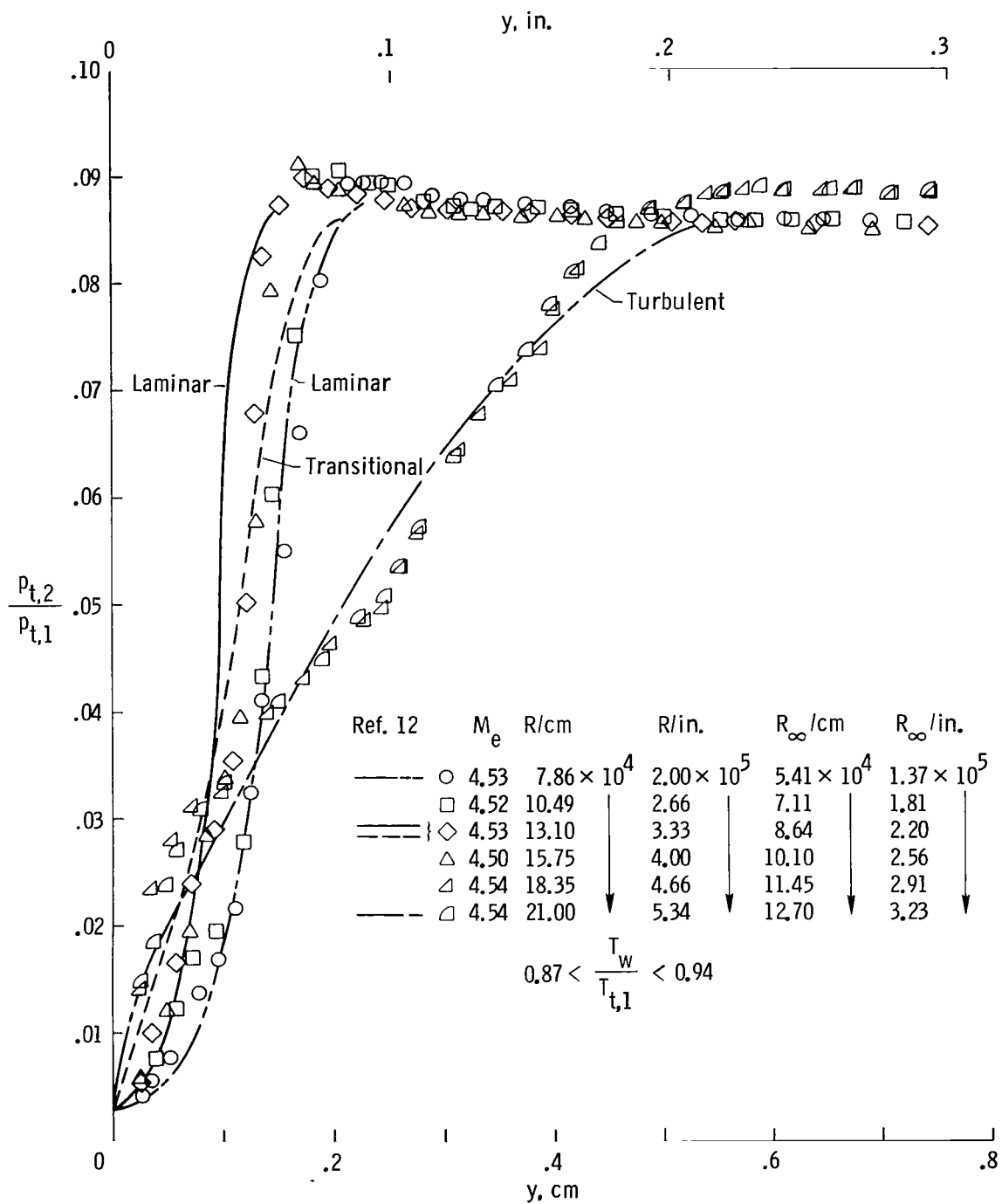
(b) Displacement thickness.

Figure 11.- Continued.



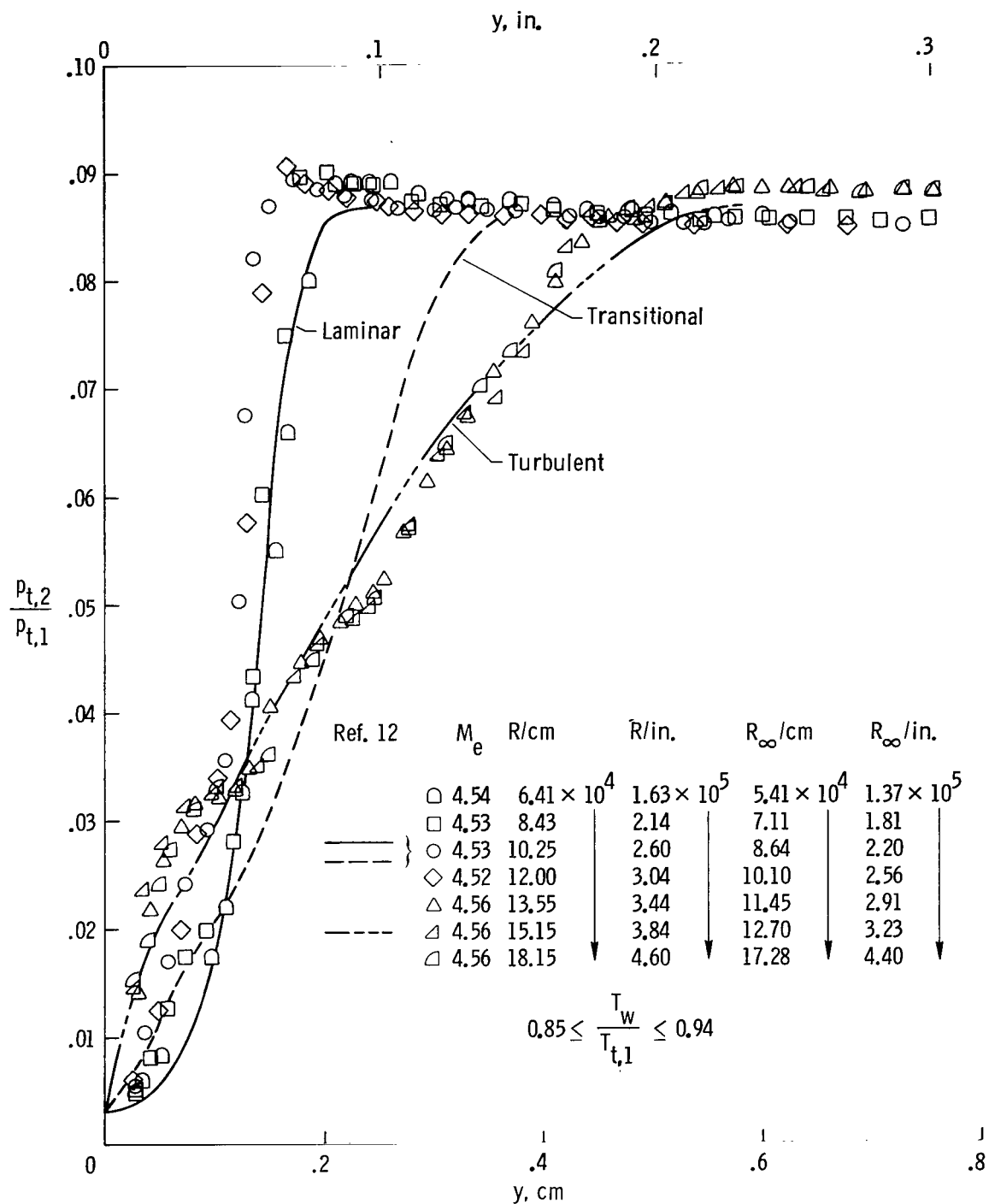
(c) Momentum thickness.

Figure 11.- Concluded.



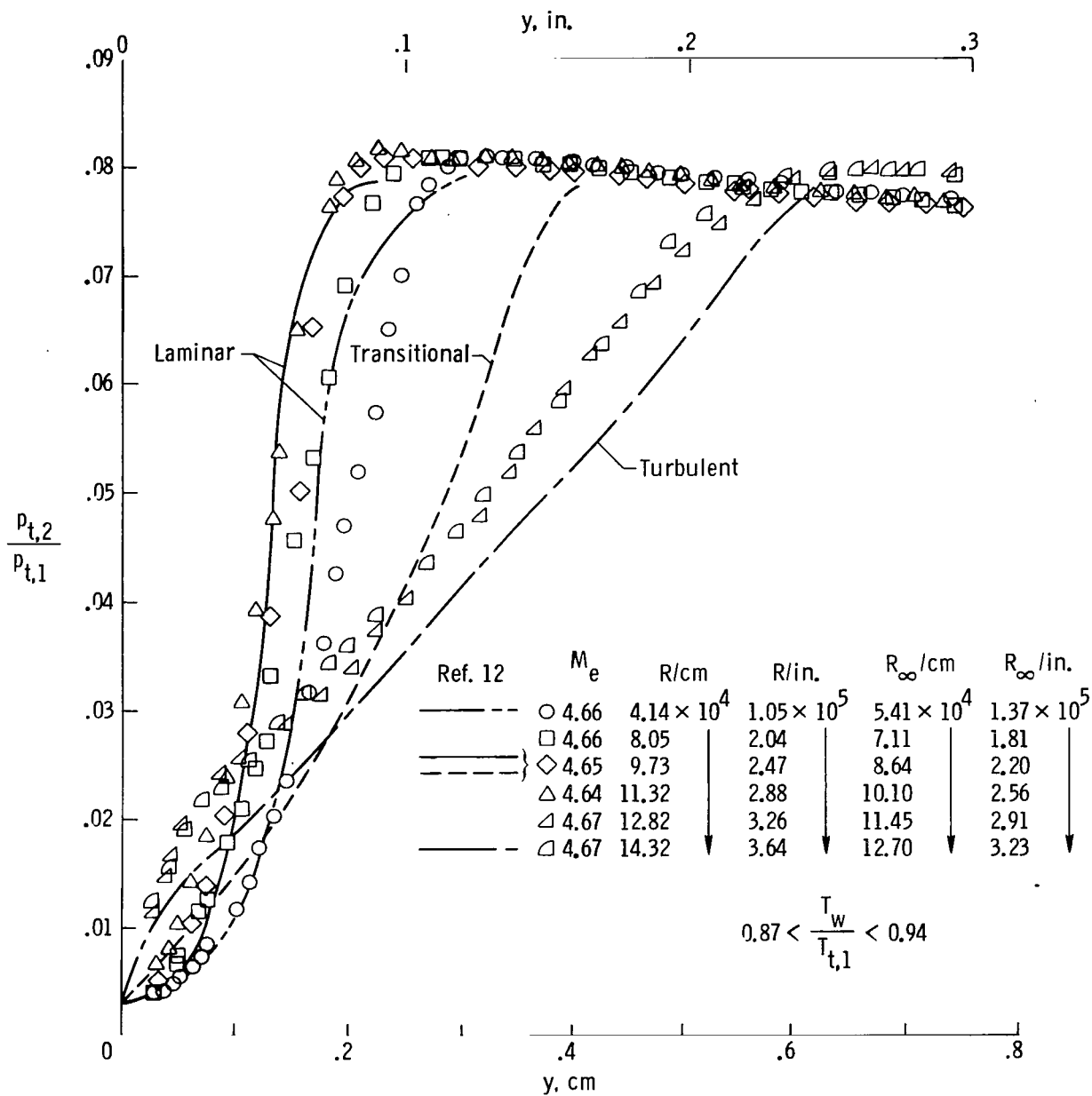
(a) Pitot profiles in physical coordinates, $x = 22.1$ centimeters (8.7 in.).

Figure 12.- Variation of laminar to turbulent flow over low Reynolds number range.



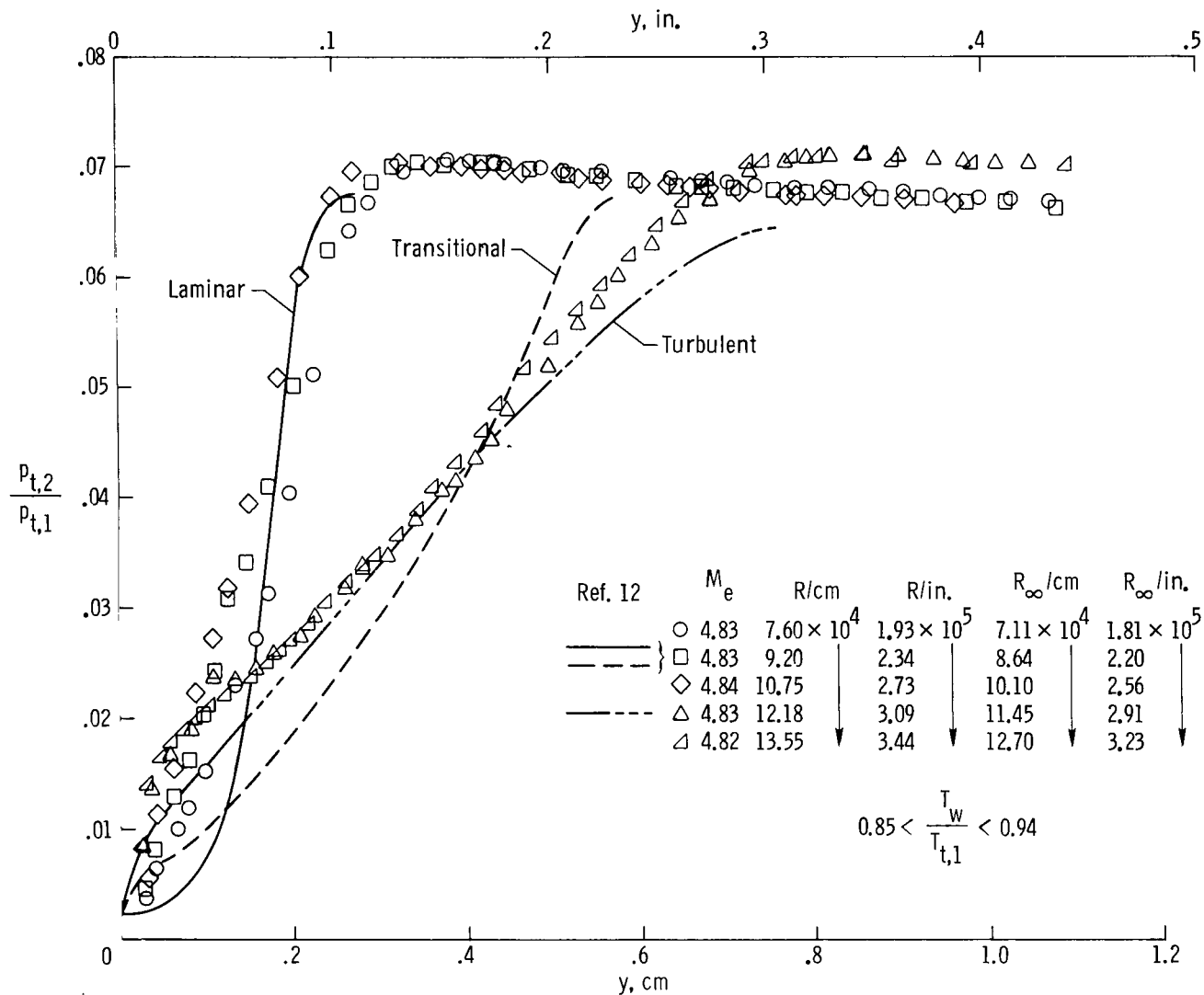
(b) Pitot profiles in physical coordinates, $x = 27.2$ centimeters (10.69 in.).

Figure 12.- Continued.



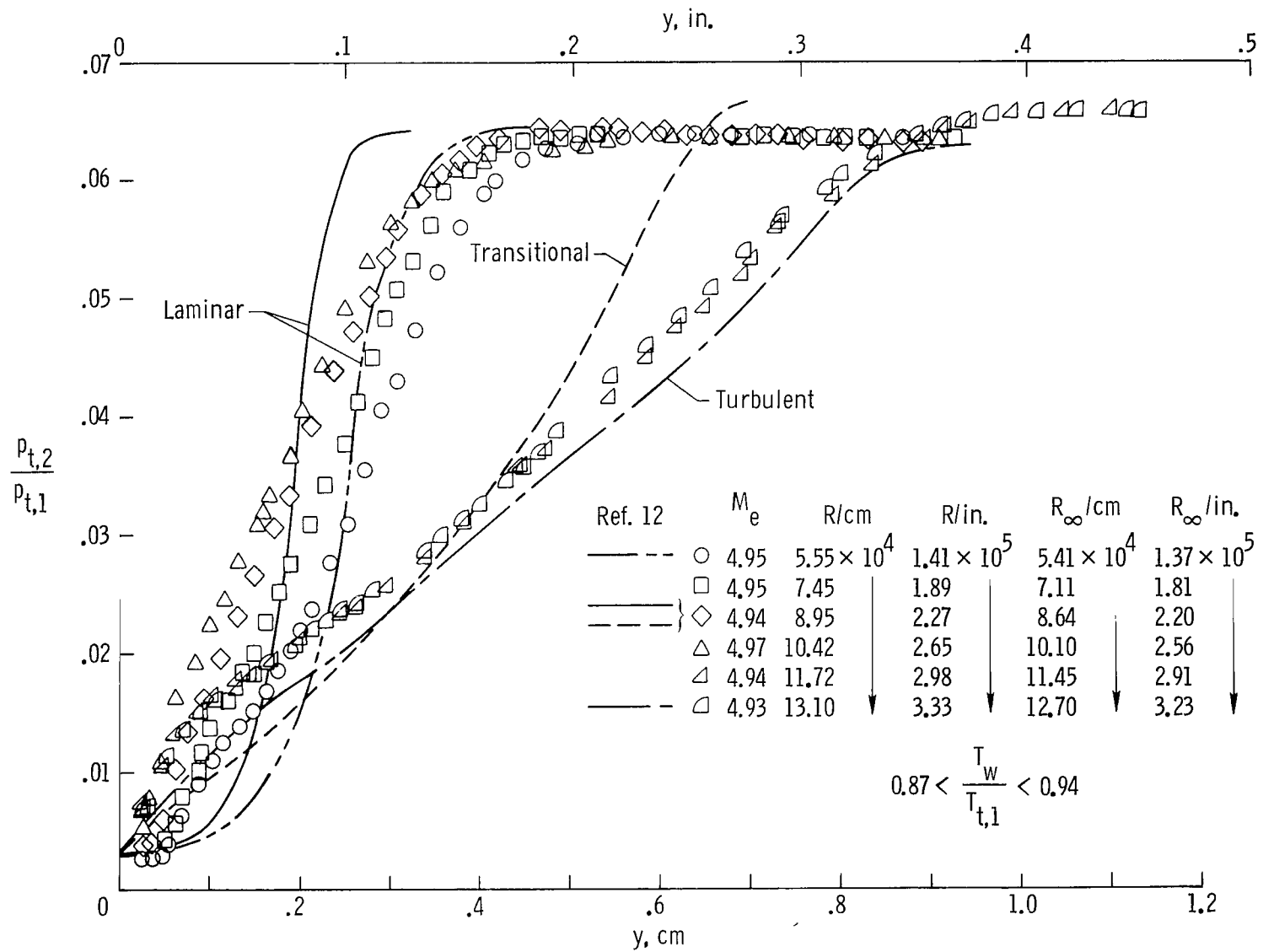
(c) Pitot profiles in physical coordinates, $x = 31.0$ centimeters (12.2 in.).

Figure 12.- Continued.



(d) Pitot profiles in physical coordinates, $x = 37.4$ centimeters (14.69 in.).

Figure 12.- Continued.



(e) Pitot profiles in physical coordinates, $x = 42.9$ centimeters (16.9 in.).

Figure 12.- Continued.

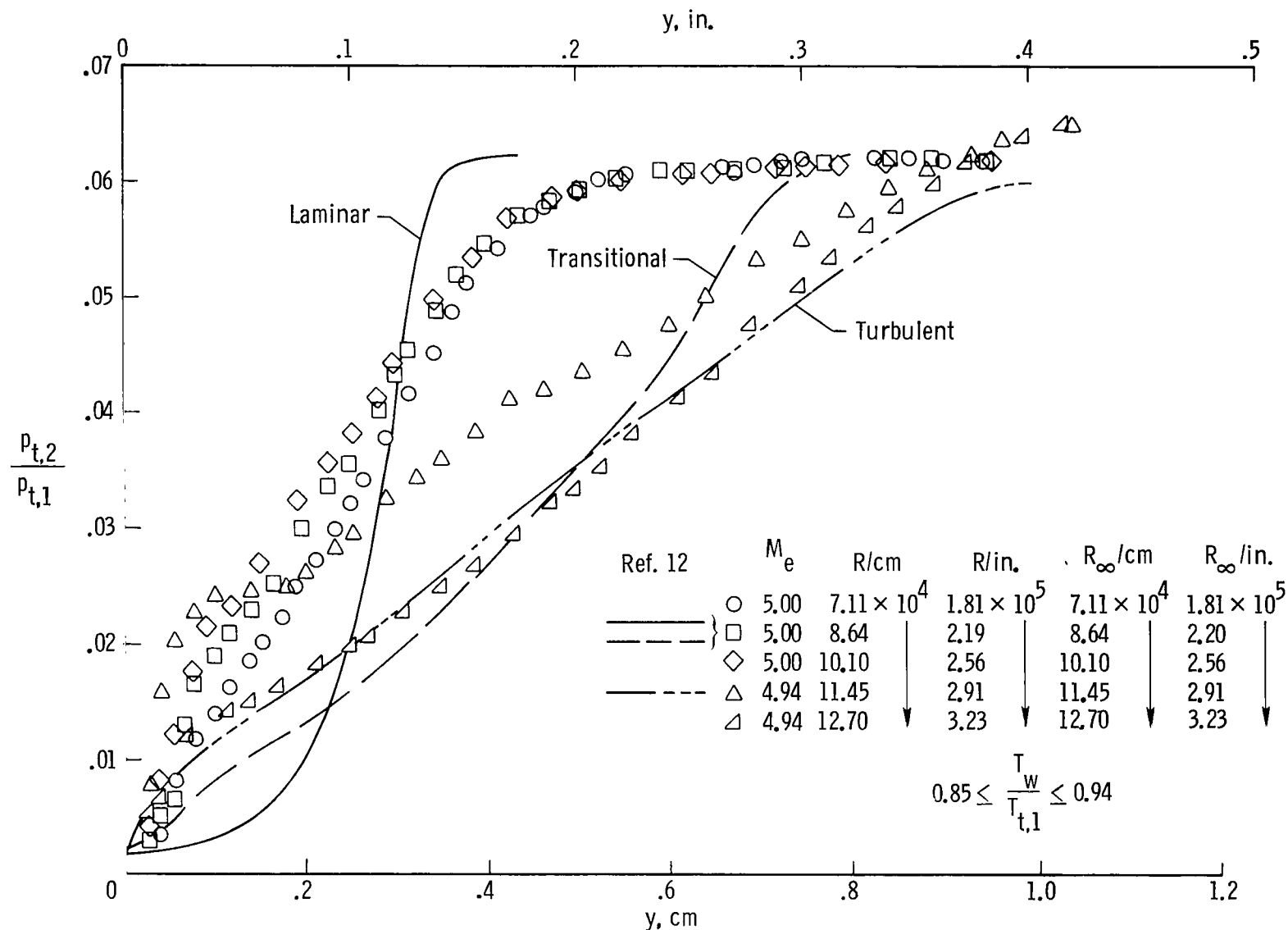
(f) Pitot profiles in physical coordinates, $x = 48.1$ centimeters (18.94 in.).

Figure 12.- Concluded.

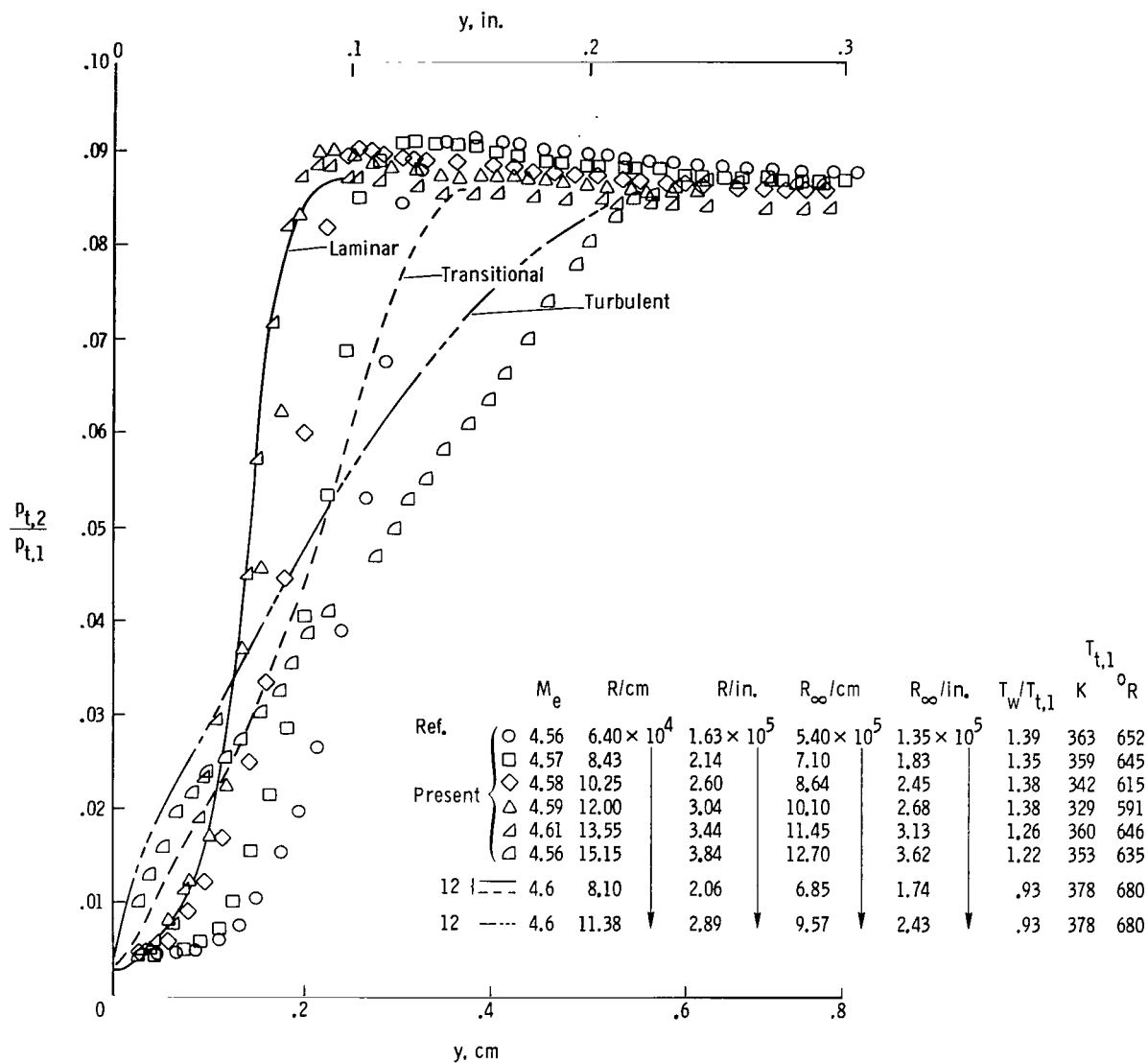
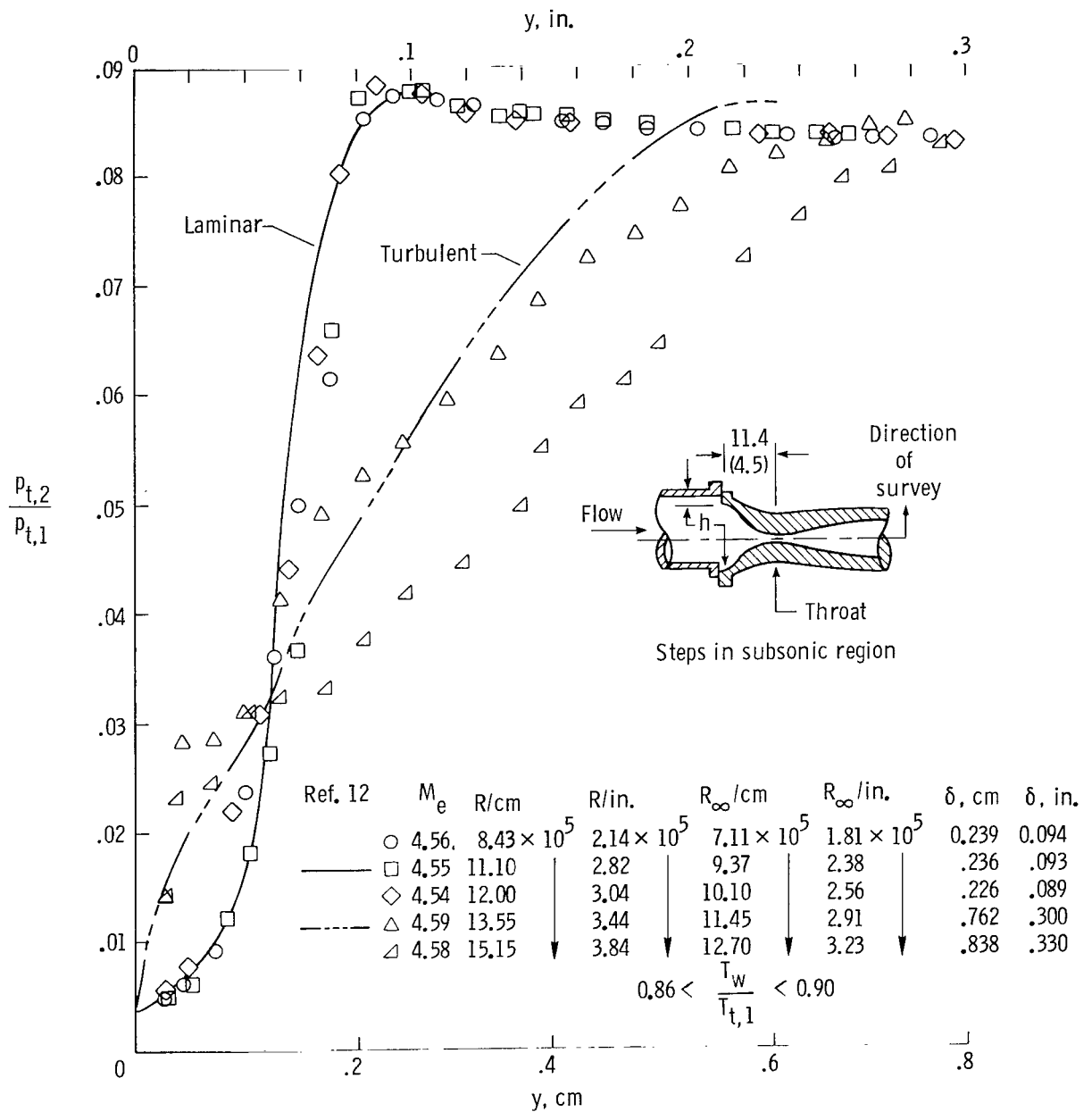
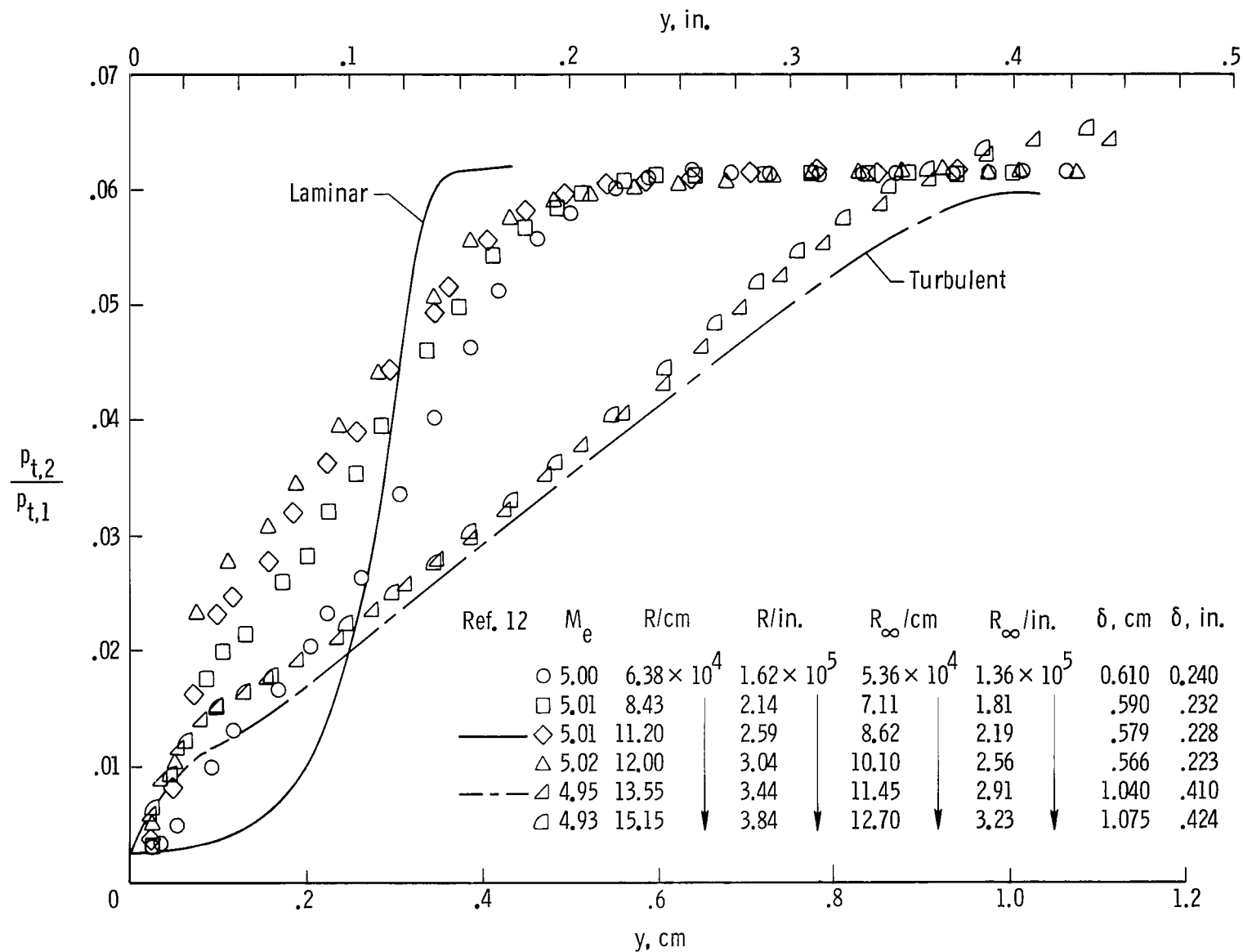


Figure 13.- Boundary-layer pitot profiles with heated nozzle wall.
 $x = 27.18$ centimeters (10.69 in.).



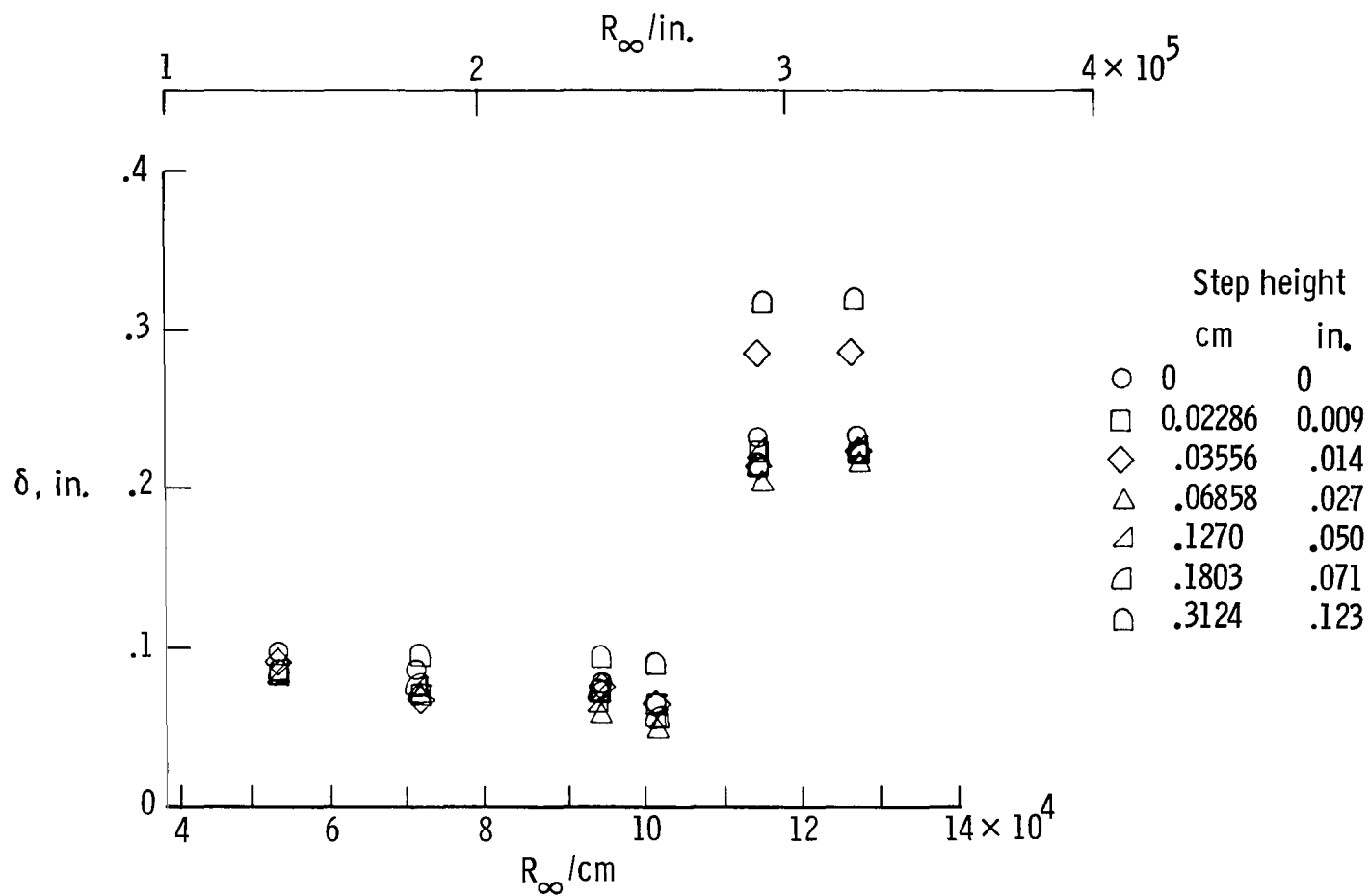
(a) Station $x = 27.2$ centimeters (10.7 in.); $h = 0.3124$ centimeters (0.123 in.).

Figure 14.- Effect of two-dimensional step at top and bottom of subsonic approach to nozzle throat. Screen configuration 1 (table III).



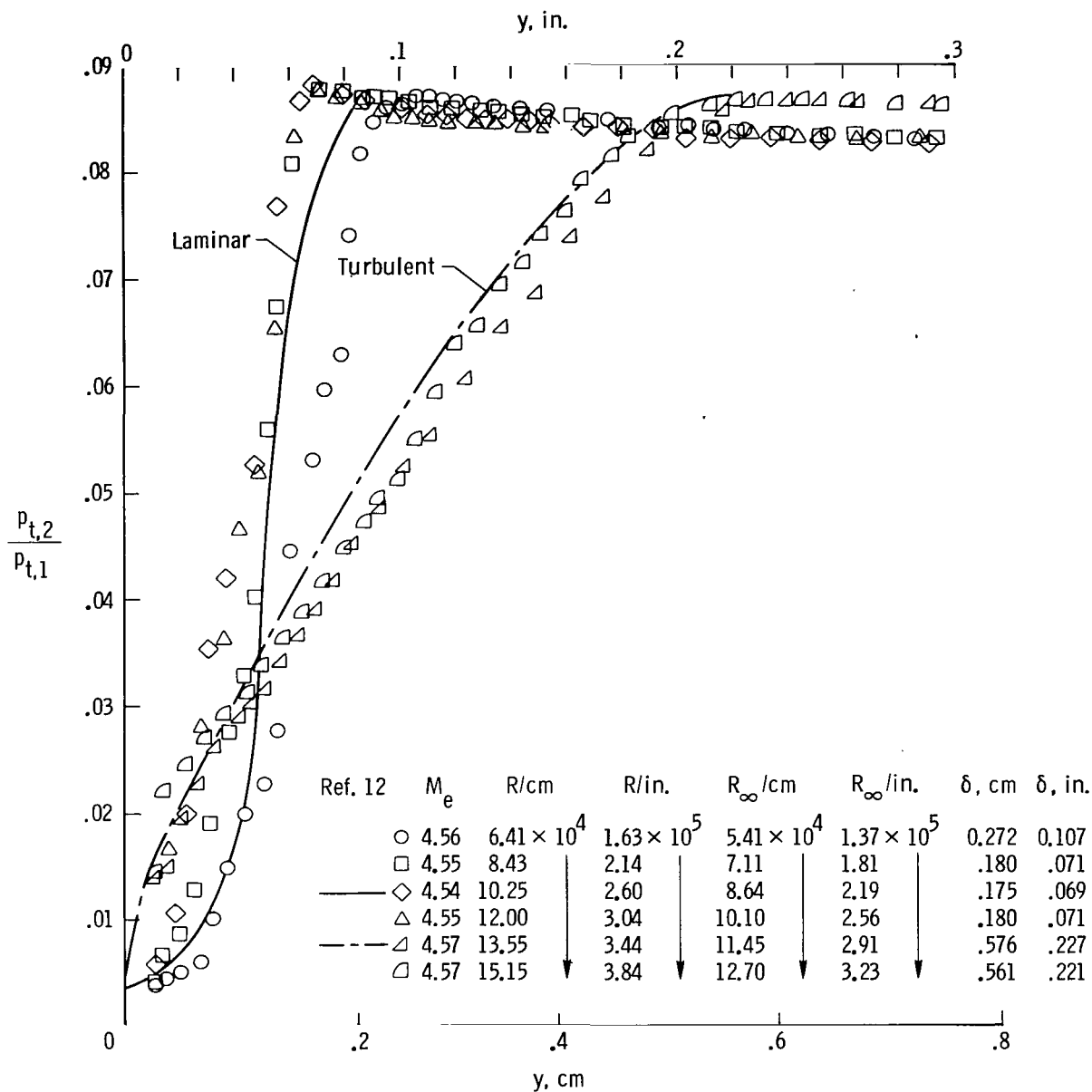
(b) Station $x = 48.1$ centimeters (18.94 in.); $h = 0.3124$ centimeters (0.123 in.)

Figure 14.- Continued.



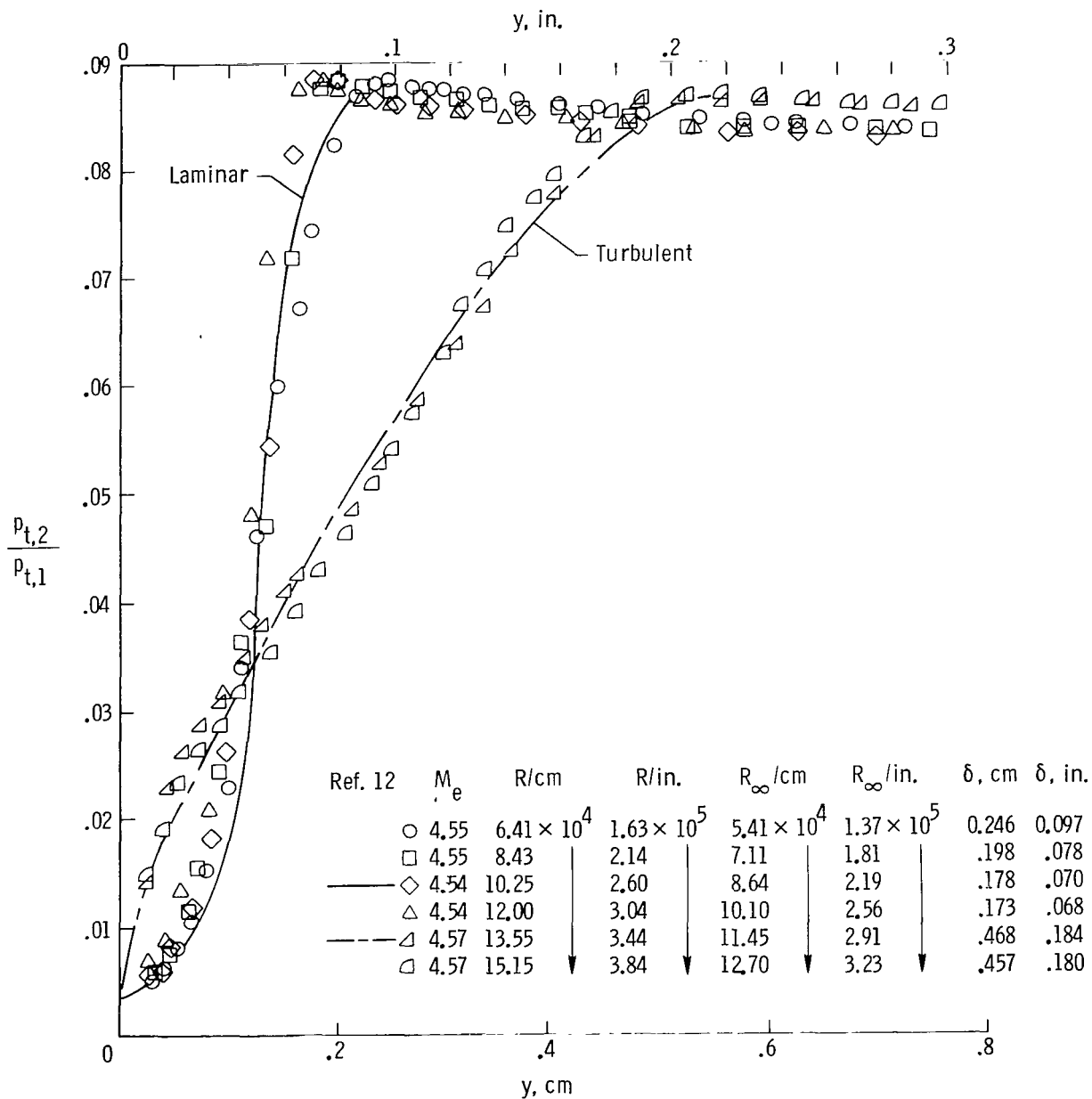
(c) Station $x = 27.2$ centimeters (10.7 in.); all step heights tested.

Figure 14.- Concluded.



(a) Screen configuration 2 (table III).

Figure 15.- Effect of settling-chamber screen configuration on boundary-layer profiles and transition. $x = 27.2$ centimeters (10.7 in.).



(b) Screen configuration 4 (table III).

Figure 15.- Concluded.

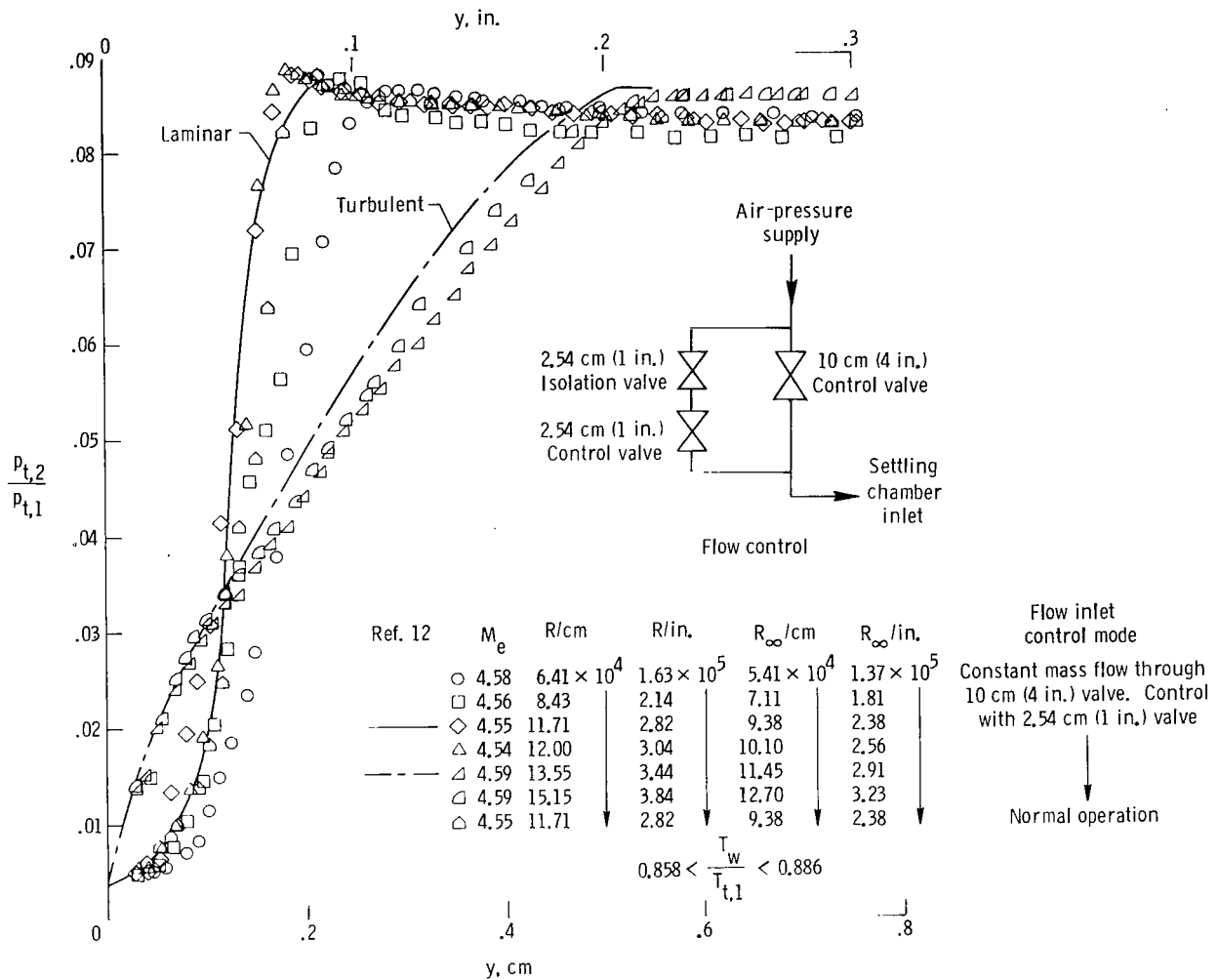


Figure 16.- Effect of flow control valve on pitot-pressure profiles and transition, with and without flow through bypass valve. $x = 27.2$ centimeters (10.7 in.).

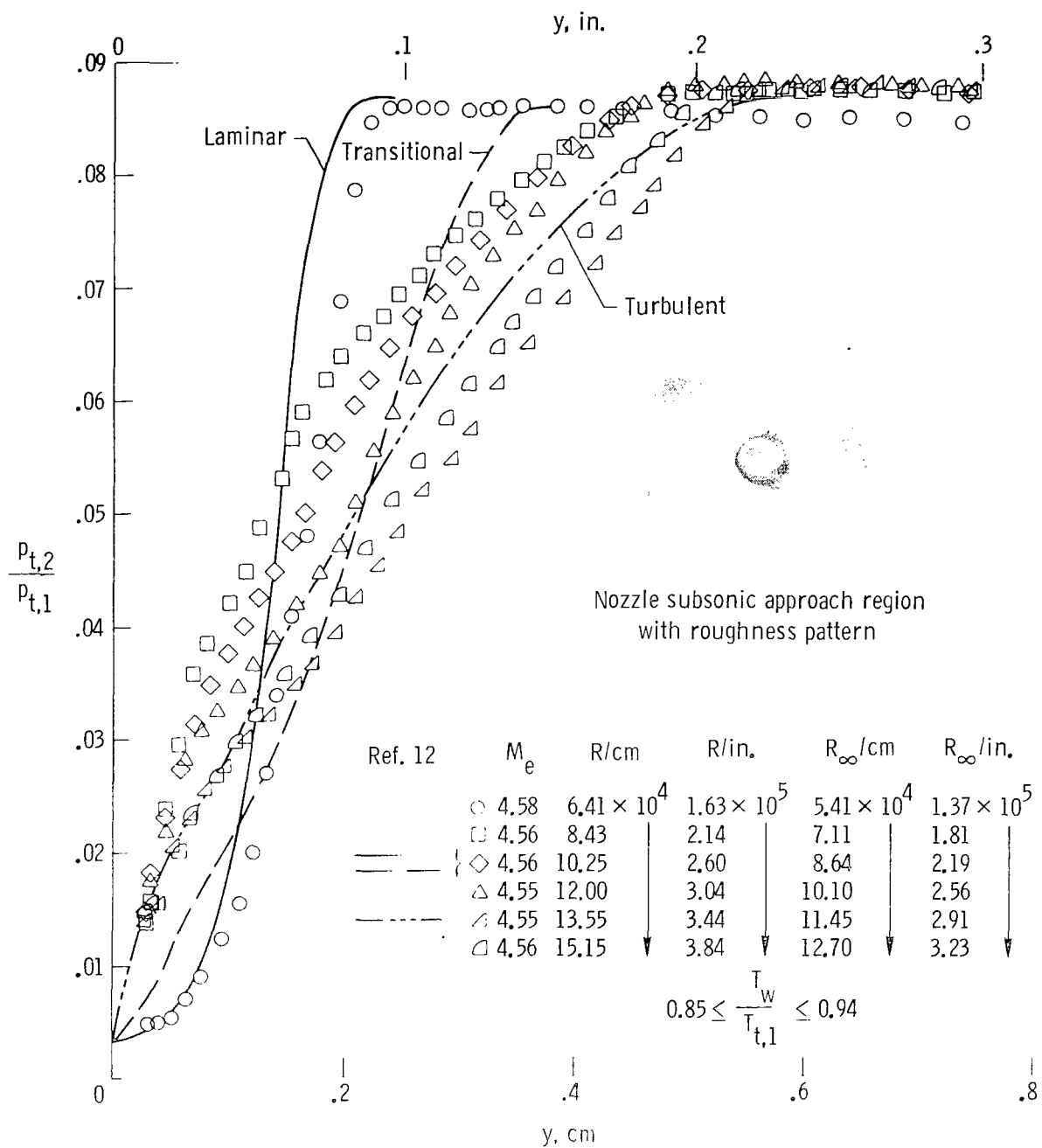


Figure 17.- Pitot-pressure profiles in physical coordinates for $x = 27.2$ centimeters (10.69 in.) with roughness located in nozzle subsonic approach region.

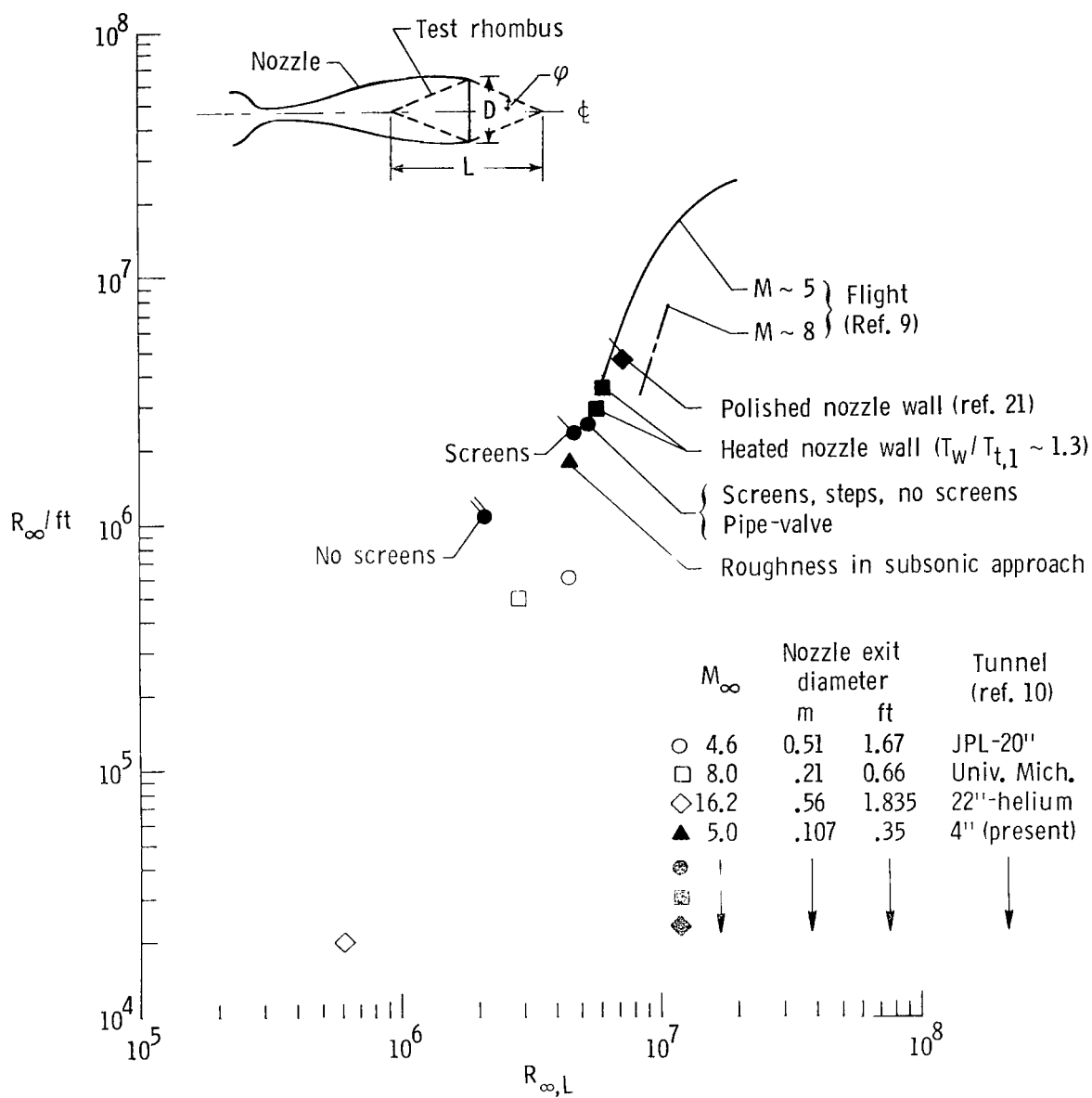


Figure 18.- Comparison of maximum test Reynolds numbers for laminar nozzle-wall boundary layers. (Solid symbols represent mean data; solid flagged symbols represent fluctuating data (ref. 11).)

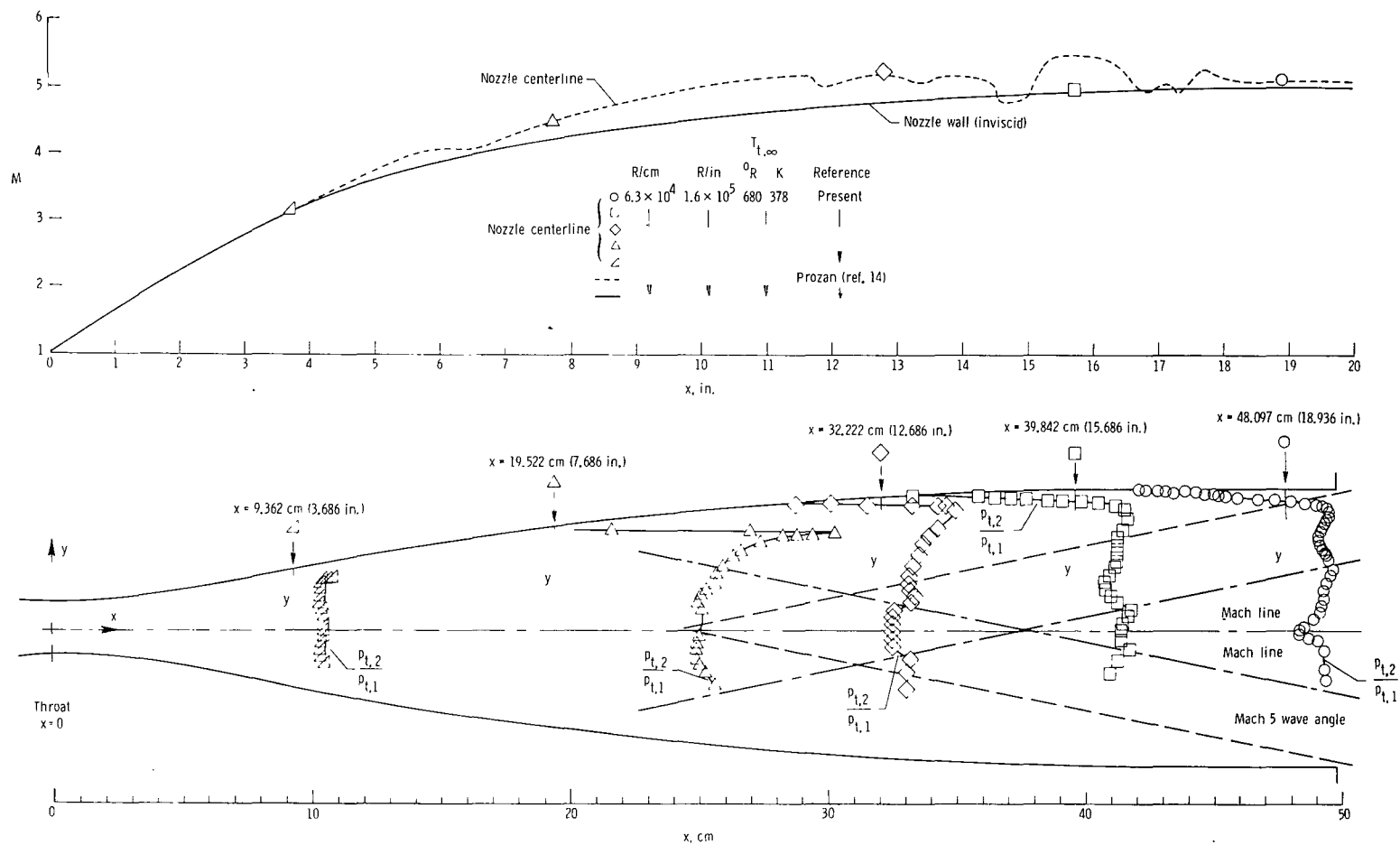


Figure 19.- Flow-field characteristics of Mach 5 nozzle.



001 001 C1 U D 751017 S00903DS
DEPT OF THE AIR FORCE
AF WEAPONS LABORATORY
ATTN: TECHNICAL LIBRARY (SUL)
KIRTLAND AFB NM 87117

POSTMASTER:

If Undeliverable (Section 158
Postal Manual) Do Not Return

"The aeronautical and space activities of the United States shall be conducted so as to contribute . . . to the expansion of human knowledge of phenomena in the atmosphere and space. The Administration shall provide for the widest practicable and appropriate dissemination of information concerning its activities and the results thereof."

—NATIONAL AERONAUTICS AND SPACE ACT OF 1958

NASA SCIENTIFIC AND TECHNICAL PUBLICATIONS

TECHNICAL REPORTS: Scientific and technical information considered important, complete, and a lasting contribution to existing knowledge.

TECHNICAL NOTES: Information less broad in scope but nevertheless of importance as a contribution to existing knowledge.

TECHNICAL MEMORANDUMS: Information receiving limited distribution because of preliminary data, security classification, or other reasons. Also includes conference proceedings with either limited or unlimited distribution.

CONTRACTOR REPORTS: Scientific and technical information generated under a NASA contract or grant and considered an important contribution to existing knowledge.

TECHNICAL TRANSLATIONS: Information published in a foreign language considered to merit NASA distribution in English.

SPECIAL PUBLICATIONS: Information derived from or of value to NASA activities. Publications include final reports of major projects, monographs, data compilations, handbooks, sourcebooks, and special bibliographies.

TECHNOLOGY UTILIZATION PUBLICATIONS: Information on technology used by NASA that may be of particular interest in commercial and other non-aerospace applications. Publications include Tech Briefs, Technology Utilization Reports and Technology Surveys.

Details on the availability of these publications may be obtained from:

SCIENTIFIC AND TECHNICAL INFORMATION OFFICE

NATIONAL AERONAUTICS AND SPACE ADMINISTRATION
Washington, D.C. 20546